AD 748810

RADC-TR-72-196
Final Report
August 1972

ELECTRONICALLY TUNABLE HIGH-POWER FILTER FOR INTERFERENCE REDUCTION IN AIR FORCE COMMUNICATION SYSTEMS

Stanford Research Institute

Rome Air Development Center
Air Force Systems Command
Griffiss Air Force Base, New York

132

UNCLASSIFIED

Security Classification

DOCUMENT CONTROL DATA - R & D

(Security classification of title, body of abstract and indexing annotation must be entered when the overall report is classified)

1. ORIGINATING ACTIVITY (Corporate author) Stanford Research Institute Menlo Park, California 94025	2a. REPORT SECURITY CLASSIFICATION UNCLASSIFIED 2b. GROUP N/A

3. REPORT TITLE

ELECTRONICALLY TUNABLE HIGH-POWER FILTER FOR INTERFERENCE REDUCTION IN AIR FORCE COMMUNICATION SYSTEMS

4. DESCRIPTIVE NOTES (Type of report and inclusive dates)

Final Report 21 April 1971 to 21 May 1972

5. AUTHOR(S) (First name, middle initial, last name)

Arthur Karp
William B. Weir

6. REPORT DATE August 1972	7a. TOTAL NO. OF PAGES 126	7b. NO. OF REFS 4
8a. CONTRACT OR GRANT NO. F30602-71-C-0255 Job Order No. 45400351	9a. ORIGINATOR'S REPORT NUMBER(S) Final Report SRI Project 1201 9b. OTHER REPORT NO(S) (Any other numbers that may be assigned this report) RADC-TR-72-196	

10. DISTRIBUTION STATEMENT

Approved for public release; distribution unlimited.

11. SUPPLEMENTARY NOTES None	12. SPONSORING MILITARY ACTIVITY Rome Air Development Center (RBCI) Griffiss Air Force Base, New York 13440

13. ABSTRACT

A novel, high-Q, high-power VHF/UHF bandpass filter is described that is electronically tuned according to a binary logic. A high-Q, TEM-line resonator is distributively loaded with N independent capacitive irises, such that the opening and closing of switches within each iris makes its capacitance two-valued. The irises are positioned in the resonator field such that the respective tuning increments resulting from the switching of each are proportional to the series 1/2, 1/4, 1/8, $1/16,\ldots,1/2^N$. The 2^N possible resonances are thus (very nearly) uniformly distributed over the tuning range and may be selected by a control code of N binary digits.

Mathematical modeling and design relations were developed and a working, 512-channel (9 iris) bandpass filter was completed for the range 294 to 359 MHz. The use of heavily biased PIN diodes as switches resulted in high peak and average power ratings, low intermodulation distortion, and moderately high unloaded Q. Under novel methods for computer and Network Analyzer control, the filter system was made to rapidly tune itself through all possible resonances and measure, compute, tabulate, and display the pertinent performance parameters for each tuning channel.

High-speed mercury-film switches (Logcells) were also studied and a two-channel demonstrational bandpass filter was completed having higher unloaded Q and lower intermodulation distortion.

DD FORM 1 NOV 65 1473

UNCLASSIFIED

Security Classification

UNCLASSIFIED
Security Classification

14. KEY WORDS	LINK A		LINK B		LINK C	
	ROLE	WT	ROLE	WT	ROLE	WT
Bandpass filter Electronic tuning Binary logic UHF band VHF band High-power filter Air Force communication systems Interference reduction PIN diode switching Mercury-film switches Two-valued capacitive iris Network-analyzer application Automatic measuring system Intermodulation distortion Multichannel filter						

UNCLASSIFIED
Security Classification

ELECTRONICALLY TUNABLE HIGH-POWER FILTER FOR INTERFERENCE REDUCTION IN AIR FORCE COMMUNICATION SYSTEMS

Arthur Karp
William B. Weir

Stanford Research Institute

i c

FOREWORD

This Final Report, under SRI Project 1201, describes research accomplished under contract F30602-71-C-0255, Job Order Number 45400351 by Stanford Research Inst. te, Menlo Park, California, for Rome Air Development Center, Griffiss A... Force Base, New York. It covers the period 21 April 1971 to 21 May 1972. Mr. Fred F. Moore (RBCI) was the RADC Project Engineer.

This report has been reviewed by the Information Office (OI) and is releasable to the National Technical Information Service.

This technical report has been reviewed and is approved.

Approved: Gary L. Seasholtz
GARY L. SEASHOLTZ, CAPTAIN, USAF
Asst Chief, Compatibility Branch
Reliability & Compatibility Division

Approved: Joseph J. Naresky
JOSEPH J. NARESKY
Chief, Reliability & Compatibility Division

FOR THE COMMANDER: Fred I. Diamond
FRED I. DIAMOND
Acting Chief, Plans Office

ABSTRACT

A novel, high-Q, high-power VHF/UHF bandpass filter is described that is electronically tuned according to a binary logic. A high-Q, TEM-line resonator is distributively loaded with N independent capacitive irises, such that the opening and closing of switches within each iris makes its capacitance two-valued. The irises are positioned in the resonator field such that the respective tuning increments resulting from the switching of each are proportional to the series 1/2, 1/4, 1/8, 1/16,..., $1/2^N$. The 2^N possible resonances are thus (very nearly) uniformly distributed over the tuning range and may be selected by a control code of N binary digits.

Mathematical modeling and design relations were developed and a working, 512-channel (9 iris) bandpass filter was completed for the range 294 to 359 MHz. The use of heavily biased PIN diodes as switches resulted in high peak and average power ratings, low intermodulation distortion, and moderately high unloaded Q. Under novel methods for computer and Network Analyzer control, the filter system was made to rapidly tune itself through all possible resonances and measure, compute, tabulate, and display the pertinent performance parameters for each tuning channel.

High-speed mercury-film switches (Logcells) were also studied and a two-channel demonstrational bandpass filter was completed having higher unloaded Q and lower intermodulation distortion.

EVALUATION:

The effort fell short of its goal in providing a breadboard model to cover the entire UHF band (294 to 359 MHz vs 225 to 400 MHz). The band width (1200 to 1800 vs 400 KHz required) and intermodulation (-25 vs -65 dBmW required) was not achieved due to pin diode limitations, however insertion loss, VSWR, power handling, tuning time, weight and size was achieved. The technique of modeling the filter and switching scheme to digitally control the TEM resonant mode is the significant achievement of the effort. This will provide the basis to further perfect 100 watt filters as new type switches (such as "logcells") or better pin diodes become available. A developed filter of this type is a needed item in the Air Force inventory for the new generation of digital controlled VHF and UHF transmitters. This filter with its 5 micro second switching time will be compatible with new rapid electronic tuned transmitters.

Fred F. Moore
FRED F. MOORE
Project Engineer

ACKNOWLEDGMENTS

The authors wish to acknowledge valuable suggestions and contributions from other SRI staff members: Don Parker (project supervision), Allen F. Podell (phase-lock systems, IMD measurements, etc.), Donald R. Chambers (diode selection, computer modeling of multiple-iris resonator, etc.), and Lloyd A. Robinson (network analyzer utilization). Contributions to the Proposal for Research (dated 21 December 1970) subsequently used during the project were also due to Edward G. Cristal (now at McMasters University) and Bernard M. Schiffman (now retired). James L. Huber was associated with the project during its initial months.

York Sato was Engineering Associate for the duration of the project and took charge of component and instrument preparation and maintenance, filter assembly, and much of the electrical measurements and mechanical design.

Valuable directions in steering the research program toward the more immediately useful objectives were received from RADC monitors Capt. Lee W. Wagenhals and Mr. Fred Moore.

The cooperation of the staff of Fifth Dimension, Inc. (Princeton, N.J.) during the study of mercury-film switches, and of Dr. Paul Chorney (Unitrode Corp., Watertown, Mass.) during the study of high-power PIN diodes, is also hereby acknowledged.

CONTENTS

I INTRODUCTION 1

II OPERATING PRINCIPLES AND DESIGN RELATIONS. 9

A. Two-Valued Capacitive Irises and Their Distribution. 9

B. Coarse- and Fine-Tuning Irises. 17

C. Switch Losses 18

III DESCRIPTION AND PERFORMANCE OF FLAUTO I. 23

A. General 23

B. Choice of Diode Switches. 31

C. Bias Chokes 34

D. Coupling Loops. 37

E. Performance 38

F. Trimming of Irises. 54

IV FLAUTO I: POWER HANDLING AND INTERMODULATION DISTORTION 57

A. Power Rating. 57

B. Intermodulation Distortion. 61

V AUTOMATIC MULTICHANNEL-FILTER MEASUREMENT SYSTEM 67

A. Hardware for the Automated Measurement System . . . 68

Preceding page blank

B.	Software for the Automated Measurement System . . .	77
	1. HP 2115A Computer Program.	77
	2. CDC 6400 Computer Program.	84
VI	MERCURY-FILM SWITCHES.	89
	A. General	89
	B. Flauto II Bandpass Filter	96
	C. Repackaging of the Logcell Switch	101
VII	SUGGESTIONS FOR FUTURE WORK.	105
VIII	SUMMARY AND CONCLUSIONS.	109
Appendix A	FILTER CIRCUIT REQUIREMENTS AND RELATIONS	113
Appendix B	HEWLETT-PACKARD 8541A AUTOMATIC NETWORK ANALYZER. .	121

ILLUSTRATIONS

Figure II-1	"Flauto" Principle: Doubly-Shorted (Half-Wave) TEM-Line Resonator Distributively Loaded with Independent Switch-Controlled Capacitive Irises	10
Figure II-2	Variation on Figure II-1: Singly-Shorted (Quarter-Wave) TEM-Line Resonator Distributively Loaded with Switch-Controlled Capacitive Irises	11
Figure II-3	Predicted Resonance Frequencies of TEM-Line Cavity with Five Two-Valued Capacitive Irises Spaced Such that $\sin^2 \theta_i$ = 1/16, 1/4, 1, 1/2, 1/8	14
Figure II-4	Tuning Chart for UHF Filter with Five Two-Valued Capacitive Irises.	15
Figure II-5	Equivalent Circuit of TEM-Line Resonator Loaded Centrally by a Capacitive Iris Controlled by n Paralleled Switches	19
Figure III-1	Flauto I, a 512-Channel, Binary-Programmed, Electronically Tuned, High-Power, High-Q, UHF Bandpass Filter with Diode-Biasing Control Breadboard in Background.	24
Figure III-2	Five-Digit, Electronically Tuned, High-Power, Narrow-Bandpass UHF Filter.	25
Figure III-3	Interior of UHF Filter with End Plate Removed . .	26
Figure III-4	Coarse-Tuning Iris-Half Subassembly	27
Figure III-5	Fine-Tuning Iris Subassembly.	28
Figure III-6	Outlines of Flauto I: 2^9-Channel UHF Bandpass Filter, Showing Locations of Coarse-Tuning (1-5) and Fine-Tuning (6-9) Irises, and Coupling Loops	29
Figure III-7	Cross Section of Flauto I: Binary-Program Electronically Tuned, High-Power, High-Q, UHF Bandpass Filter	30

Figure III-8	Proposed Biasing in Series of an Even Number of PIN Diodes per Iris Half; (a) Not Recommended, (b) Recommended	34
Figure III-9	Bandpass-Filter Characteristics for the 32 Channels of the Five-Iris Filter of Figure III-2	40
Figure III-10	Representative Page from CDC 6400 Printout Listing Flauto I Data Measured by HP Network Analyzer.	42
Figure III-11	Representative Page from CDC 6400 Printout Listing Computed Filter Parameters for Flauto I.	44
Figure III-12	Low-end Portion of Plot of Insertion Loss vs. Frequency for Flauto I Bandpass Filter, as Generated by CDC 6400 Page Printer.	46
Figure III-13	Tuning Data for Flauto I Bandpass Filter.	47
Figure III-14	Computer Plot of Parameters for Flauto I Bandpass Filter	52
Figure III-15	Computer Plot of Parameters for Flauto I Bandpass Filter (Continued)	53
Figure IV-1	Equivalent Circuit of Flauto I Filter with All Diodes Forward-Biased	57
Figure IV-2	Equivalent Circuit of Flauto I Filter with All Diodes Reverse-Biased	59
Figure IV-3	Test Setup for Measuring Intermodulation Distortion in UHF Bandpass Filter.	63
Figure IV-4	IMD Data for Flauto I Filter at Channel Code 00000.	65
Figure V-1	Automated Measurement System.	69
Figure V-2	Transistor-Driven-Relay Biasing Circuit for Each Iris	71
Figure V-3	Phase-Lock-Loop Bias and Integrator Circuit . . .	73
Figure V-4	Input-Flag Logic Circuit.	76
Figure V-5	HP 2115A Computer Program Flow Diagram.	78
Figure VI-1	Photograph, Approximately 15.5X, of Logcell Mercury-Film Switch Capsule (Part No. 3000-1C-WL, Fifth Dimension, Inc, Princeton, N.J.). . . .	90

Figure VI-2 Details of Mounting Logcell Switch Capsule, Accessories, and Drive Components in RF Cavity. 94

Figure VI-3 Flauto II, A Two-Channel (One-Iris) Electronically Tunable, High-Power, High-Q, UHF Bandpass Filter Using 10 Logcell I Mercury-Film Switches. 97

Figure VI-4 Interior View of Flauto II Filter 98

Figure VI-5 Close-Up of Iris Half for Flauto II Filter, Showing Two Dielectric Spacers and Five Logcell I Switches Installed. 100

Figure VI-6 Proposed Molybdenum/Ceramic Package Modification of "Logcell" Switch for High-Q, High-Frequency, Resonant Cavity Applications. 103

Figure VI-7 Proposed Package Idea for High-Q Mercury-Film Switch of Figure VI-6 104

Figure A-1 Equivalent Circuits of a Single-Resonator Bandpass Filter with Loss 117

Figure B-1 Computer-Controlled Automatic Network Analyzer (Hewlett-Packard Model 8541A) Used to Measure VHF, UHF, and Microwave Components at Stanford Research Institute 124

TABLES

Table II-1 Iris Placement for a Binary Tuning Program 12

Table III-1 Gap Dimensions for Irises of Flauto I After Final Trimming 31

Table III-2 Diode Biasing Recommendations. 39

Table VIII-1 Summary of Design Objectives and Performance Parameters 111

I INTRODUCTION

This report summarizes one year's research effort on high-Q, high-power, UHF/VHF bandpass filters that are electronically tuned according to a novel concept based on a binary logic. Such filters would be useful to reduce interference in Air Force communication systems when located between transmitter and antenna. This application thus dictates that the filter have high selectivity (high Q), handle high power, and not engender excessive intermodulation distortion (IMD) at the required power levels. Electronic tuning replaces mechanical tuning so that tuning may be much more rapid and reliable over a longer period in service.

The novel concept on which these filters are based is the use of the simplest mode of resonance in a coaxial (or modified coaxial) TEM resonator distributively loaded with several identical but independent capacitive irises containing switches that enable the effective capacitance of an iris to be two-valued. Since the switches themselves are two-state devices, IMD is minimized, rather than being large as in the case of a high-power, high-Q system containing continuously variable, electronically tunable elements like varactors. Additionally, the distribution pattern for the irises is determined such that the tuning increments resulting from the switching of each member of the series of irises are related, very nearly, by the ratios

$$1/2,\ 1/4,\ 1/8,\ 1/16,\ \ldots,\ 1/2^N\ .$$

where N is the total number of irises in the resonator.* Accordingly, the electronic tuning is said to follow a "binary logic" and, to the first order of approximation, one may call up a desired tuning channel (out of a total of 2^N resonances) by expressive its number in binary form and using the 0's and 1's to represent the required states of the switches in each iris.

During the course of the research program, the following were the major achievements:

- Development of the design concept and experimental confirmation of its validity.
- Development of mathematical modeling of the filter with regard to iris placement, the effects of switch losses, and the RF voltages and currents in individual switches at high power levels.
- Development of design relationships applicable to non-ideal switches and prediction of the resulting limitations on filter selectivity.
- Evaluation of two kinds of switching device (PIN diodes and Logcell I mercury-film switches).
- Completion of a working breadboard-model bandpass filter, based on PIN diodes, and having 512 tuning channels in the range 294 to 359 MHz.
- Evaluation of worst-case third-order intermodulation generation of this filter.
- Development of hardware and software serving to rapidly tune this filter through a list of tuning channels and

---

*The same series of tuning-increment ratios could be achieved with several unequal capacitive elements connected at a common location in the resonator, rather than with a spatial distribution of equal capacitive elements. However, the ratio of the largest to the smallest capacitance needed would then have to be 2^{N+1}, and such a design would not be feasible at VHF and higher frequencies.

automatically measure, record, and display the corresponding filter parameters.

- Completion of a demonstrator breadboard-model bandpass filter based on Logcell I mercury-film switches and having two channels (at 299 and 323 MHz) with superior selectivity.

- Generation of recommendations for improvements in mercury-film switches.

- Generation of recommendations for future work in all of the above areas.

The design parameters used as objectives during the conduct of the above were the following:

Frequency range of primary interest:	225 - 400 MHz
Frequency range of secondary interest:	116 - 150 MHz
Tuning increments:	100 kHz
3-dB bandwidth:	400 kHz (max)
30-dB bandwidth:	14 MHz (max)
Passband insertion loss:	2.25 dB (max)
Passband VSWR:	1.5:1 (max)
Power-handling capacity, peak:	100 watts
Power-handling capacity, average:	20 watts
Input impedance:	50 ohms
Tuning time:	1 second, max
Volume:	0.5 ft^3, max
Weight:	15 pounds, max
Third-order intermodulation products with two in-band or out-of-band inputs at +40 dBm:	-60 dBm, max

The technical approach followed by SRI is to cover the frequency range of primary interest with four switch-selected filters. The subranges for these filters would then be

225 - 269, 269 - 313, 313 - 356, 356 - 400 MHz

or

225 - 260,	260 - 300,	300 - 346,	346 - 400 MHz
("bass)	("tenor")	("alto")	("soprano")*

depending on whether the subranges are desired to be equal in MHz, or in percentage width. The completed, working-model filter based on PIN diodes (henceforth referred to as "Flauto I") covers the range 294 - 359 MHz, and hence would amply cover the third ("alto") subrange no matter how defined. (The range 116 - 150 MHz could probably be covered with a single resonator.)

The weight allowance for Flauto I--if assumed to be 1/4 of 15 pounds--has been exceeded by the "breadboard" model, but there is no doubt that, in a production model, substitution of aluminum for brass, and the thinning and ribbing of walls to provide low weight without loss of mechanical rigidity, would yield the desired result. The volume allowance--if 1/4 of 0.5 ft^3--would permit each filter to be 3 by 6 by 12 inches, whereas the Flauto I resonator now measures 3.25 by 6.5 by 13.5 inches internally. However, design relationships indicate that the small required reduction in cross-sectional area, in a production model, would not result in a degradation of performance of Flauto I.

Tuning-time specifications have been amply met: PIN diodes can be switched in a few microseconds (even when RF current is large compared with bias current) and mercury-film switches can be operated in a few milliseconds. Design objectives for insertion loss, VSWR, power handling, and input impedance are readily achievable.

---

*The musical notations have been added since analogies with musical instruments have been found to be helpful, and historically intriguing (cf. Helmholtz), in writing about these filters.

Design objectives for bandwidth, however, cannot be met with presently available PIN diodes due to their inherent RF losses, and the steps one may take to reduce loss under forward bias (more diodes in parallel) and under reverse bias (fewer diodes in parallel) are mutually opposed. Even after making the most of possible design tradeoffs, the 3-dB bandwidths of the 512 tuning channels of Flauto I exceed the design objective by factors of 3 to 4.5.*

As a consequence of the increased bandwidth, the design objective on tuning increment was relaxed by a factor of 3 (i.e., 300 kHz). However, the design of Flauto I and its driving circuitry is quite compatible with a tuning increment of 100 kHz, since the addition of a fine-tuning iris to the resonator (and of a digit to the tuning code) is relatively simple and inexpensive.

The electrical parameters of mercury-film switches can allow design objectives for bandwidth to be met. However, the construction of the corresponding filter was not undertaken, pending a repackaging of the Logcell I switch to decrease mechanical fragility and package losses. A demonstrator filter was completed with Logcell I switches, and the unloaded Q observed for its two tuning channels exceeds that which could be obtained with PIN diodes (indicating reduced bandwidth for a given insertion loss).

Intermodulation products are generated in PIN diodes due to the internal physics of the junction, and the conditions are exceptionally severe in high-Q resonators where large swings of RF voltage are developed. (RF voltage varies as the +1/2 power of both power input and loaded Q.) As a result of in-situ measurements and carefully considered

---

*Decreases in bandwidth at the expense of increased insertion loss and VSWR are assumed undesirable.

extrapolations, it appears that worst-case third-order intermodulation products in Flauto I would be above the design objective by about 35 dB, and that very little improvement would result from redesign of the filter or from substitution of diodes from another manufacturer.

The generation of intermodulation products in mercury-film switches is expected to be negligible and due only to inadvertent occurrences of metal/oxide interfaces in the circuit. Meeting design objectives on IMD with these switches should be readily achievable.

In Section II of this report, the operating principle of a single-resonator filter covering a 15- to 20-percent tuning range by means of spatially distributed, switch-controlled, independent capacitive irises is discussed in more detail. Part of SRI's technical approach has been to group these irises into two sets: a coarse-tuning group of five irises providing an average tuning increment of 2 MHz, and a fine-tuning (or interpolating) group of four irises providing an average tuning increment of 125 kHz. Mathematical modeling of the filter is developed and design relations are derived.

In Section III, physical components, design decisions, adjustments, and performance are discussed in general and in detail for Flauto I, a working high-power, high-Q, bandpass filter using nine irises with PIN diode switches and resonant bias chokes in conjunction therewith.

In Section IV, currents, voltages, and dissipation in the diodes of Flauto I at high RF power levels are investigated and intermodulation-distortion experiments are described.

In Section V are described the hardware and software comprising a novel system for automatically measuring and displaying the performance of a multichannel, binary-programmed, electronically tuned bandpass filter such as Flauto I.

In Section VI, the theory and application of mercury-film (Logcell) switches in filters of the present type are covered, and the construction and performance of a demonstrator bandpass filter using these switches is discussed.

Recommendations for future research and development work on these filters and the components thereof are listed in Section VII.

A summary of the results of the project is given in Section VIII and conclusions stated.

II OPERATING PRINCIPLES AND DESIGN RELATIONS

A. Two-Valued Capacitive Irises and Their Distribution

The equivalent circuit of a TEM-line (generally coaxial) resonator distributively loaded with independent switch-controlled capacitive irises is shown in Figure II-1. The transmission line is short-circuited at both ends and hence is half-wave resonant.* In the absence of the irises, the fundamental resonant frequency, f_0, would be $c/4\ell$, where c is the velocity of light, and the (transverse) electric field in the resonator would have a half-sine-wave distribution with a maximum in the mid-plane. The irises that are added are identified according to their distance from the nearest short-circuiting plane; it is convenient to specify the distances θ_i as "electrical angles" relative to θ_1 (distance from short to mid-plane) being defined as 90°. An iris is considered to be more or less "significant" to the resonator as θ is larger or smaller, respectively.

In Figure II-1, the "significance" succession is achieved by using both sides of the resonator in alternation. This scheme appears to be the most convenient, and the only one tried experimentally, but it is not essential. In Figure II-2, the resonator is intended to be equivalent, but it is shorter and quarter-wave resonant, with one end open-circuited and the other end shorted. No doubt the choice between the two embodiments would depend on the particular application to be served. For the present work, the resonator of Figure II-2 appears the

---

*Only this simplest mode of resonance is considered throughout this report.

Preceding page blank

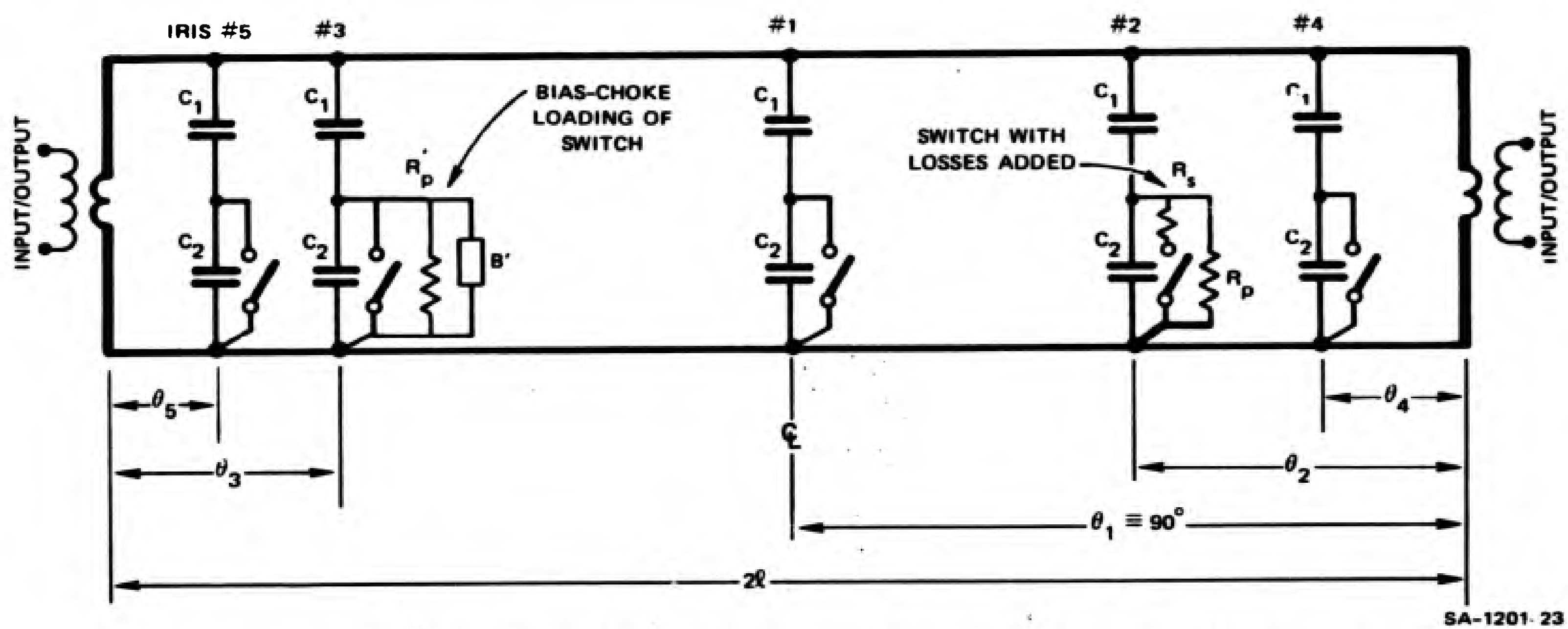

FIGURE II-1 "FLAUTO" PRINCIPLE: DOUBLY-SHORTED (half-wave) TEM-LINE RESONATOR DISTRIBUTIVELY LOADED WITH INDEPENDENT SWITCH-CONTROLLED CAPACITIVE IRISES

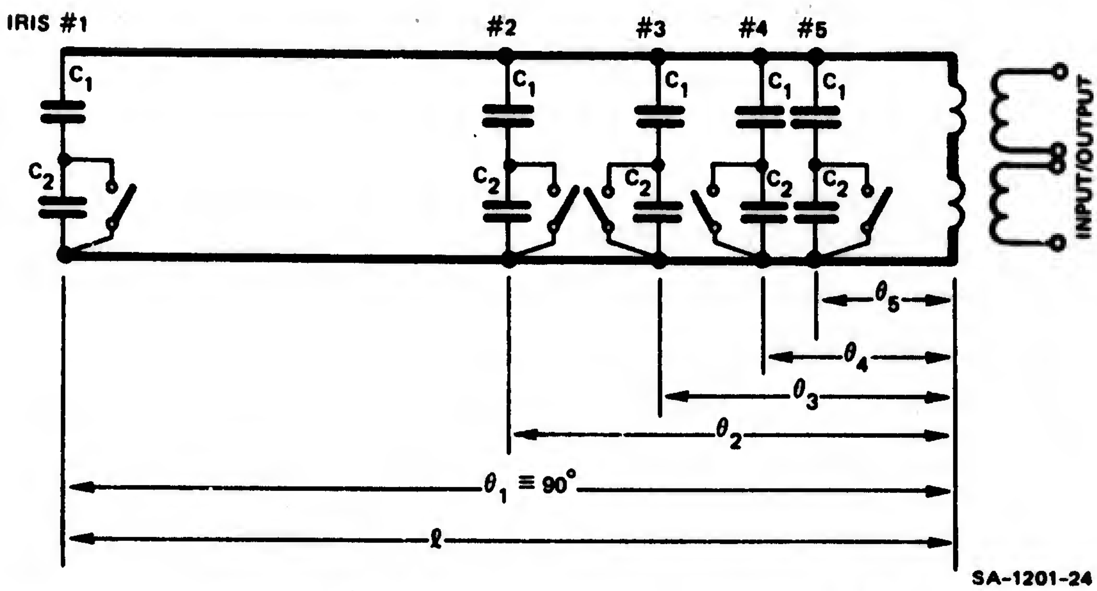

FIGURE II-2 VARIATION ON FIGURE II-1: SINGLY-SHORTED (quarter-wave) TEM-LINE RESONATOR DISTRIBUTIVELY LOADED WITH SWITCH-CONTROLLED CAPACITIVE IRISES

less advantageous due to the mechanical inconvenience of having irises closer together and the greater likelihood of unwanted interactions between irises. In addition, the effective fringing capacitance (not shown) at the open-circuited end may depend on the state of the nearby irises and thus make computations difficult.

The principal capacitance provided by the iris is C_1, but since the switches exhibit capacitance when "open," and are supported between conductors providing additional capacitance, it is necessary to include the capacitances C_2, as shown. The iris capacitance is thus two-valued:

$$C_{max} = C_1 \qquad \text{with switch closed} \qquad \text{(II-1)}$$

and

$$C_{min} = \frac{C_1 C_2}{C_1 + C_2} \qquad \text{with switch open} \quad . \qquad \text{(II-2)}$$

Since the usefulness of an iris depends on having C_{max}/C_{min} large, it is seen as desirable to have $C_2 < C_1$, and preferably $C_2 \ll C_1$.

Having all the irises identical has many advantages, including keeping C_{max}/C_{min} optimal. The "significance" of an iris for tuning purposes is then determined solely by its location relative to the E-field distribution. If iris loading is assumed not to alter this half-sine-wave distribution, and if irises are assumed not to interact with one another, the "capacitive effect" of an iris should be weighted as

$$\sin \theta_i \quad , \qquad i = 1, 2, 3, \ldots, N \quad .$$

Further, assuming that it is a law of nature for a "frequency-tuning effect" to vary as the (-1/2) power of a "capacitive effect," a binary tuning program would be achieved if

$$\sin^2 \theta_i = 1, 1/2, 1/4, 1/8, \ldots, 1/2^{N-1} \qquad \text{(II-3)}$$

where N is the total number of irises present. The following table is obtained from Eq. (II-3):

Table II-1

IRIS PLACEMENT FOR A BINARY TUNING PROGRAM

Iris No. (i =)	Nominal "Frequency-Tuning Effect"	$\sin^2\theta_i$	θ_i	Distance from Short
1	1/2 of the range	1	90°	ℓ
2	1/4 of the range	1/2	45°	$0.500\ \ell$
3	1/8 of the range	1/4	30°	$0.333\ \ell$
4	1/16 of the range	1/8	20.7°	$0.230\ \ell$
5	1/32 of the range	1/16	14.5°	$0.161\ \ell$
⋮	⋮	⋮	⋮	⋮
N	$1/2^N$ of the range	$1/2^{N-1}$	$\sin^{-1}[2^{-(N-1)/2}]$	$2\theta_i \ell/180$

The above inductive (if not intuitive) reasoning is far from rigorous and the assumptions made are tenous. Nevertheless, it has in practice proved very workable; computations and measurements made with a resonator loaded with five irises positioned as indicated have yielded an essentially binary tuning logic, as evidenced by a roughly uniform spacing of the 32 resonances. Using the computer program UHFFILT (see below), the distribution of resonances plotted in Figure II-3 was obtained for a representative case. While the spacings are not entirely uniform, they are much more so than was obtained with any of several other distributions considered. In addition, all attempts to improve the uniformity by various small adjustments of one or more positions were of no avail.

To facilitate computations on iris-loaded resonators like that of Figure II-1, a CDC 6400 computer program UHFFILT was written (in FORTRAN) with capacity to handle nine two-valued irises. Input data are line length and Z_0, the N values of C_{max} and of C_{min} (whether or not all irises are the same), and the N+1 longitudinal spacings. The computer sequences through the 2^N combinations and, for each, solves (by iteration) the transcendental equation which yields the resonant frequency. The 2^N frequencies are then listed in descending order and printed out or graphed along with corresponding codes and frequency separations between resonances.

The model of Figure II-1 should be a good approximation to the physical case to the degree that the irises are thin and not too close to one another, and, if not actually filling the entire transverse cross section, at least do not cause substantial changes in the distribution pattern of fields in the transverse plane upon being switched. The validity of the model is demonstrated in Figure II-4, where the 32 resonant frequencies of an actual filter (see later) with five equal

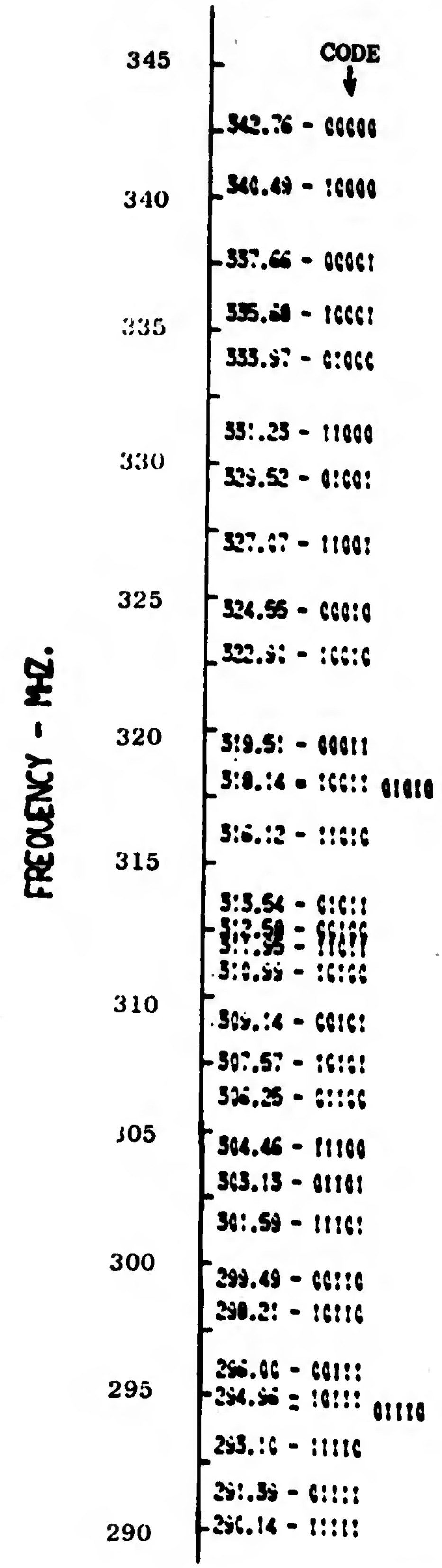

All Capacitance Values:

Code "0", C_{min} = 3.2 pF

Code "1", C_{max} = 6.4 pF

Z_0 = 56 ohms

Spacings (inches):(see Fig. II-1)

left short to iris 5:	1.090
iris 5 to iris 3:	1.155
iris 3 to iris 1:	4.500
iris 1 to iris 2:	3.375
iris 2 to iris 4:	1.830
iris 4 to right short:	1.550
Total: 2ℓ =	13.500

SA-1201-25

FIGURE II-3 PREDICTED RESONANCE FREQUENCIES OF TEM-LINE CAVITY WITH FIVE TWO-VALUED CAPACITIVE IRISES SPACED SUCH THAT $\sin^2 \theta_i$ = 1/16, 1/4, 1, 1/2, 1/8

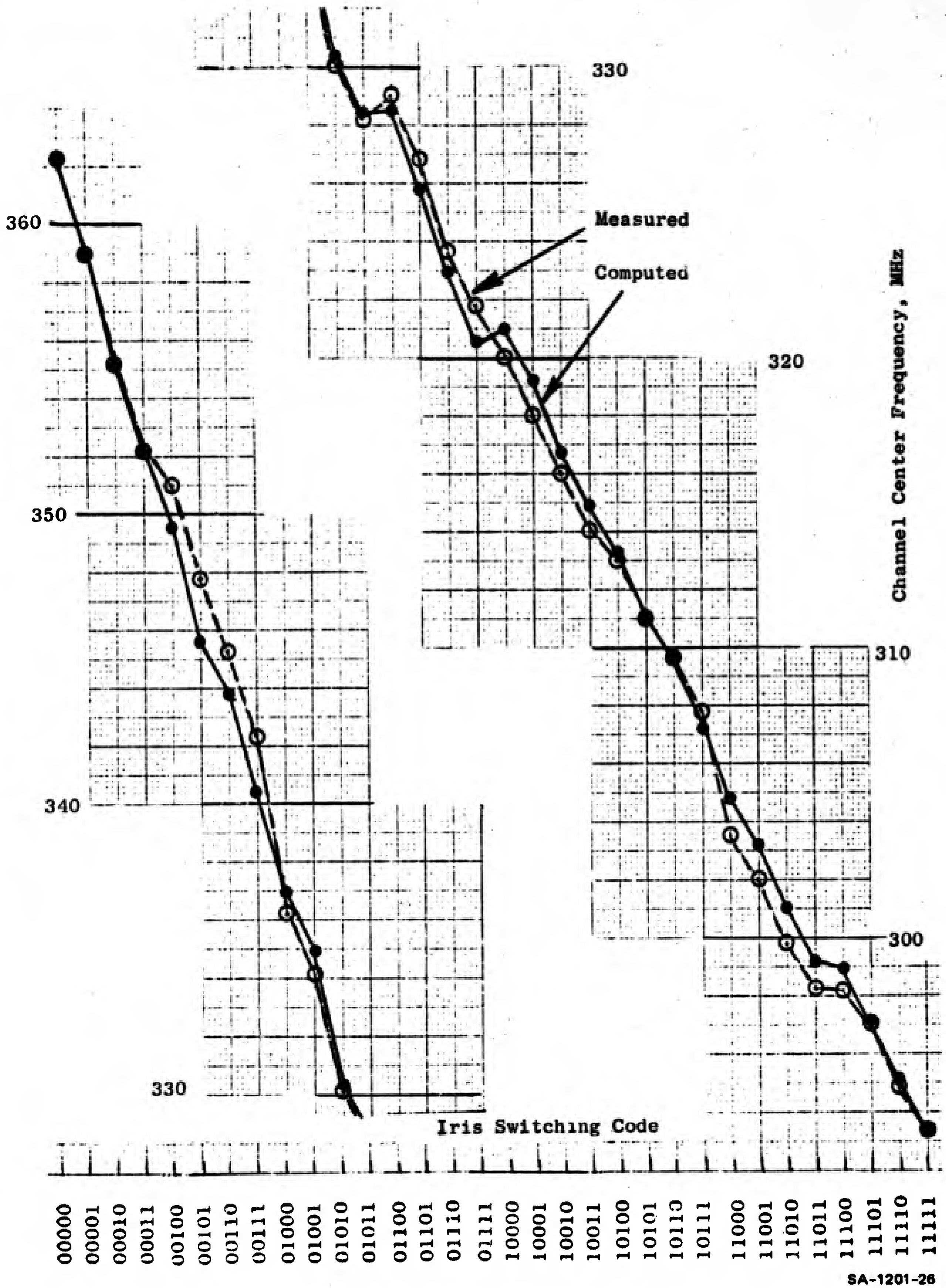

FIGURE II-4 TUNING CHART FOR UHF FILTER WITH FIVE TWO-VALUED CAPACITIVE IRISES

irises are plotted. For the comparison points, the computer model used the same Z_0 (56 ohms), length, and spacings as the filter (see Figure II-3), and capacitances were inserted as

$$C_{max} = 6.15 \text{ pF}$$

$$C_{min} = 2.35 \text{ pF} \quad .$$

These values are within the range of estimates one may make for the actual iris constructed, but were more particularly chosen to give agreement at the end points, 362.3 MHz (all switches open) and 293.4 MHz (all switches closed). It is seen that, at points in between, agreement is excellent both in general and in detail, despite the approximations and simplifications made in setting up the model. In addition, the essentially uniform slope of the curves indicates that, with only two or three exceptions, the resonances are fairly uniformly spaced in frequency.

In conclusion, use may be made of the analogies between electromagnetic resonators and acoustic resonators (e.g., musical instruments) such as Helmholtz enjoyed. If a VHF, UHF, or microwave bandpass filter utilized a separate resonator for each tuning channel, it could be likened to a piano or organ. If the filter is tuned by mechanically changing a physical dimension, it could be compared with a trombone or violin. The present filter consists of a single resonator distributively loaded with two-valued reactive elements. It is therefore like a flute (flauto), or the older and simpler recorder (flauto dolce), having a relatively small number of finger holes on the surface that can be either open or closed. In all cases, the numerous possible combinations of open and closed elements allows a relatively small number of them to engender a large gamut of resonances. In music, the relations between the notes and the code or pattern of open and closed holes is called a "fingering chart." The musical resonators also have the possibility of higher-order modes of resonance (via "octave keys"), but these modes have not been of interest in the present electromagnetic counterparts. The aptness of the analogy has suggested the use of "Flauto" as a useful and short name when referring to resonators and filters of the form under discussion.

B. Coarse- and Fine-Tuning Irises

In actual application it has been found that after five or six irises have been installed in a UHF filter, the spacings between irises, and between an iris and an end wall, start to become inconveniently small. Hence, if the tuning range is required to be divided into more than 32 or 64 parts, more irises must be added, though not very many since the number of tuning channels doubles for each additional iris. Although there are several solutions to this problem, the scheme chosen here was to design each of the five original "coarse-tuning" irises so as not to fill up the entire resonator cross section, but to leave room for a small, interpolating or "fine-tuning" iris (see later, in Figure III-7) in the same transverse plane. If the tuning effectiveness of the auxiliary iris is 1/32 of that of the original iris, and if there is negligible interaction between them,* the progressive halvings of tuning increment by each iris in turn will be continuous from Iris 1 through Iris 10 (of which 1 through 5 are original irises and 5 through 10 are auxiliary). A total of 1028 resonances would be available.

---

*The complexity of the possible interactions between a multiplicity of iris segments lying in the same transverse plane indicates that further use of this possibility, beyond the use already made, would not be advisable.

Admittedly, having a large and a small capacitance in the same place in the resonator is in part a return to a principle (see footnote, p. 2) that was rejected in conceiving the present filter. However, the ratio 32:1 is not as unattractive as 1028:1, and has been found to be manageable in practice.

As will be seen from the course of the discussion in the remainder of this report, a very appealing feature of this filter is the fact that the filter parameters (range limits, loaded and unloaded Q, bandwidth, VSWR, and insertion loss) are determined almost solely by the first few of the more-significant irises. Thus, a filter design can be developed that is independent of the ultimate tuning increment desired. Less-significant irises can be added or deleted at any time, giving a smaller or larger tuning increment, without affecting filter performance for any one channel.

C. Switch Losses

In practice, it is found that the principal limitation on the attainable unloaded Q, Q_u, of a "Flauto" resonator is due to switch losses. The resistivity of resonator walls and end plates does play a part, as does increased cavity loss due to crowding of RF currents near an iris, but these factors alone would still allow Q_u to be in the range 5000 to 9000 without exceeding the permissible resonator volume. With PIN-diode switches, however, it does not appear possible for Q_u to exceed 1500 as an average over the band.*

*As indicated in Appendix A, a 3-dB bandwidth of 400 kHz would require Q_u = 5000 as limited by switch losses, with the Q_u of the resonator alone substantially larger. Bandwidth specifications have consequently been relaxed for a filter using diodes.

It is also found that the limitations on Q_u are imposed almost entirely by the switches in Iris 1. Since the square of the RF voltage at Iris i is about half that at Iris i-1, it is seen that the less-significant irises have very little effect on Q_u. Indeed, during testing of Flauto I (see later) it was confirmed that switch resistance in the less-significant irises may be allowed to increase quite a bit (via decreases in diode forward-bias current) before any detrimental effect on Q_u is observed. Economic advantage of this effect was taken by using progressively less bias current for the diodes in Irises 2, 3, 4, . . ., and/or using fewer switches in parallel.

The equivalent circuit of a TEM resonator loaded by Iris 1 and its associated losses is shown in Figure II-5. If there is an inductive length of resonator on both sides of Iris 1 (as in Figure II-1), one should interpret Z_0 as <u>half</u> that of the line. The resistance r accounts for cavity wall, end plate, and crowding losses, but will be neglected

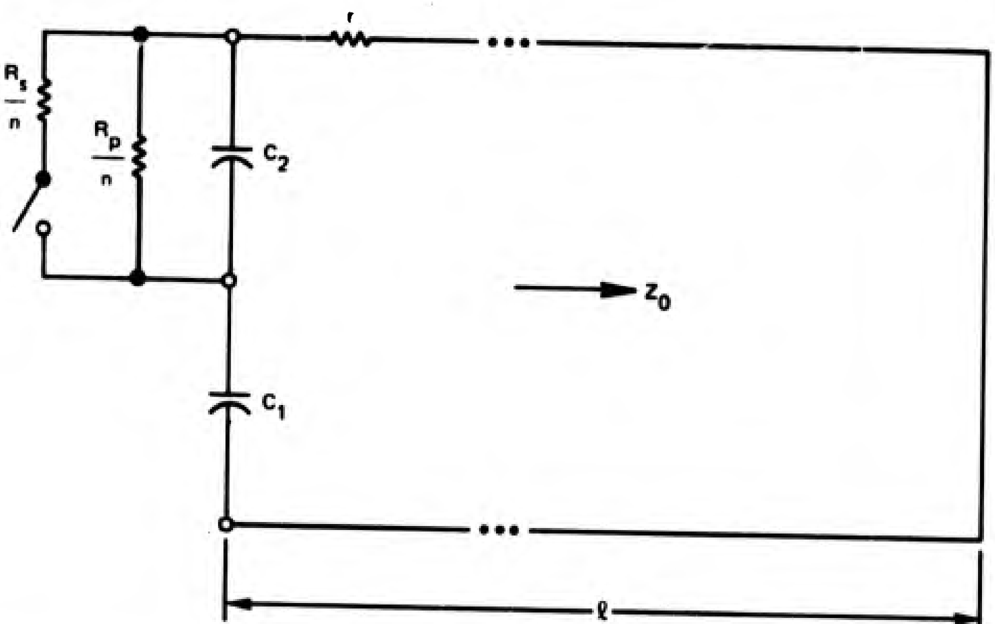

FIGURE II-5 EQUIVALENT CIRCUIT OF TEM-LINE RESONATOR LOADED CENTRALLY BY A CAPACITIVE IRIS CONTROLLED BY n PARALLELED SWITCHES here. The resistance of a closed switch (denoted by subscript a) is R_s, with $R_s < 1$ ohm, and of an open switch (subscript b), R_p, with $R_p > 10^4$ ohms (shunting the switch capacitance). The number of switches in parallel is n. For the two states, one readily finds:

$$Q_{ua} = \frac{nZ_0 \tan \theta_a}{R_s} \tag{II-4}$$

and

$$Q_{ub} = \frac{R_p}{nZ_0 \tan \theta_b} \left(\frac{C_1 + C_2}{C_1}\right)^2 \tag{II-5}$$

where $\theta_a = 2\pi f_a \ell/c$ and $\theta_b = 2\pi f_b \ell/c$ are the electrical lengths at resonant frequencies f_a and f_b and c is the velocity of propagation.

The above equations indicate major design relations for the filter. It is seen that increasing the accessible design variables n, Z_0, or ℓ to enhance Q_{ua} would have the opposite effect on Q_{ub}, since $(nZ_0 \tan \theta)$ is the numerator of Eq. (II-4) but in the denominator of Eq. (II-5). Depending on the parameters of the switches chosen, a compromise design such that $Q_{ua} \approx Q_{ub}$ would be the best one could do.

Given wide freedom in the choice of n, Z_0, and ℓ it would be of interest to compute an upper limit for Q_u, but having C_1, C_2, f_a, f_b and ℓ related through transcendental equations renders this excessively difficult. However, experimentation with different diodes and much numerical figuring during the course of the project seem to indicate that 1200 would be an upper limit for available PIN diodes near 300 MHz. This low value was originally unexpected since PIN diodes were not expected to have such a low R_p, which is due to a high effective dielectric loss tangent for the depleted I layer. Some diode manufacturers do not even quote R_p, since it is of little interest for diodes used to switch low-impedance lines, as opposed to use in the interior of a high-Q resonator. [Since mercury film switches (see later) have an R_p that is two or three orders of magnitude higher and an R_s that is less than one order of magnitude higher than for PIN diodes, the upper limit for Q_u there should be much higher.]

Alternative forms of Eqs. (II-4) and (II-5) are

$$Q_{ua} = [2\pi f_a C_1 R_s/n]^{-1} \tag{II-6}$$

and

$$Q_{ub} = 2\pi f_b (C_2^2/C_1) R_p/n \quad . \tag{II-7}$$

If one defines

$$\Psi \equiv C_{max}/C_{min} = (C_1 + C_2)/C_2 \tag{II-8}$$

and assumes that C_2 is comprised entirely of the capacitance (C_d) of the n open switches

$$C_2 \approx nC_d \tag{II-9}$$

one obtains

$$Q_{ua} = [2\pi f_a C_d R_s (\Psi - 1)]^{-1} \tag{II-10}$$

and

$$Q_{ub} = 2\pi f_b C_d R_p \Psi/(\Psi - 1) \quad . \tag{II-11}$$

These expressions are independent of the number of switches in parallel, and for a given C_d, R_s, and R_p,

$$Q_{ua} \propto \frac{f_a^{-1}}{\Psi - 1} \tag{II-12}$$

and

$$Q_{ub} \propto \frac{f_b \Psi}{\Psi - 1} \quad . \tag{II-13}$$

From the above, it is seen that Q_{ua} and Q_{ub} will generally be enhanced by making $\Psi - 1$ small, which means that C_{max}/C_{min} should be only minimally greater than unity. The consequence of this stipulation is that the resonator tuning range will be reduced, since f_b/f_a should be of the order of $(C_{max}/C_{min})^{1/2}$. In conclusion, it appears that the smaller the tuning range of a resonator, the higher the attainable Q_u, and this was one of the arguments in favor of covering the range 225 to 400 MHz (1.78:1) with four filters (with frequency ratio about 1.16:1 each) instead of one. (Another advantage is having two irises fewer per resonator.)

III DESCRIPTION AND PERFORMANCE OF FLAUTO I

A. General

Flauto I is a working, breadboard-model, UHF bandpass filter designed according to the principles given above, and employing UM 7000-C-series PIN diodes as switches. It has nine capacitive irises (five coarse-tuning and four fine-tuning) and hence 512 tuning channels covering the range 293.2 to 359.3 MHz (1.22:1, or 20 percent) with a tuning increment that is 130 kHz average, and 300 kHz maximum.

The completed filter is shown in Figure III-1. Each coarse-tuning iris consists of two half-iris subassemblies; five of these are seen mounted on the broad wall of the resonator (the other halves are not visible in the photograph), and the four fine-tuning iris subassemblies are seen mounted on the narrow wall. Input/output coupling loops are at the top, and the inner conductor of the TEM resonator (not visible) runs the full length of the cavity. Another view of the filter is shown in Figure III-2, which was photographed before adding the fine-tuning irises. Figure III-3 shows the interior of the filter--also photographed before addition of the fine-tuning irises. Two of the subassemblies shown in Figure III-4 comprise a coarse-tuning iris whose components, such as the diodes, bias choke, and bypass capacitor, will be discussed below. A fine-tuning iris subassembly (Figure III-5) is seen to be similar, but much smaller. The significant dimensions of the filter are included in the outline sketch of Figure III-6, with Figure III-7 showing a cross section (with irises) in more detail. Parts were initially planned to be silver-plated brass (or copper), but in view of the dominance of switch losses over other losses, the plating was frequently omitted. Dielectric

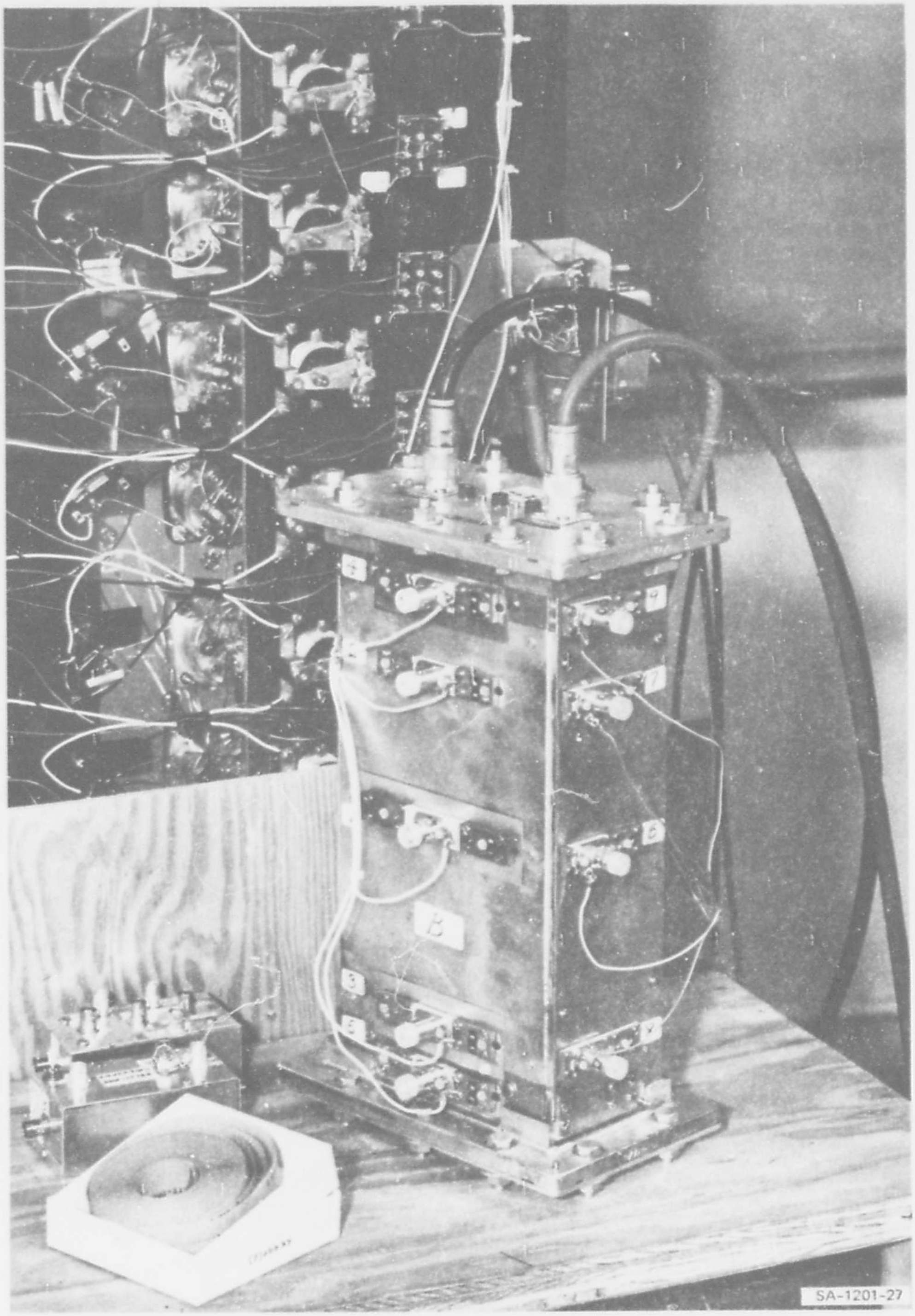

FIGURE III-1 FLAUTO I, A 512-CHANNEL, BINARY-PROGRAMMED, ELECTRONICALLY TUNED, HIGH-POWER, HIGH-Q, UHF BANDPASS FILTER WITH DIODE-BIASING CONTROL BREADBOARD IN BACKGROUND. (Small boxes contain OPAMPS for phase-locking and automatic measuring systems; punched tape is read into HP Network Analyzer to start automatic measurement program.)

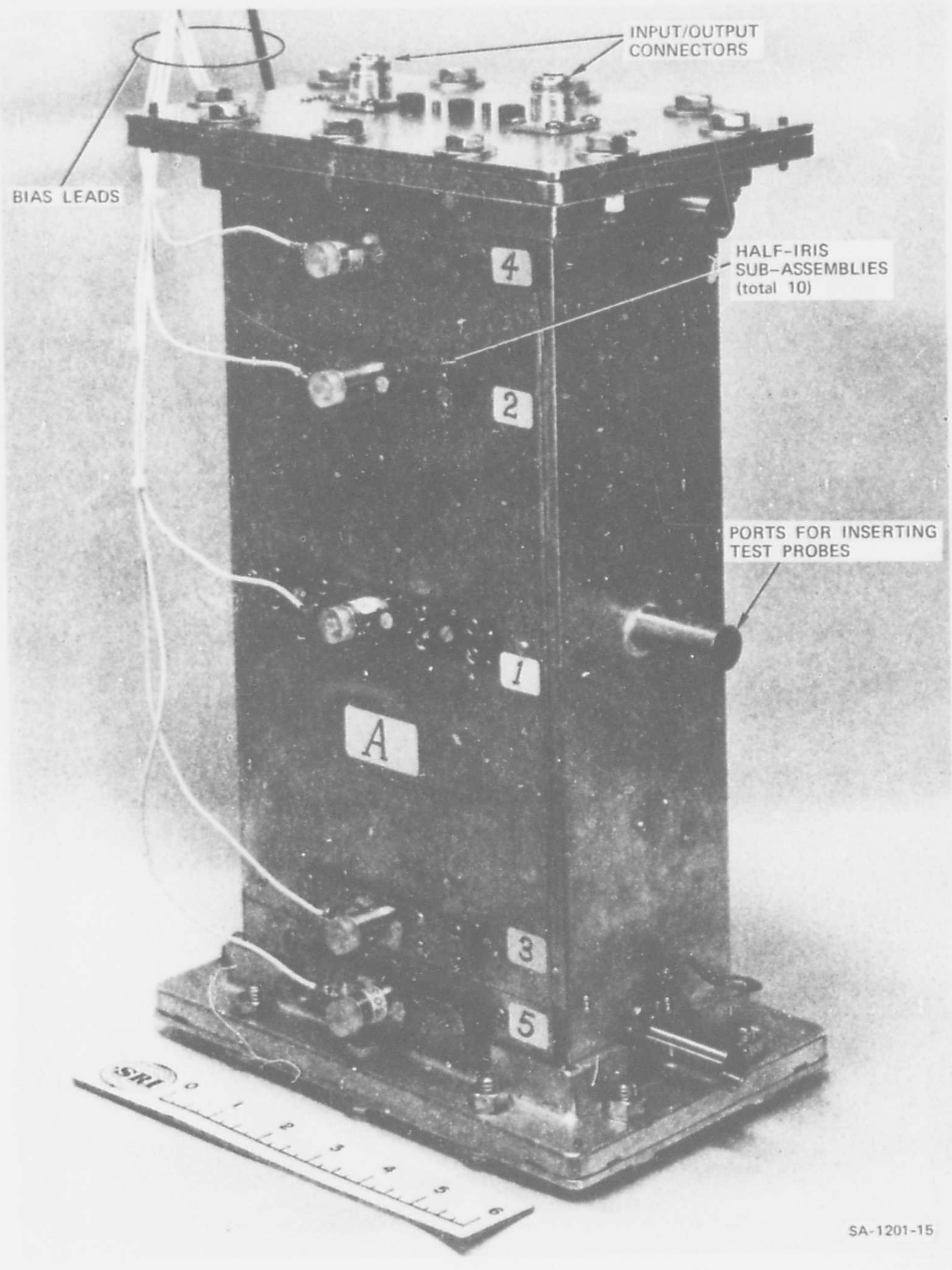

FIGURE III-2 FIVE-DIGIT, ELECTRONICALLY TUNED, HIGH-POWER, NARROW-BANDPASS UHF FILTER

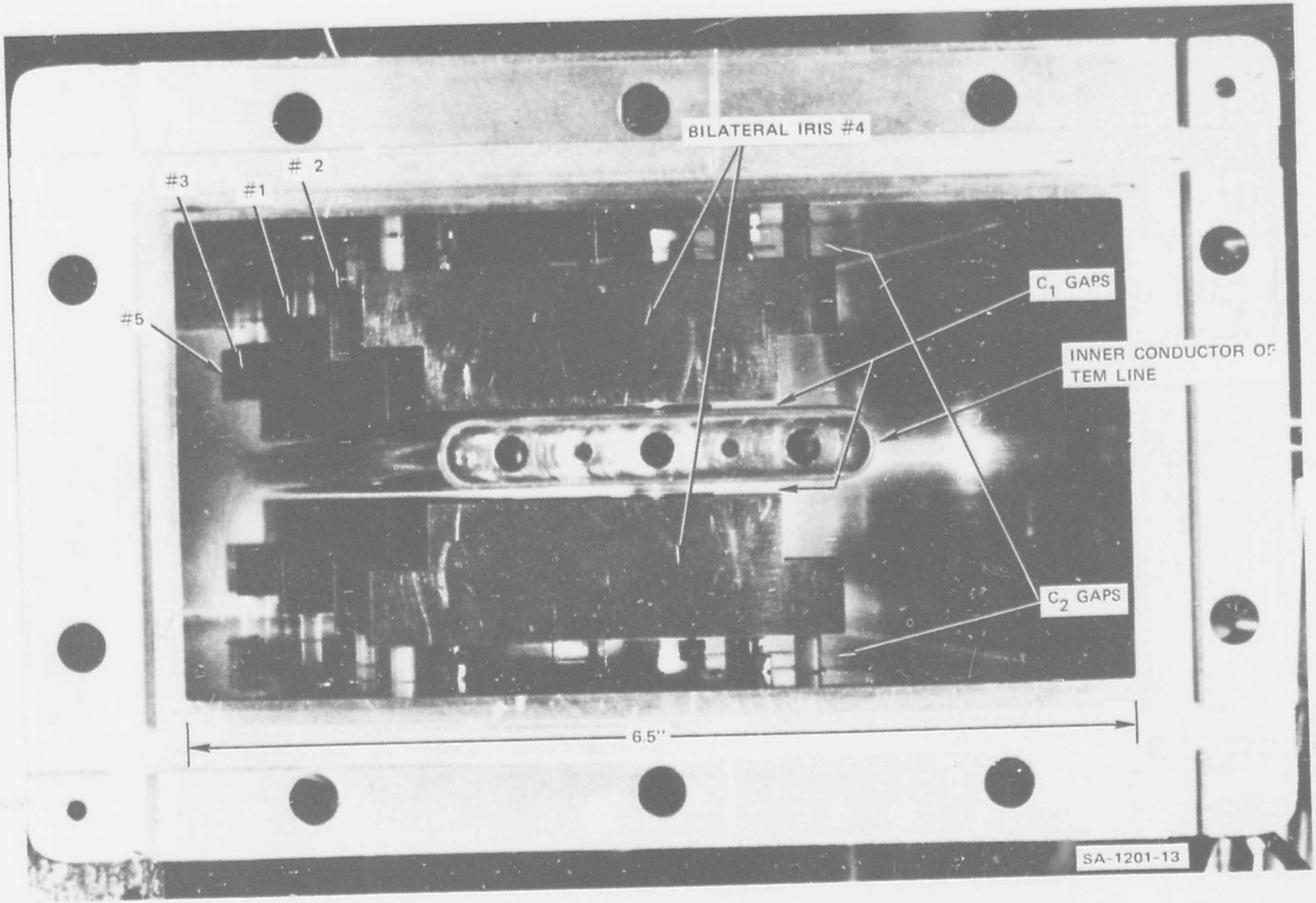

FIGURE III-3 INTERIOR OF UHF FILTER WITH END PLATE REMOVED (fine-tuning irises absent)

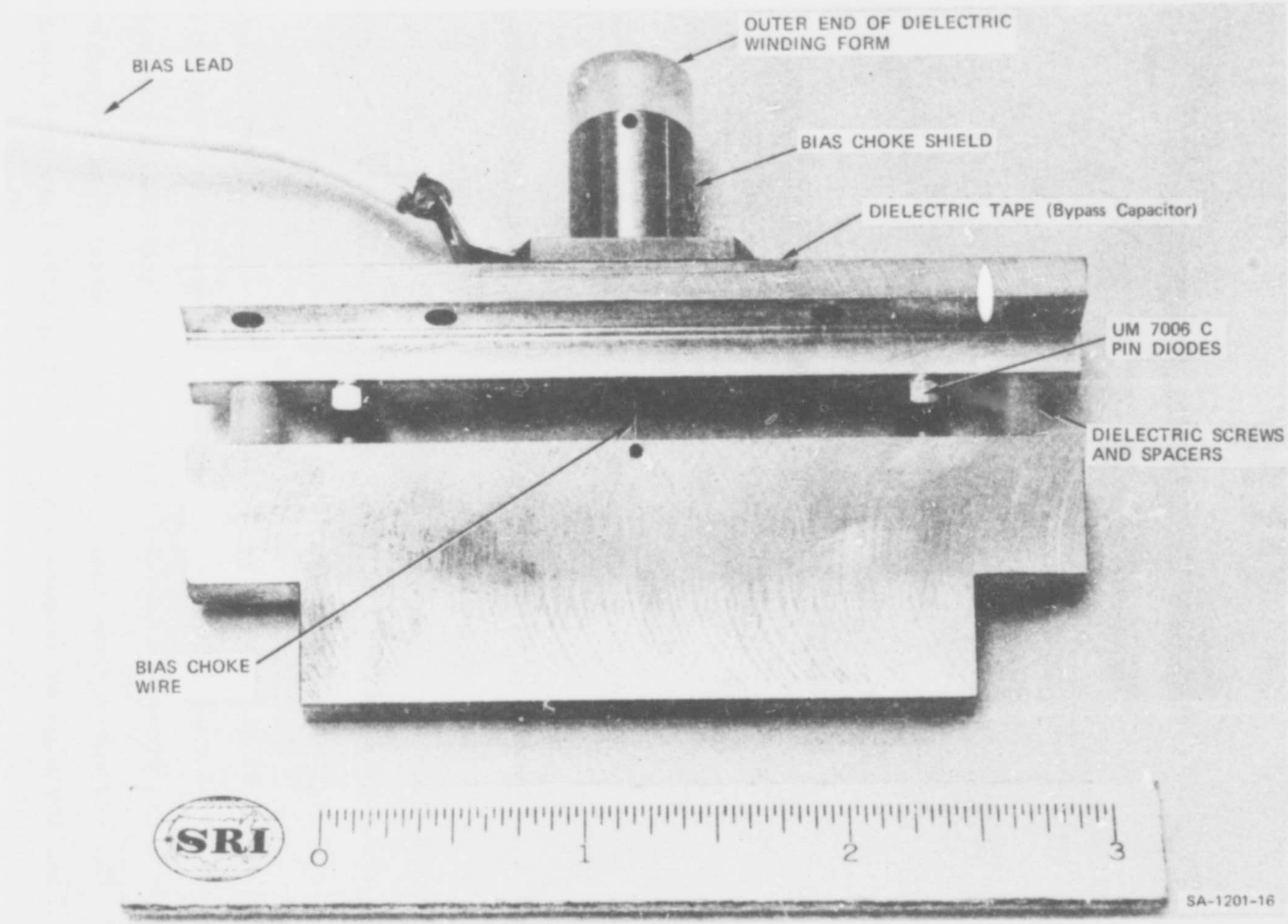

FIGURE III-4 COARSE-TUNING IRIS-HALF SUBASSEMBLY

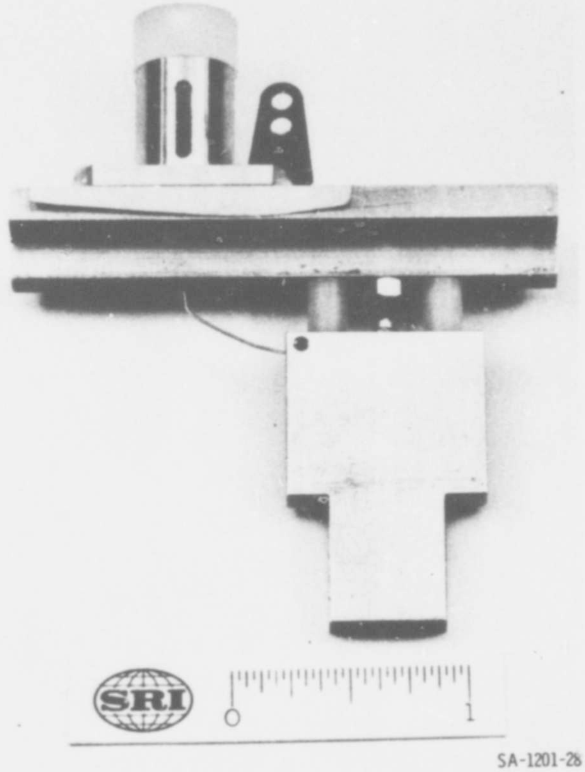

FIGURE III-5 FINE-TUNING IRIS SUBASSEMBLY

parts are of Rexolite, with nylon screws. Mylar tape forms the bypass capacitor adjoining the bias choke. The critical C_1 inner gaps (S_1 and S_1') and the much less critical C_2 outer gaps (S_2 and S_2') formed by the irises are listed in Table III-1; the small variations are the result of a final "trimming" of the iris capacitances (see later).

Although originally chosen because of the ease of construction and availability of materials, the rectangular cross section (Figures III-3 and III-7) has proven to be very convenient for the TEM line required here. (A circularly symmetrical cross section might lead to smaller dimensions for a given resonator Q_u, but it appears that iris assembly would be more difficult, and that an alternative scheme for the fine-tuning irises would have to be found.) A highly asymmetrical rectangular

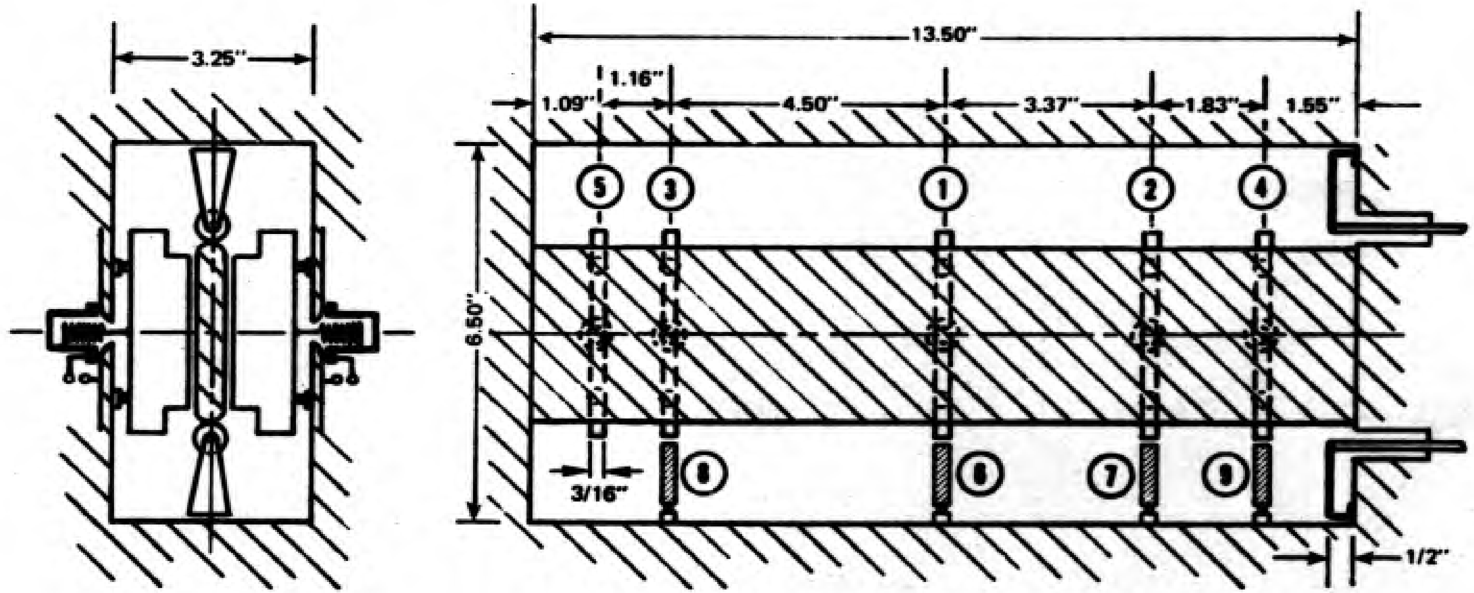

TRANSVERSE SECTION
(without Irises 6-9)

LONGITUDINAL SECTION

SA-1201-14R

FIGURE III-6 OUTLINES OF FLAUTO I: 2^9-CHANNEL UHF BANDPASS FILTER, SHOWING LOCATIONS OF COARSE-TUNING (1-5) AND FINE-TUNING (6-9) IRISES, AND COUPLING LOOPS

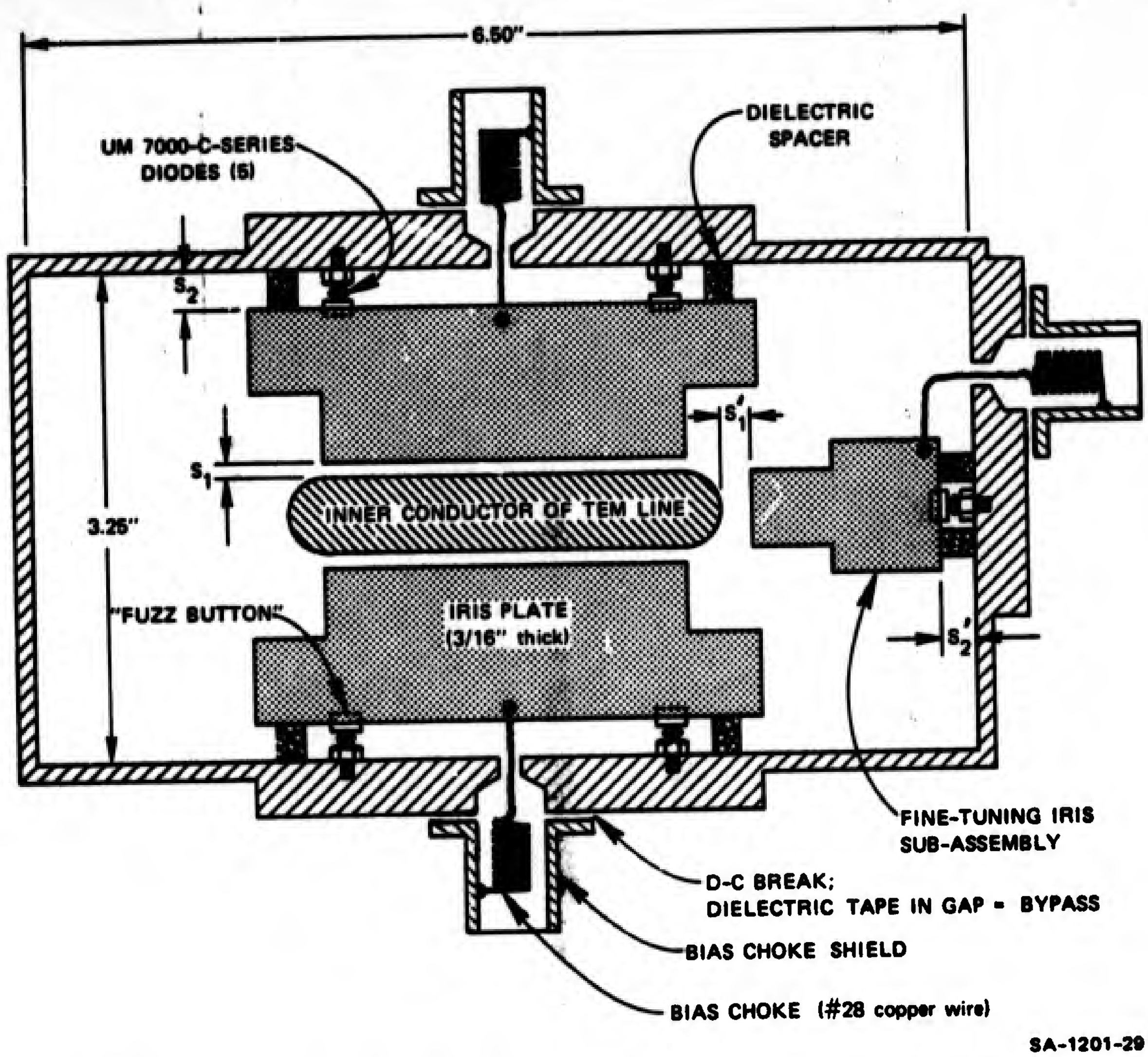

FIGURE III-7 CROSS SECTION OF FLAUTO I: BINARY-PROGRAM ELECTRONICALLY TUNED, HIGH-POWER, HIGH-Q, UHF BANDPASS FILTER

cross section was considered, with the RF fields concentrated on one side, so that a single iris plate (instead of two) would suffice, located on that same side. It was found, however, that for the same Z_0 and resonator Q_u, an excessively large volume would be needed on the unused side. That is, when resonator volume and hence cross-sectional area are limited, one obtains the greatest Q_u for a given Z_0 when using the available area for a bilaterally symmetrical cross section.

Table III-1

GAP DIMENSIONS FOR IRISES OF FLAUTO I AFTER FINAL TRIMMING

	Iris No.	Total Diodes	Inner Gap, S_1 or S'_1 (inch)	Outer Gap, S_2 or S'_2 (inch)
Coarse Tuning	1	4	0.090	0.250
	2	4	0.100	0.250
	3	4	0.080	0.250
	4	4	0.100,0.095	0.250
	5	4	0.085	0.250
Fine Tuning	6	1	0.212	0.225
	7	1	0.174	0.264
	8	1	0.150	0.225
	9	1	0.150	0.225

B. <u>Choice of Diode Switches</u>

Criteria affecting the choice of PIN diodes include voltage rating (since wide RF voltage swings are to be expected in a high-Q, high-power filter, and high reverse bias voltages are also needed), R_s, C_d (including package), R_p, and intermodulation-distortion considerations. A common diode figure of merit--cutoff frequency--is inversely proportional to both R_s and C_d. However, care must be used in considering this figure, since R_s is normally quoted for 0.1 A forward-bias current, whereas higher bias currents are generally possible, especially in diodes having superior heat sinking (e.g., Unitrode).* R_p may vary among diodes

*A (-1/2) power dependence of R_s on bias current generally applies.

from a given source and some manufacturers do not include it in their specifications. HPA diodes are generally somewhat superior to Unitrode in this regard, but other considerations may count more.

In considering filter designs, it was soon realized that the lowest available C_d would be a strong recommendation. If C_d, and hence C_2, are high, C_1 must be high and Z_0 low because of tuning considerations. Construction then becomes difficult (e.g., very narrow S_1 gaps) and the lowering of Q_{ua} demands more diodes be placed in parallel, increasing C_2 further, and aggravating rather than improving the situation. The diode choice thus narrowed to types like HPA 5082-3304 and the UM 7000 series, and excluded types like MA-47084. The fact that package capacitance forms a large part of the diode capacitance in HPA diodes but not in Unitrode could seem to be a detracting factor for the former in the present application. Roughly, a parallel combination of three of the HPA diodes (biased at 0.5 A) would be equivalent to two of the Unitrode diodes (biased at 1.2 A each) with regard to R_s/n and R_p/n, while C_2 could be about half except for the influence of the supporting structure. In the final choice, however, the rate of deterioration of diode performance at higher RF power levels, and the availability of higher voltage ratings and of a more convenient package design, strongly favored the UM 7000 C series. [Parameters for this series are $C_d = 0.9$ pF; $R_s = 0.8$ ohm at 0.1 A bias or 0.23 ohm at 1.2 A bias; $R_p \approx 30$ to 60 kilohms (quoted as minimum) at appropriate frequency and bias voltage,* but experimentally, and fortunately, found to be about 280 kilohms.]

Lastly, intermodulation distortion (IMD) was to be considered. Presumably, diode differences in this regard could be due to different

---

*Application Note MW-70-1, Unitrode Corporation, Watertown, Mass. 02172 (1970).

doping levels and profiles in the semiconductor.* RADC has indicated the order of preference to be Microwave Associates, Unitrode, and HPA. These observations were made with the diodes in a 50-ohm line, rather than in a filter structure. Therefore, it is felt that these data require normalization relative to some diode parameter (or combination of parameters) that affects the impedance level in the filter or the number of diodes to be paralleled per iris. After the filter design was optimized for each diode type, the ranking with regard to IMD might well be different. (Incidentally, it can be shown that combining diodes in "antiparallel" or "back-to-back" combinations is of no avail in reducing third-order intermodulation products.)

As for the number of UM 7000-C series diodes to be paralleled for each iris half of the type shown in Figure III-7, it was noted from experiments with "dummy" diodes (i.e., brass studs simulating forward-biased diodes and having comparable inductance but negligible R_s) that a minimum of three switches is needed to render the inductive and loss effects of RF-current crowding negligible. However, it was noted that the values of $R_p/6$ and $R_s/6$ would then be such that Q_{ub} would be too low relative to Q_{ua}, and the consequent unbalance across the tuning band (where combinations of irises with reverse-biased and forward-biased diodes are generally the case) would be disadvantageous. It was therefore decided to use only two diodes per iris half, and tolerate some added inductance and loss due to crowding, in order to avoid having $Q_{ua} > Q_{ub}$. One diode was considered sufficient for a fine-tuning iris.

---

*For example, some association of lower R_p with lower IMD has been noted in a survey of diode data. Both factors could well reflect higher I-layer conductivity under reverse bias. In any case, their association is unfortunate.

C. Bias Chokes

A tedious concomitant of using PIN diodes in a filter structure is the need to bring bias leads into the RF region without degrading RF performance. Early in the project, anticipating that diodes would be used in pairs, it was decided to use the biasing arrangement of Figure III-8(a), where the diodes are in series for biasing purposes, but in parallel for RF purposes. The first effect then noticed was that the residual reactance contributed by the bypass capacitor in series with its associated diode creates an imbalance in the division of RF current between the two diodes and an increase in loss due to crowding.

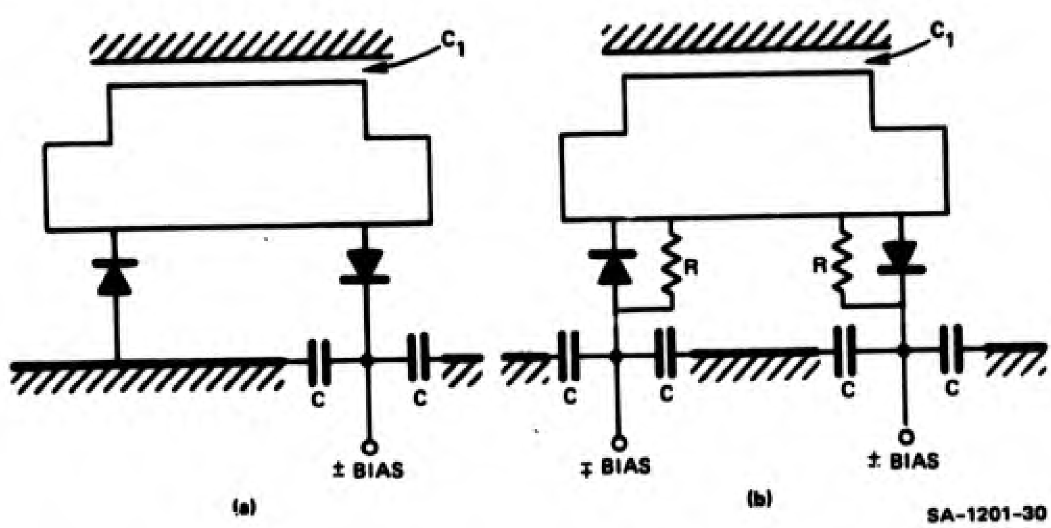

FIGURE III-8 PROPOSED BIASING IN SERIES OF AN EVEN NUMBER OF PIN DIODES PER IRIS HALF; (a) NOT RECOMMENDED, (b) RECOMMENDED

A second observation was that the effective series resistance of the bypass capacitor could not be neglected for the various commercially available ceramic capacitors suitable for the UHF band, although a large variation in capacitor Q may be encountered. After much experimentation, including the preparation of anodized-sleeve capacitors and sputtered-film capacitors, it was concluded that (with sufficient diligence) high-Q capacitors could be procured having losses small compared with those of available PIN diodes but not compared with those of a superior diode capable of yielding the desired $Q_u \sim 5000$.

Lastly, a third observation made with the arrangement of Figure III-8(a) was that, following application of full reverse bias, it takes some tens of seconds for Q_u to reach its final value. It appears that it is necessary here to charge C_1 through the dc leakage resistance ($\sim 10^{12}$ ohms) of one reverse-biased diode before bias voltage exists across the second diode. To remedy these problems (including unequal division of reverse-bias voltage), it appears that the only way to carry out the original biasing scheme is in the form shown in Figure III-8(b), where complete symmetry is observed. Ideally, the "bleeder" resistors, R, should have a dc resistance that is much less than their RF resistance, which should in turn be large compared with R_p.

As an alternative, it was decided to change over to the bias-choke arrangement shown in three places in Figure III-7. Here, the diodes are biased in parallel, and despite some dire predictions, no instability in the partition of bias current has been observed. Apparently, although the rate of change of R_s with bias current is negative, the reverse is true of the dc resistance (at least for the diodes and heat sinking chosen) and instabilities do not occur. Additional advantages are that n can now be odd as well as even, that diodes need not be ordered with two polarities relative to heat sink, and that heat sinking cannot be interfered with by bypass capacitors.*

---

*It is possible that in a microwave version of the filter, a coaxial stub would replace the helix, or that the biasing scheme of Figure III-8 would now be preferred.

The usefulness of the bias chokes shown is due to their being resonant within the relatively narrow tuning range (~ 20%) of the filter. Consequently, the susceptance and admittance they place across the outer gaps (S_2 or S_2') is very small compared with $2\pi fC_2$ and n/R_p, respectively. If Q_u', Z_0', and ℓ_1 are the parameters of the helical transmission line,

$$\mathrm{Re}[Y_{in}] \approx \frac{1 + \cot^2 (2\pi f\ell_1/c)}{4Q_u'Z_0'/\pi} \quad . \tag{III-1}$$

A consequence is that the shunting resistance due to the choke, R_p', is within 10% of $4Q_u'Z_0'/\pi$ over a 40% band.

Following the literature* on quarter-wave resonant helices, and adopting the recommended aspect ratios, the product $Q_u'Z_0'$ is found to be substantially independent of helix diameter even though Q_u' decreases and Z_0' increases as the diameter decreases. For copper wire and frequencies near 400 MHz, one predicts $R_p' \approx 335{,}000$ ohms.

The susceptance presented by the choke,

$$B' \approx - \cot (2\pi f\ell_1/c)/Z_0' \tag{III-2}$$

for $Q_u' > 10$ and $(2\pi f\ell_1/c) \rightarrow \pi/2$. Thus, it is advantageous to make Z_0' as large as possible by making the helix diameter as small as mechanical and thermal considerations will permit. A design based on 28 gauge copper wire (10 to 12 turns wound at 40 T.P.I. on a 3/16-inch rexolite sleeve) was therefore chosen. Since $Z_0' \approx 620$ ohms and $Q_u' \approx 400$, the

---

*W.W. Macalpine and R.O. Schildknecht, "Coaxial Resonators with Helical Inner Conductor," Proc. IRE, Vol. 47, p. 2099 (December 1959).

effect of a choke tuned to the center of a 20% band is to increase or decrease C_2 by about ±0.1 pF at the edges of the band. When the 14 chokes for Flauto I were tuned (by adjusting the number of turns), the chokes for Iris 1 were tuned to the center of the upper half of the tuning range because the diodes short this choke over the entire lower half. All other chokes were tuned to approximately the center of the tuning range. The possibilities of very finely "trimming" the effective C_2 capacitances of the final filter by modifying the tuning of the chokes (via a ceramic plug) were considered but not attempted.

To complete the discussion of the diode biasing arrangements, one must mention the dc breaks (between choke shield and filter wall) shown in Figure III-7. These breaks have very little effect on the circuit since they are located as close as possible to the high-impedance end of the choke such that the break is in series with the very high R'_p. However, to minimize any RF leakage due to the break, the gap contains thin mylar tape forming a bypass capacitance of at least 65 pF. Due to the way it is used, this capacitor can be of relatively very low quality compared with the bypass capacitors needed for the schemes of Figure III-8.

D. Coupling Loops

The installation of input and output coupling loops in the Flauto I resonator is shown in Figure III-6. The loops were formed by adding copper strips onto type-N connectors so as to minimize loop resistive losses. Loops were deemed preferable to E-field probes since the H-fields of the resonator are the less likely to change in distribution over the tuning range due to the switching in and out of capacitive irises. It appeared the most convenient to locate both loops at the same end of the resonator, but other arrangements should also be satisfactory, or even preferable, in the future.

For a rectangular loop in a resonant cavity of constant length, the external Q, Q_E, should be independent of frequency and, for a given longitudinal location, be determined by the ratio of loop self-inductance to the net mutual inductance between the center conductor of the coaxial line and the two portions of the loop that parallel it. (These two components of mutual inductance are of opposite sign.) Thus, Q_E should decrease with increasing loop area and proximity to the center conductor, but be substantially independent of the wire thickness (except for the effects of ohmic losses).

After completion of the resonator with the coarse-tuning irises, the areas of the loops were readily adjusted to give the desired insertion loss and VSWR (which established Q_E and Q_L, given Q_u--see Appendix A). It was not found necessary to readjust the loops after addition of the fine-tuning irises. The two loop areas were assumed to be equal. If one loop (in a filter with loss and with one direction of power flow) is made larger than the other, by design or as the result of accidental mechanical variation, and gives a slightly lower Q_E, it is advantageous for it to be used for the filter input.*

E. Performance

Diode biases appropriate for Flauto I are listed in Table III-2. Forward-bias currents greater than about 1.1 amps per diode produce no visible improvement in filter performance. Reverse-bias voltages greater than about 200 volts produce no visible change in resonant frequencies or Q, but are required for power handling and for minimizing IMD; the reverse bias for the diodes in Iris 1 should be as high as the

*L. Young, private communication.

diode PIV (peak inverse voltage) rating will allow. Forward or reverse biasing beyond that indicated for the less-significant irises produces no enhancement in filter performance.

Table III-2

DIODE BIASING RECOMMENDATIONS

	Iris No.	Diode Type	Number of Diodes	Forward-Bias Current, A	Current, A	Reverse-Bias Voltage, V
Coarse Tuning	1	UM7010C	4	1.13	4.5	1000
	2	UM7010C	4	1	4.0	700
	3	UM7006C	4	0.75	3.0	500
	4	UM7006C	4	0.5	2.0	350
	5	UM7006C	4	0.3	1.2	250
Fine Tuning	6	UM7006C	1	0.3	0.3	200
	7	UM7006C	1	0.3	0.3	200
	8	UM7006C	1	0.3	0.3	200
	9	UM7006C	1	0.3	0.3	200
Total			24		15.9	

Some representative bandpass-filter characteristics for Flauto I are shown in Figure III-9, as plotted by the HP network analyzer. The 32 responses shown are those obtained with the fine-tuning irises left out, hence only 5-digit codes are indicated, with "0" and "1" indicating reverse- and forward-biased diodes, respectively. Some idea of the minimal variations of insertion loss and 3-dB and 30-dB bandwidths across the tuning range may be obtained by inspection, and the freedom from spurious responses may be noted.

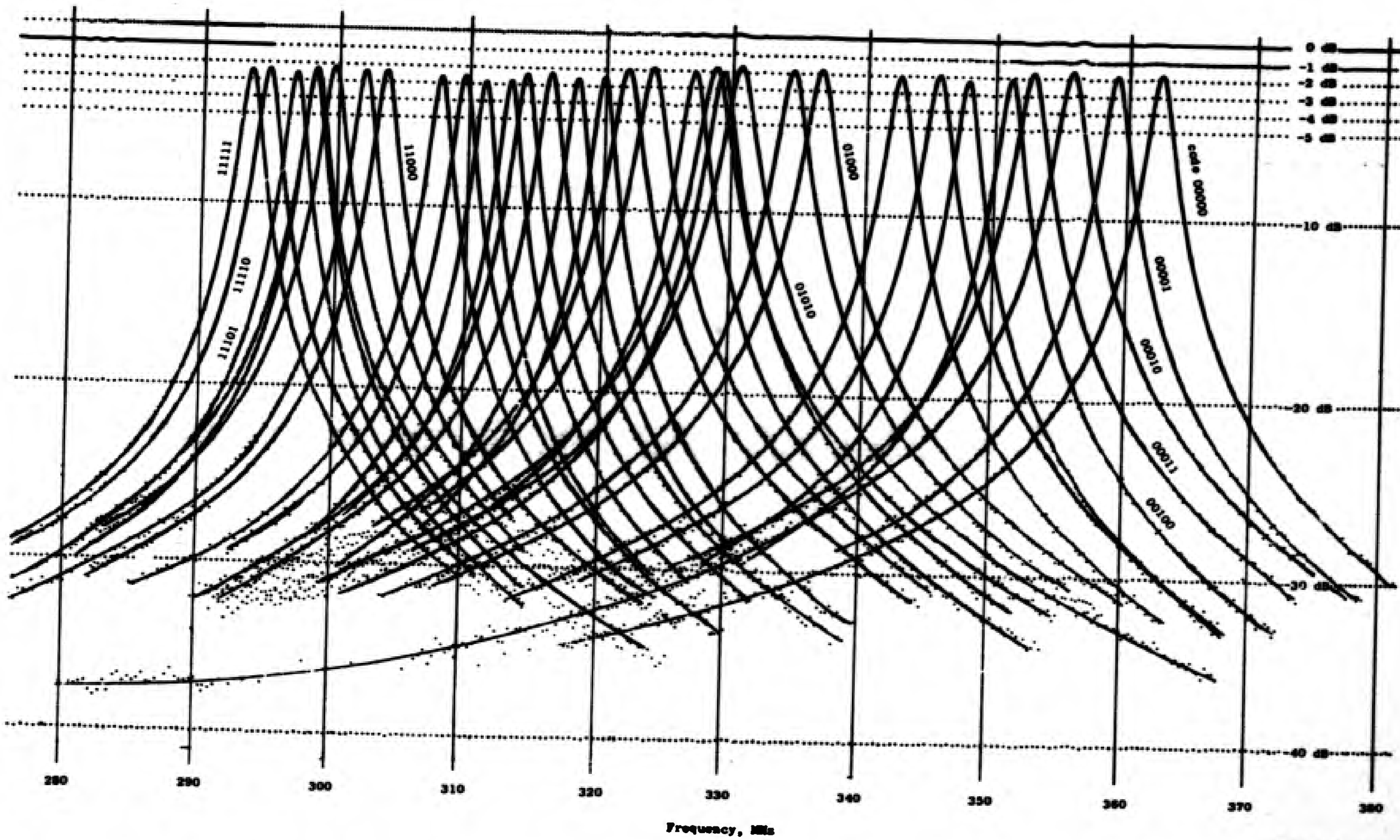

FIGURE III-9 BANDPASS-FILTER CHARACTERISTICS FOR THE 32 CHANNELS OF THE FIVE-IRIS FILTER OF FIGURE III-2

It is to be recalled that each of the five coarse-tuning irises is comprised of two halves that could be switched separately, if so desired (although the 1024 resulting resonances would definitely not cover the band uniformly). In general, asymmetrical iris switching results in RF current crowding that is very detrimental to the unloaded Q. When the switches are low-loss, such asymmetries must be avoided; however, in Flauto I, diode losses predominate, and so mask these asymmetry-crowding losses. Nevertheless, Flauto I was developed to be compatible with low-loss switches, whenever they become available, and the halves of the coarse-tuning irises are switched in unison.

To verify the performance of all 512 tuning channels of the nine-iris filter, automatic measurement methods were required. The hardware and software for doing this are described in full in Section V. Briefly, using the HP Network Analyzer and a special program, the computer sequences through a partial or complete list of codes and causes the appropriate diode biases to be applied. For each code, after phase-locking an RF oscillator to the resonance of the filter, frequency is counted and insertion loss automatically measured and recorded via teletypewriter (TTY) or punched tape. For spot-checking a few resonances and the tuning increment between them (or checking for insufficient biasing, as evidenced by excessive apparent insertion loss), the TTY output is the more convenient. For a complete filter-performance run, the punched tape is used. Three such runs can be completed in less than ten minutes. The second and third runs are made with the phase-locking arranged to obtain the frequencies for which the phase shift through the filter differs from that at resonance by $\pm 45^\circ$. Thus, bandwidth and other parameters can be computed by the CDC 6400, which subsequently processes the tape and its data.

Several formats are available for the results from the CDC 6400 page printer. Figure III-10 shows a typical page among several listing

CODE	DEAC	PHASE=-45 FREQ-MHZ	DIF-MHZ	LOSS-DB	PHASE=0 FREQ-MHZ	DIF-MHZ	LOSS-DB	PHASE=45 FREQ-MHZ	DIF-MHZ	LOSS-DB
001110000	112	338.87	.01	4.4	339.59	-.02	2.0	340.37	-.06	5.6
001110001	113	338.69	-.18	4.4	339.42	-.17	2.0	340.21	-.16	5.6
001110010	114	338.51	-.18	4.4	339.22	-.20	2.0	340.00	-.21	5.6
001110011	115	338.33	-.18	4.4	339.05	-.17	2.0	339.84	-.16	5.6
001110100	116	338.06	-.27	4.3	339.78	-.27	2.0	339.57	-.27	5.6
001110101	117	337.89	-.17	4.3	338.62	-.16	1.9	339.42	-.15	5.6
001110110	118	337.71	-.18	4.3	338.42	-.20	2.0	339.21	-.21	5.6
001110111	119	337.54	-.17	4.3	338.26	-.16	1.9	339.05	-.16	5.6
001111000	120	337.37	-.17	4.3	338.08	-.18	2.0	338.85	-.20	5.7
001111001	121	337.19	-.18	4.3	337.91	-.17	1.9	338.69	-.16	5.6
001111010	122	337.01	-.18	4.4	337.72	-.19	2.0	338.48	-.21	5.6
001111011	123	336.83	-.18	4.4	337.55	-.17	1.9	338.33	-.15	5.6
001111100	124	336.56	-.27	4.4	337.28	-.27	1.9	338.06	-.27	5.6
001111101	125	336.39	-.17	4.4	337.12	-.16	1.9	337.91	-.15	5.6
001111110	126	336.21	-.18	4.4	336.92	-.20	2.0	337.70	-.21	5.6
001111111	127	336.04	-.17	4.4	336.76	-.16	1.9	337.55	-.15	5.6
010000000	128	336.25	.21	4.1	337.06	.30	1.7	337.96	.41	5.3
010000001	129	335.97	-.28	4.1	336.79	-.27	1.7	337.71	-.25	5.2
010000010	130	335.87	-.10	4.1	336.67	-.12	1.7	337.57	-.14	5.3
010000011	131	335.59	-.28	4.1	336.41	-.26	1.7	337.32	-.25	5.3
010000100	132	335.58	-.01	4.1	336.39	-.02	1.7	337.30	-.02	5.3
010000101	133	335.31	-.27	4.1	336.14	-.25	1.6	337.05	-.25	5.2
010000110	134	335.20	-.11	4.1	336.01	-.13	1.7	336.90	-.15	5.2
010000111	135	334.93	-.27	4.1	335.76	-.25	1.6	336.65	-.25	5.2
010001000	136	334.77	-.16	4.1	335.58	-.18	1.7	336.45	-.20	5.2
010001001	137	334.50	-.27	4.1	335.31	-.27	1.6	336.20	-.25	5.2
010001010	138	334.39	-.11	4.2	335.19	-.12	1.7	336.06	-.14	5.2
010001011	139	334.11	-.28	4.2	334.93	-.26	1.6	335.81	-.25	5.2

SA-1201-32

FIGURE III-10 REPRESENTATIVE PAGE FROM CDC 6400 PRINTOUT LISTING FLAUTO I DATA MEASURED BY HP NETWORK ANALYZER "raw data." The CODE column refers to the biasing ("0" = reverse, "1" = forward) of the diodes in the nine irises in sequence, and DEBC refers to the decimal equivalent of this code taken as a binary number. The remaining columns list frequency and insertion loss corresponding to phase shifts through the filter of -45°, 0 (resonance), and $+45^{\circ}$, respectively. Frequency difference from the previous entry is also listed. Theoretically, the loss figures in Columns 5 and 11 should be 3 dB greater than those in Column 8. The errors in measuring loss should not exceed ±0.1 dB. The error in determining frequency--about ±50 kHz--is principally due to a $\pm 3^{\circ}$ tracking error in relating "resonance" to "zero phase shift" over the tuning range. (At resonance, there appears to be a residual phase shift of about 30° between the connectors, and this value fluctuates about $\pm 3^{\circ}$ as one moves over the tuning range.)

Figure III-11 is a sample page of processed data. The 512 channel center frequencies have been rearranged in ascending order (Column 2) and have been assigned channel numbers (CH) from 1 to 512. Frequency differences (tuning increments) are printed interlinearly in Column 2. CODE and DEBC indicate the biasing pattern required. Ideally, DEBC should run monotonically from 511 to 0, while CH runs from 1 to 512. However, when the four fine-tuning irises are involved, resonant frequency is not altogether a smooth function of DEBC, although it is when the coarse-tuning irises alone are used (codes $\delta\delta\delta\delta\delta$ 0000).* The next columns list, respectively, insertion loss, 3-dB bandwidth (actually, the bandwidth defined on the $\pm 45^{\circ}$ phase-shift basis) and loaded Q, external Q,† unloaded Q, and VSWR,† all computed from the relations given in Appendix A.

---

*The symbol δ may represent either 0 or 1, wherever it occurs.

†Assumed the same for both loops.

CH	FO-MHZ	CODE	DEBC	LOSS-DB	DF3-MHZ	UL	JE	QU	VSWR	F1-MHZ	DLOSS(-45)-DB	F2-MHZ	DLOSS(+45)-DB
141	307.35	101110011	371	2.4	1.31	235	621	961	1.6	306.69	2.7	308.00	3.2
	.12												
142	307.47	101110010	370	2.5	1.29	238	633	967	1.7	306.82	2.7	308.11	3.2
	.14												
143	307.61	101110001	369	2.4	1.31	235	621	962	1.6	306.94	2.7	308.25	3.2
	.12												
144	307.73	101110000	368	2.5	1.30	237	629	958	1.7	307.07	2.7	308.37	3.2
	.02												
145	307.75	101101111	367	2.3	1.33	231	600	1010	1.6	307.08	2.8	308.41	3.2
	.12												
146	307.87	101101110	366	2.3	1.32	233	607	1005	1.6	307.20	2.8	308.52	3.2
	.15												
147	308.02	101101101	365	2.3	1.34	230	597	998	1.6	307.33	2.8	308.67	3.2
	.11												
148	308.13	101101100	364	2.3	1.32	233	609	1001	1.6	307.46	2.8	308.78	3.2
	.23												
149	308.36	101101011	363	2.3	1.33	232	605	993	1.6	307.68	2.8	309.01	3.2
	.12												
150	308.48	101101010	362	2.3	1.31	235	617	997	1.6	307.82	2.8	309.13	3.2
	.11												
151	308.59	101100111	359	2.3	1.34	230	601	986	1.6	307.91	2.8	309.25	3.1
	.03												
152	308.62	101101001	361	2.3	1.33	232	606	990	1.6	307.94	2.8	309.27	3.1
	.09												
153	308.71	101100110	358	2.3	1.32	234	613	989	1.6	308.04	2.8	309.36	3.1
	.03												
154	308.74	101011111	351	2.5	1.23	251	676	1003	1.7	308.10	2.8	309.33	3.1
	.01												
155	308.75	101101000	360	2.4	1.31	236	618	994	1.6	308.08	2.8	309.39	3.2
	.11												
156	308.86	101100101	357	2.3	1.34	230	601	987	1.6	308.17	2.8	309.51	3.1
	.03												
157	308.89	101011110	350	2.5	1.21	255	684	1008	1.7	308.27	2.8	309.48	3.1
	.09												
158	308.98	101100100	356	2.3	1.32	234	613	991	1.6	308.30	2.8	309.62	3.1
	.02												
159	309.00	101011101	349	2.5	1.23	251	670	1006	1.7	308.37	2.9	309.60	3.1
	.16												
160	309.16	101011100	348	2.5	1.21	256	684	1010	1.7	308.53	2.9	309.74	3.1
	.04												
161	309.20	101100011	355	2.3	1.33	232	609	985	1.6	308.52	2.9	309.85	3.1
	.12												
162	309.32	101011011	347	2.5	1.22	254	679	999	1.7	308.69	2.9	309.91	3.1
	.01												
163	309.33	101100010	354	2.4	1.32	234	616	978	1.6	308.65	2.8	309.97	3.1
	.13												
164	309.46	101100001	353	2.4	1.33	233	610	979	1.6	308.78	2.9	310.11	3.1
	.02												
165	309.48	101011010	346	2.6	1.20	258	695	998	1.7	308.86	2.9	310.06	3.1
	.10												
166	309.58	101010111	343	2.5	1.24	250	670	981	1.7	308.94	2.9	310.18	3.1
	.01												
167	309.59	101100000	352	2.4	1.32	235	618	974	1.6	308.91	2.8	310.23	3.1
	0.00												
168	309.59	101011001	345	2.6	1.22	254	681	996	1.7	308.96	2.9	310.18	3.1
	.14												

SA-1201-33

FIGURE III-11 REPRESENTATIVE PAGE FROM CDC 6400 PRINTOUT LISTING COMPUTED FILTER PARAMETERS FOR FLAUTO I

Columns 11 and 13 list the frequencies that were ±45° away from resonance in terms of phase-shift and Columns 12 and 14 list the difference between the loss at these frequencies and that at resonance--ideally, 3 dB, but not so in practice, although the average for the two columns is always 3 dB.

Figure III-12 shows the beginning of a plot of insertion loss vs. frequency (rounded off to the nearest 100 kHz) made by the page printer (with additional tuning data included). The symbol I=X=I was used for a data point to suggest the rounding-off error in the loss. This plot has omitted some 18.5% of the tuning channels due to "redundancy." That is, when two channels were less than 100 kHz apart in frequency (after rounding off), the chosen program allowed only the channel having lower loss to be plotted. One function of this plot is to rapidly show whether any tuning increments are present that exceed the allowable.

A complete listing of tuning information in "fingering chart" form--channel number, center frequency, increment, and biasing code in binary and decimal forms--is given in Figure III-13.

Computed and measured filter parameters are plotted (by computer) versus frequency in Figures III-14 and III-15. Unloaded Q, Q_u, is seen to increase with frequency from about 900 to about 1500. The increase indicates that paired diodes under reverse bias (dominating the top of the band) introduce somewhat less effective loss than do paired diodes under forward bias (dominating the bottom of the band) for the resonator chosen--see Eqs. (II-4) and (II-5). Also, losses arising external to the diodes should also make Q_u decrease with decreasing frequency, although the contribution would be small. This variation in Q_u does not seem to be objectionable. Since the external Q, Q_E, has a general tendency to increase with decreasing frequency, the net effect is to make the bandwidth-determining loaded Q, Q_L, more nearly independent

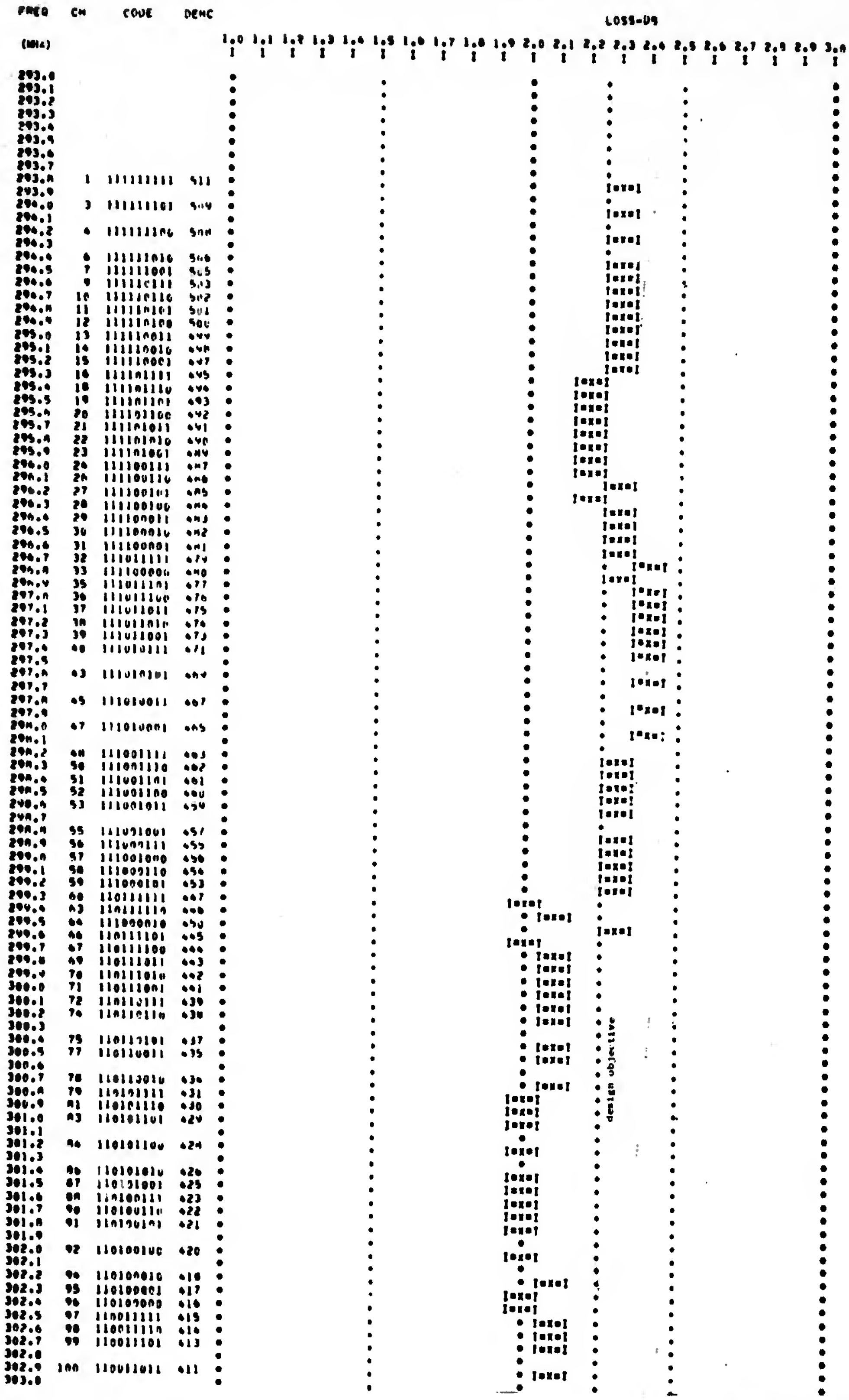

SA-1201-34

FIGURE III-12 LOW-END PORTION OF PLOT OF INSERTION LOSS vs. FREQUENCY FOR FLAUTO I BANDPASS FILTER, AS GENERATED BY CDC 6400 PAGE PRINTER. (Channels omitted are within 100 kHz of another channel having lower loss.)

CH	FO-MHZ	CODE	DEBC	CH	FO-MHZ	CODE	DEBC	CH	FO-MHZ	CODE	DEBC	CH	FO-MHZ	CODE	DEBC
1	293.84	111111111	511	29	296.43	111100011	483	57	298.97	111001000	456	85	301.23	110101011	427
	.11				.12				.12				.13		
2	293.95	111111110	510	30	296.55	111100010	482	58	299.09	111000110	454	86	301.36	110101010	426
	.10				.09				.07				.15		
3	294.05	111111101	509	31	296.64	111100001	481	59	299.16	111000101	453	87	301.51	110101001	425
	.11				.01				.14				.05		
4	294.16	111111100	508	32	296.65	111011111	479	60	299.30	110111111	447	88	301.56	110100111	423
	.08				.12				.02				.08		
5	294.24	111111011	507	33	296.77	111100000	480	61	299.32	111000100	452	89	301.64	110101000	424
	.12				.03				.04				.04		
6	294.36	111111010	506	34	296.80	111011110	478	62	299.36	111000011	451	90	301.68	110100110	422
	.09				.07				.06				.16		
7	294.45	111111001	505	35	296.87	111011101	477	63	299.42	110111110	446	91	301.84	110100101	421
	.12				.15				.10				.12		
8	294.57	111111000	504	36	297.02	111011100	476	64	299.52	111000010	450	92	301.96	110100100	420
	.01				.04				.06				.05		
9	294.58	111110111	503	37	297.06	111011011	475	65	299.58	111000001	449	93	302.01	110100011	419
	.11				.16				0.00				.14		
10	294.69	111110110	502	38	297.22	111011010	474	66	299.58	110111101	445	94	302.15	110100010	418
	.10				.06				.12				.15		
11	294.79	111110101	501	39	297.28	111011001	473	67	299.70	110111100	444	95	302.30	110100001	417
	.11				.13				.05				.13		
12	294.90	111110100	500	40	297.41	111010111	471	68	299.75	111000000	448	96	302.43	110100000	416
	.09				.03				0.00				.02		
13	294.99	111110011	499	41	297.44	111011000	472	69	299.75	110111011	443	97	302.45	110011111	415
	.12				.12				.13				.17		
14	295.11	111110010	498	42	297.56	111010110	470	70	299.88	110111010	442	98	302.62	110011110	414
	.09				.07				.14				.12		
15	295.20	111110001	497	43	297.63	111010101	469	71	300.02	110111001	441	99	302.74	110011101	413
	.06				.15				.06				.16		
16	295.26	111101111	495	44	297.78	111010100	468	72	300.08	110110111	439	100	302.90	110011011	411
	.06				.04				.07				.01		
17	295.32	111110000	496	45	297.82	111010011	467	73	300.15	110111000	440	101	302.91	110011100	412
	.05				.16				.05				.17		
18	295.37	111101110	494	46	297.98	111010010	466	74	300.20	110110110	438	102	303.08	110011010	410
	.10				.06				.15				.11		
19	295.47	111101101	493	47	298.04	111010001	465	75	300.35	110110101	437	103	303.19	110011001	409
	.12				.12				.13				.06		
20	295.59	111101100	492	48	298.16	111001111	463	76	300.48	110110100	436	104	303.25	110010111	407
	.09				.04				.04				.12		
21	295.68	111101011	491	49	298.20	111010000	464	77	300.52	110110011	435	105	303.37	110011000	408
	.12				.12				.13				.05		
22	295.80	111101010	490	50	298.32	111001110	462	78	300.65	110110010	434	106	303.42	110010110	406
	.09				.06				.12				.12		
23	295.89	111101001	489	51	298.38	111001101	461	79	300.77	110101111	431	107	303.54	110010101	405
	.12				.16				.03				.17		
24	296.01	111100111	487	52	298.54	111001100	460	80	300.80	110110001	433	108	303.71	110010100	404
	.01				.04				.10				0.00		
25	296.02	111101000	488	53	298.58	111001011	459	81	300.90	110101110	430	109	303.71	110010011	403
	.11				.17				.03				.18		
26	296.13	111100110	486	54	298.75	111001010	458	82	300.93	110110000	432	110	303.89	110010010	402
	.10				.06				.12				.11		
27	296.23	111100101	485	55	298.81	111001001	457	83	301.05	110101101	429	111	304.00	110010001	401
	.11				.12				.13				.02		
28	296.34	111100100	484	56	298.93	111000111	455	84	301.18	110101100	428	112	304.02	110001111	399
	.09				.04				.05				.16		

SA-1201-35(a)

FIGURE III-13 TUNING DATA FOR FLAUTO I BANDPASS FILTER

CH	FO-MHZ		CODE	DEMC	CH	FO-MHZ		CODE	DEMC	CH	FO-MHZ		CODE	DEMC	CH	FO-MHZ		CODE	DEMC
113	304.18	.01	110010000	400	141	307.35	.12	101110011	371	169	309.73	.02	101010110	342	197	313.51	.13	100111011	315
114	304.19	.12	110001110	398	142	307.47	.14	101110010	370	170	309.75	.10	101011000	344	198	313.64	.10	100111010	314
115	304.31	.17	110001101	397	143	307.61	.12	101110001	369	171	309.85	.15	101010101	341	199	313.74	.11	100110111	311
116	304.48	.01	110001011	395	144	307.73	.02	101110000	368	172	310.00	.17	101010100	340	200	313.85	.02	100111001	313
117	304.49	.17	110001100	396	145	307.75	.12	101101111	367	173	310.17	.16	101010011	339	201	313.87	.12	100110110	310
118	304.66	.12	110001010	394	146	307.87	.15	101101110	366	174	310.33	.11	101010010	338	202	313.99	.08	100111000	312
119	304.78	.05	110001001	393	147	308.02	.11	101101101	365	175	310.44	.16	101010001	337	203	314.07	.14	100110101	309
120	304.83	.13	110000111	391	148	308.13	.23	101101100	364	176	310.60	.06	101010000	336	204	314.21	.18	100110100	308
121	304.96	.04	110001000	392	149	308.36	.12	101101011	363	177	310.66	.16	101001111	335	205	314.39	.14	100110011	307
122	305.00	.13	110000110	390	150	308.48	.11	101101010	362	178	310.82	.11	101001110	334	206	314.53	.21	100110010	306
123	305.13	.17	110000101	389	151	308.59	.03	101100111	359	179	310.93	.16	101001101	333	207	314.74	0.00	100110001	305
124	305.30	0.00	110000100	388	152	308.62	.09	101101001	361	180	311.09	.18	101001100	332	208	314.74	.14	100101111	303
125	305.30	.18	110000011	387	153	308.71	.03	101100110	358	181	311.27	.16	101001011	331	209	314.88	0.00	100110000	304
126	305.48	.11	110000010	386	154	308.74	.01	101011111	351	182	311.43	.09	101001010	330	210	314.88	.21	100101110	302
127	305.59	.19	110000001	385	155	308.75	.11	101101000	360	183	311.52	.02	101000111	327	211	315.09	.13	100101101	301
128	305.78	.16	110000000	384	156	308.86	.03	101100101	357	184	311.54	.14	101001001	329	212	315.22	.20	100101100	300
129	305.94	.11	101111111	383	157	308.89	.09	101011110	350	185	311.68	.03	101000110	326	213	315.42	.14	100101011	299
130	306.05	.14	101111110	382	158	308.98	.02	101100100	356	186	311.71	.09	101001000	328	214	315.56	.08	100101010	298
131	306.19	.12	101111101	381	159	309.00	.16	101011101	349	187	311.80	.16	101000101	325	215	315.64	.12	100100111	295
132	306.31	.21	101111100	380	160	309.16	.04	101011100	348	188	311.96	.17	101000100	324	216	315.76	.01	100101001	297
133	306.52	.13	101111011	379	161	309.20	.12	101100011	355	189	312.13	.17	101000011	323	217	315.77	.14	100100110	294
134	306.65	.11	101111010	378	162	309.32	.01	101011011	347	190	312.30	.11	101000010	322	218	315.91	.08	100101000	296
135	306.76	.02	101110111	375	163	309.33	.13	101100010	354	191	312.41	.17	101000001	321	219	315.99	.07	100100101	293
136	306.78	.10	101111001	377	164	309.46	.02	101100001	353	192	312.58	.27	101000000	320	220	316.06	.06	100011111	287
137	306.88	.02	101110110	374	165	309.48	.10	101011010	346	193	312.85	.13	100111111	319	221	316.12	.12	100100100	292
138	306.90	.12	101111000	376	166	309.58	.01	101010111	343	194	312.98	.21	100111110	318	222	316.24	.08	100011110	286
139	307.02	.11	101110101	373	167	309.59	0.00	101100000	352	195	313.19	.13	100111101	317	223	316.32	.10	100100011	291
140	307.13	.22	101110100	372	168	309.59	.14	101011001	345	196	313.32	.19	100111100	316	224	316.42	.04	100011101	285

SA-1201-35(b)

FIGURE III-13 (Continued)

CH	FO-MHZ	CODE	DEBC	CH	FO-MHZ	CODE	DEBC	CH	FO-MHZ	CODE	DEBC	CH	FO-MHZ	CODE	DEBC
225	316.46	100100010	290	253	319.68	100000011	259	281	323.23	011100111	231	309	326.74	011001011	203
	.13				.19				.16				.22		
226	316.59	100011100	284	254	319.87	100000010	258	282	323.39	011100110	230	310	326.96	011001010	202
	.08				.05				.11				.07		
227	316.67	100100001	289	255	319.92	011111111	255	283	323.50	011100101	229	311	327.03	011001001	201
	.05				.13				.16				.23		
228	316.72	100011011	283	256	320.05	100000001	257	284	323.66	011100100	228	312	327.26	011001000	200
	.09				.02				.12				.07		
229	316.81	100100000	288	257	320.07	011111110	254	285	323.78	011100011	227	313	327.33	010111111	191
	.10				.12				.17				.17		
230	316.91	100011010	282	258	320.19	011111101	253	286	323.95	011100010	226	314	327.50	010111110	190
	.07				.05				.03				.04		
231	316.98	100010111	279	259	320.24	100000000	256	287	323.98	011011111	223	315	327.54	011000111	199
	.10				.10				.08				.13		
232	317.08	100011001	281	260	320.34	011111100	252	288	324.06	011100001	225	316	327.67	010111101	189
	.07				.11				.12				.09		
233	317.15	100010110	278	261	320.45	011111011	251	289	324.18	011011110	222	317	327.76	011000110	198
	.12				.16				.05				.08		
234	317.27	100011000	280	262	320.61	011111010	250	290	324.23	011100000	224	318	327.84	011000101	197
	.06				.11				.04				.01		
235	317.33	100010101	277	263	320.72	011111001	249	291	324.27	011011101	221	319	327.85	010111100	188
	.18				.16				.20				.08		
236	317.51	100010100	276	264	320.88	011111000	248	292	324.47	011011100	220	320	327.93	010111011	187
	.13				.32				.05				.13		
237	317.64	100010011	275	265	321.20	011110111	247	293	324.52	011011011	219	321	328.06	011000100	196
	.18				.15				.21				.05		
238	317.82	100010010	274	266	321.35	011110110	246	294	324.73	011011010	218	322	328.11	011000011	195
	.18				.12				.08				.01		
239	318.00	100010001	273	267	321.47	011110101	245	295	324.81	011011001	217	323	328.12	010111010	186
	.07				.15				.21				.16		
240	318.07	100001111	271	268	321.62	011110100	244	296	325.02	011011000	216	324	328.28	010111001	185
	.11				.11				.30				.06		
241	318.18	100010000	272	269	321.73	011110011	243	297	325.32	011010111	215	325	328.34	011000010	194
	.07				.17				.21				.07		
242	318.25	100001110	270	270	321.90	011110010	242	298	325.53	011010110	214	326	328.41	011000001	193
	.18				.02				.08				.05		
243	318.43	100001101	269	271	321.92	011101111	239	299	325.61	011010101	213	327	328.46	010111000	184
	.18				.09				.21				.18		
244	318.61	100001100	268	272	322.01	011110001	241	300	325.82	011010100	212	328	328.64	011000000	192
	.14				.07				.04				.05		
245	318.75	100001011	267	273	322.08	011101110	238	301	325.86	011010011	211	329	328.69	010110111	183
	.19				.09				.22				.18		
246	318.94	100001010	266	274	322.17	011110000	240	302	326.08	011010010	210	330	328.87	010110110	182
	.06				.02				.08				.17		
247	319.00	100000111	263	275	322.19	011101101	237	303	326.16	011010001	209	331	329.04	010110101	181
	.12				.16				.01				.18		
248	319.12	100001001	265	276	322.35	011101100	236	304	326.17	011001111	207	332	329.22	010110100	180
	.06				.12				.20				.08		
249	319.18	100000110	262	277	322.47	011101011	235	305	326.37	011010000	208	333	329.30	010110011	179
	.13				.17				.02				.02		
250	319.31	100001000	264	278	322.64	011101010	234	306	326.39	011001110	206	334	329.32	010101111	175
	.05				.11				.08				.17		
251	319.36	100000101	261	279	322.75	011101001	233	307	326.47	011001101	205	335	329.49	010110010	178
	.18				.16				.21				.01		
252	319.54	100000100	260	280	322.91	011101000	232	308	326.68	011001100	204	336	329.50	010101110	174
	.14				.32				.06				.15		

SA-1201-35(c)

FIGURE III-13 (Continued)

CH	F0-MHZ	CODE	DEBC
337	329.65	010110001	177
	.02		
338	329.67	010101101	173
	.17		
339	329.84	010110000	176
	.01		
340	329.85	010101100	172
	.09		
341	329.94	010101011	171
	.19		
342	330.13	010101010	170
	.16		
343	330.29	010101001	169
	.19		
344	330.48	010101000	168
	.22		
345	330.70	010100111	167
	.19		
346	330.89	010100110	166
	.16		
347	331.05	010100101	165
	.19		
348	331.24	010100100	164
	.09		
349	331.33	010100011	163
	.19		
350	331.52	010100010	162
	.16		
351	331.68	010100001	161
	.20		
352	331.88	010100000	160
	.21		
353	332.09	010011111	159
	.24		
354	332.33	010011110	158
	.13		
355	332.46	010011101	157
	.25		
356	332.71	010011100	156
	0.00		
357	332.71	010011011	155
	.25		
358	332.96	010011010	154
	.13		
359	333.09	010011001	153
	.25		
360	333.34	010011000	152
	.19		
361	333.53	010010111	151
	.24		
362	333.77	010010110	150
	.14		
363	333.91	010010101	149
	.25		
364	334.16	010010100	148
	0.00		

CH	F0-MHZ	CODE	DEBC
365	334.16	010010011	147
	.12		
366	334.28	010001111	143
	.14		
367	334.42	010010010	146
	.12		
368	334.54	010001110	142
	.01		
369	334.55	010010001	145
	.12		
370	334.67	010001101	141
	.13		
371	334.80	010010000	144
	.12		
372	334.92	010001100	140
	.01		
373	334.93	010001011	139
	.26		
374	335.19	010001010	138
	.12		
375	335.31	010001001	137
	.27		
376	335.58	010001000	136
	.18		
377	335.76	010000111	135
	.25		
378	336.01	010000110	134
	.13		
379	336.14	010000101	133
	.25		
380	336.39	010000100	132
	.02		
381	336.41	010000011	131
	.26		
382	336.67	010000010	130
	.09		
383	336.76	001111111	127
	.03		
384	336.79	010000001	129
	.13		
385	336.92	001111110	126
	.14		
386	337.06	010000000	128
	.06		
387	337.12	001111101	125
	.16		
388	337.28	001111100	124
	.27		
389	337.55	001111011	123
	.17		
390	337.72	001111010	122
	.19		
391	337.91	001111001	121
	.17		
392	338.08	001111000	120
	.18		

CH	F0-MHZ	CODE	DEBC
393	338.26	001110111	119
	.16		
394	338.42	001110110	118
	.20		
395	338.62	001110101	117
	.16		
396	338.78	001110100	116
	.27		
397	339.05	001110011	115
	.17		
398	339.22	001110010	114
	.20		
399	339.42	001110001	113
	.17		
400	339.59	001110000	112
	.02		
401	339.61	001101111	111
	.17		
402	339.78	001101110	110
	.20		
403	339.98	001101101	109
	.17		
404	340.15	001101100	108
	.29		
405	340.44	001101011	107
	.18		
406	340.62	001101010	106
	.19		
407	340.81	001101001	105
	.04		
408	340.85	001011111	95
	.14		
409	340.99	001101000	104
	.07		
410	341.06	001011110	94
	.10		
411	341.16	001100111	103
	.07		
412	341.23	001011101	93
	.10		
413	341.33	001100110	102
	.12		
414	341.45	001011100	92
	.08		
415	341.53	001100101	101
	.11		
416	341.64	001011011	91
	.07		
417	341.71	001100100	100
	.15		
418	341.86	001011010	90
	.14		
419	342.00	001100011	99
	.03		
420	342.03	001011001	89
	.15		

CH	F0-MHZ	CODE	DEBC
421	342.18	001100010	98
	.07		
422	342.25	001011000	88
	.13		
423	342.38	001100001	97
	.03		
424	342.41	001010111	87
	.15		
425	342.56	001100000	96
	.07		
426	342.63	001010110	86
	.17		
427	342.80	001010101	85
	.22		
428	343.02	001010100	84
	.19		
429	343.21	001010011	83
	.22		
430	343.43	001010010	82
	.17		
431	343.60	001010001	81
	.22		
432	343.82	001010000	80
	.15		
433	343.97	001001111	79
	.23		
434	344.20	001001110	78
	.17		
435	344.37	001001101	77
	.22		
436	344.59	001001100	76
	.22		
437	344.81	001001011	75
	.23		
438	345.04	001001010	74
	.17		
439	345.21	001001001	73
	.23		
440	345.44	001001000	72
	.16		
441	345.60	001000111	71
	.22		
442	345.82	001000110	70
	.18		
443	346.00	001000101	69
	.23		
444	346.23	001000100	68
	.21		
445	346.44	001000011	67
	.24		
446	346.68	001000010	66
	.17		
447	346.85	001000001	65
	.24		
448	347.09	001000000	64
	.13		

SA-1201-35(d)

FIGURE III-13 (Continued)

CH	FO-MHZ	CODE	DEBC
449	347.22	000111111	63
	.19		
450	347.41	000111110	62
	.28		
451	347.69	000111101	61
	.20		
452	347.89	000111100	60
	.27		
453	348.16	000111011	59
	.20		
454	348.36	000111010	58
	.28		
455	348.64	000111001	57
	.21		
456	348.85	000111000	56
	.05		
457	348.90	000110111	55
	.20		
458	349.10	000110110	54
	.28		
459	349.38	000110101	53
	.20		
460	349.58	000110100	52
	.27		
461	349.85	000110011	51
	.21		
462	350.06	000110010	50
	.06		
463	350.12	000101111	47
	.20		
464	350.32	000101110	46
	.02		
465	350.34	000110001	49
	.21		
466	350.55	000110000	48
	.05		
467	350.60	000101101	45
	.21		
468	350.81	000101100	44
	.30		
469	351.11	000101011	43
	.21		
470	351.32	000101010	42
	.26		
471	351.60	000101001	41
	.22		
472	351.82	000101000	40
	.03		
473	351.85	000100111	39
	.21		
474	352.06	000100110	38
	.25		
475	352.31	000011111	31
	.03		
476	352.34	000100101	37
	.21		

CH	FO-MHZ	CODE	DEBC
477	352.55	000100100	36
	.02		
478	352.57	000011110	30
	.26		
479	352.83	000011101	29
	.02		
480	352.85	000100011	35
	.22		
481	353.07	000100010	34
	.02		
482	353.09	000011100	28
	.18		
483	353.27	000011011	27
	.08		
484	353.35	000100001	33
	.19		
485	353.54	000011010	26
	.03		
486	353.57	000100000	32
	.23		
487	353.80	000011001	25
	.27		
488	354.07	000011000	24
	.02		
489	354.09	000010111	23
	.26		
490	354.35	000010110	22
	.27		
491	354.62	000010101	21
	.27		
492	354.89	000010100	20
	.17		
493	355.06	000010011	19
	.28		
494	355.34	000010010	18
	.19		
495	355.53	000001111	15
	.07		
496	355.60	000010001	17
	.21		
497	355.81	000001110	14
	.07		
498	355.88	000010000	16
	.18		
499	356.06	000001101	13
	.28		
500	356.34	000001100	12
	.21		
501	356.55	000001011	11
	.29		
502	356.84	000001010	10
	.25		
503	357.09	000001001	9
	.29		
504	357.38	000001000	8
	0.00		

CH	FO-MHZ	CODE	DEBC
505	357.38	000000111	7
	.28		
506	357.66	000000110	6
	.26		
507	357.92	000000101	5
	.29		
508	358.21	000000100	4
	.20		
509	358.41	000000011	3
	.30		
510	358.71	000000010	2
	.25		
511	358.96	000000001	1
	.29		
512	359.25	000000000	0

SA-1201-35(e)

FIGURE III-13 (Concluded)

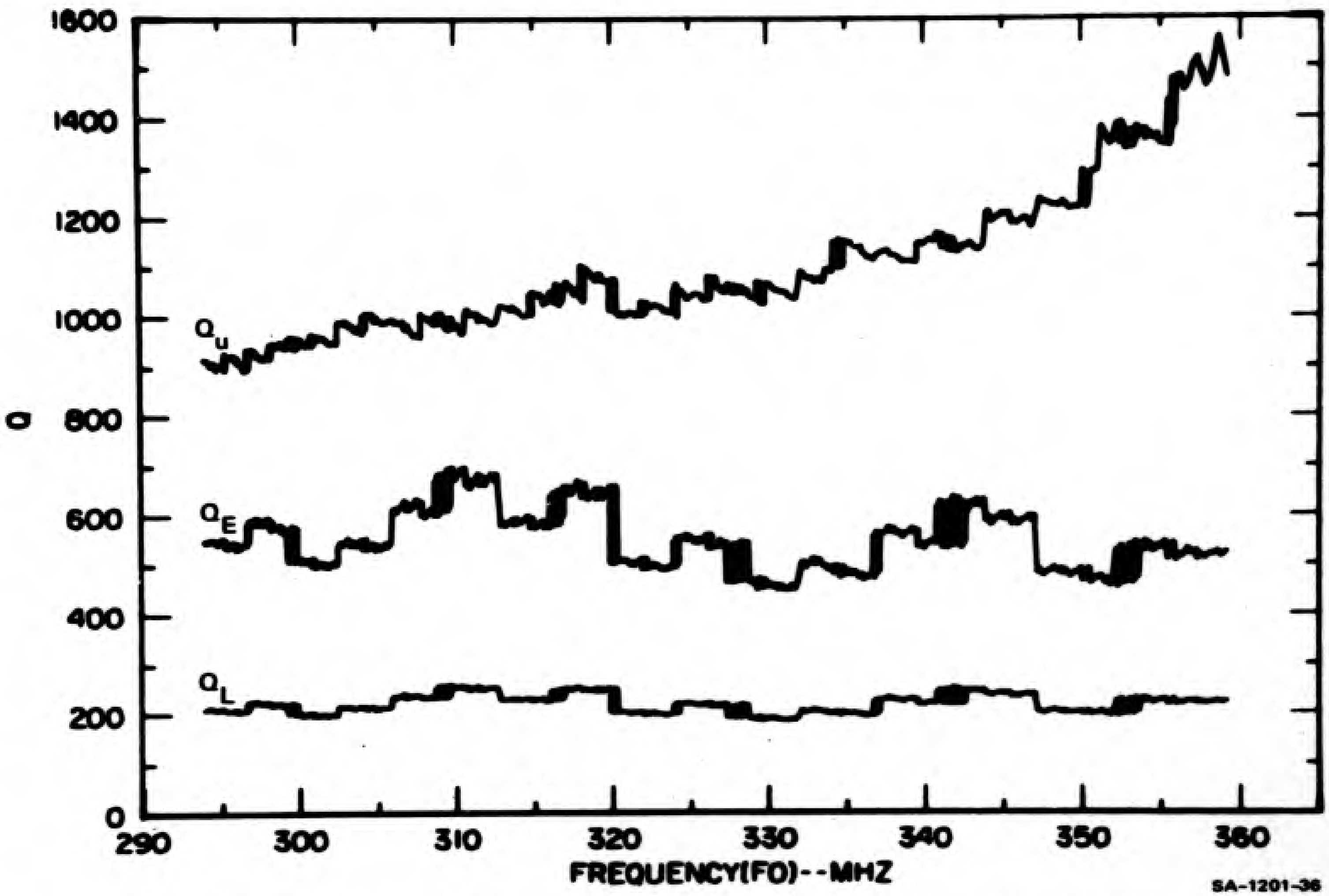

FIGURE III-14 COMPUTER PLOT OF PARAMETERS FOR FLAUTO I BANDPASS FILTER

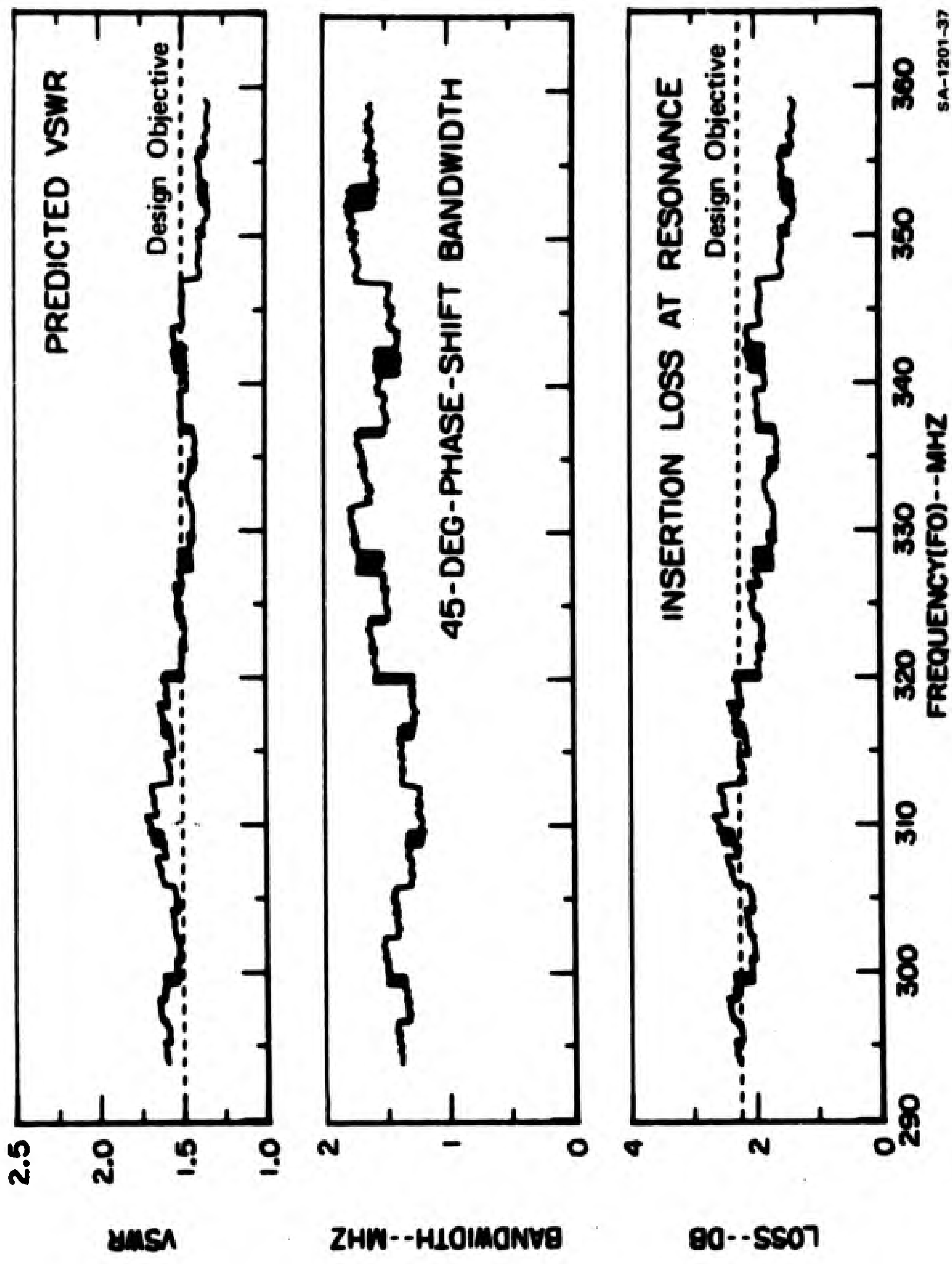

FIGURE III-15 COMPUTER PLOT OF PARAMETERS FOR FLAUTO I BANDPASS FILTER (Continued) of frequency. The apparent reason for Q_E, which is determined by the loop coupling, to rise at the lower frequencies is the shifting of RF fields away from the loops as more irises are switched from C_{min} to C_{max}. Indeed, whenever Iris 4 (the iris closest to the loops) is switched, Q_E makes a noticeable jump. (These jumps give the lower curves in Figure III-14 their stepped appearance.)

With regard to bandwidth and insertion loss, a general trend is observable for the former to rise while the latter falls, with increasing frequency, as the trend for Q_E would indicate. To level out this variation (if so desired), the effective loop area should be slightly decreased for the higher frequencies. This might possibly be realized with the aid of a compensating capacitance shunting the loop.

The VSWR data points in Figure III-15 were not measured, but were computed from the other parameters. Spot checks indicate these values are reliable since spurious sources of mismatch (e.g., connectors) can be neglected at the frequencies of interest.

F. Trimming of Irises

After the filter was assembled, it was found that the basic principle for the spatial distribution of equal irises had provided a remarkably uniform distribution of resonances across the tuning range. A method of appreciating this fact is to observe, for example, that the eight resonances corresponding to $\delta\delta\delta$ 100000 fall close to midway between the eight resonances corresponding to $\delta\delta\delta$ 000000. Similarly, the 16 resonances corresponding to $\delta\delta\delta\delta$ 10000 fall close to midway between the 16 resonances corresponding to $\delta\delta\delta\delta$ 00000, and so on. When the least-significant irises are introduced, however, some irregularities begin to occur. For example, the 128 resonances each of $\delta\delta\delta\delta\delta\delta\delta$ 10 and $\delta\delta\delta\delta\delta\delta\delta$ 00 show the desired relationship in most cases, or "on the average," but exceptions do occur. That is, two different binary words will sometimes yield substantially the same frequency (redundancy), or the curve of frequency vs. magnitude of the binary word will sometimes show a small backward overlap.

These effects are wasteful, but not detrimental. They were expected, and allowed for, since nine irises were provided even though eight irises should, ideally, be adequate for dividing the 66-MHz band into increments no greater than 300 kHz. What is undesirable is to find frequency increments greater than the allowable. For example, the frequency step encountered in going from 011111111 to 100000000 easily becomes excessive when the C_{max} of Iris 1 is too large by only a very small amount. (One is dealing with a small difference between two large and nearly equal quantities.) As a consequence, it is necessary to "trim" the C_{max} of each iris by a very small percentage after final assembly.

Ideally, continuously variable trimming (via Johanson screws, flexible diaphragms, etc.) would be desirable, but provision for this was not made in the breadboard model. Instead, trimming was accomplished by loosening and reassembling the irises with a selection of thin shims that allowed the S_1 and S_1' gaps to be slightly increased, although this technique was somewhat time-consuming. The procedure is to examine tuning increments at critical places in the band. For example, the critical places for an iris are 2^{i-1} in number and occur when digit i in the code changes from 0 to 1. After examining the preliminary list of resonances (obtained by the automatic measuring procedure) one notes where the iris in question causes the greatest tuning increment. If the increment is excessive, shims are inserted to reduce it, although redundancies and overlaps may now be introduced elsewhere in the band. In general, one should start with the trimming of the least-significant irises, but perform spot-checks continuously for all irises, since interaction between them does occur.

Trimming was deemed complete when, with the fewest and thinnest possible shims, no tuning increment exceeded the allowable increment, even though the number of redundancies and overlaps may not have been minimized. (Final measurements were taken at this time.) Actually, the trimming of the least-significant irises can be the more important in this regard. For example, if Iris 3 is inefficiently trimmed, only four redundancies or overlaps can, at worst, be introduced, whereas, if Iris 8 is inefficiently trimmed, as many as 128 redundancies or overlaps might be introduced. The thickened portions of the traces in Figures III-14 and III-15 indicate where most of the redundant or overlapped resonances occur for this filter.

Since only 220 channels are actually required to cover the 66-MHz range with 300 kHz increments, it would appear that 292 of the present 512 resonances are supernumerary and that the utilization efficiency is only 43%. On the other hand, 220 channels cannot be obtained with fewer than eight irises (and eight control bits), and since Flauto I has nine, only one unit out of nine is supernumerary, and the utilization efficiency would be 89%.

IV FLAUTO I: POWER HANDLING AND INTERMODULATION DISTORTION

A. Power Rating

The power ratings specified for the filter are 100 W peak and 20 W average. Diode currents and voltages at these input power levels were investigated analytically. The greatest magnitudes of RF diode current and voltage should occur in Iris 1 under forward bias (lowest-frequency tuning) and under reverse bias (highest-frequency tuning), respectively.

An equivalent circuit (neglecting the fine-tuning irises) for the forward-bias case (code 11111....) is shown in Figure IV-1. The 6.15-pF capacitance is the C_{max} of Iris 1. The 4.85-pF capacitance is the effective combined C_{max} of Irises 2 through 5, as required to give the resonance at 293 MHz. From the definition of loaded Q, one may write

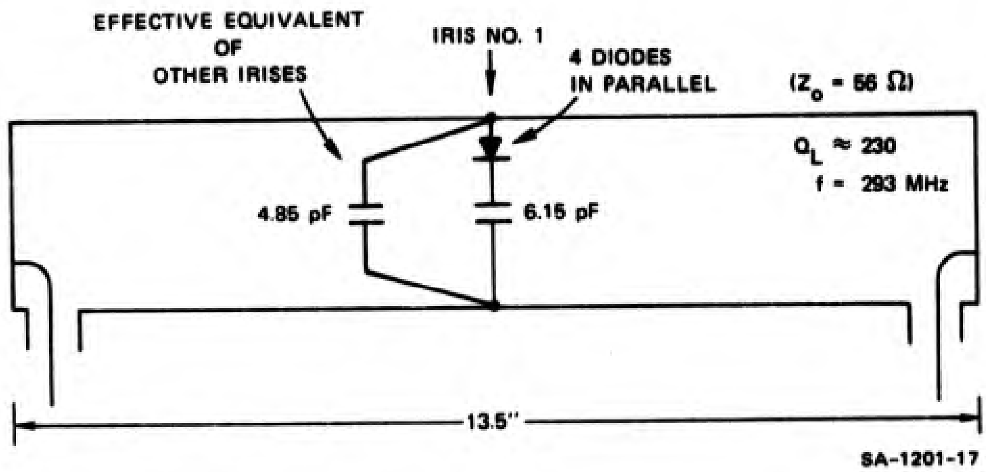

FIGURE IV-1 EQUIVALENT CIRCUIT OF FLAUTO I FILTER WITH ALL DIODES FORWARD-BIASED

$$Q_L = 2\pi f \frac{\text{energy stored}}{\text{power input}} \qquad \text{(IV-1)}$$

since the power input, P_0, must be the sum of the power delivered to the load and the power dissipated. Thus,

$$Q_L = \frac{2\pi f \cdot C\hat{V}^2/2}{P_0} \qquad \text{(IV-2)}$$

from which the peak voltage at the center of the resonator, $\hat{V}$, is

$$\hat{V} = \left(\frac{2Q_L P_0}{2\pi f C}\right)^{1/2} \qquad \text{(IV-3)}$$

where C is the total effective central capacitance. The peak current through the 6.15-pF capacitor is then $(2\pi f)(6.15)10^{-12}$ times $\hat{V}$, or 17 A when $P_0 = 100$ W, f = 293 MHz, C = 11 pF, and $Q_L \approx 230$.

Since the above current is divided among four diodes in parallel, the peak RF current per diode is about 4.3 A. Since a PIN diode having a carrier lifetime, $\tau \geq 1\ \mu s$ can carry a steady-state UHF current that is $2\pi f\tau$, or several thousand, times the forward-bias current, one may conclude that a peak power of 100 W is well within the "handling" capability of the forward-biased diodes in the Flauto I filter.

Under a duty cycle such that the average power is 20 W, the dissipation per diode would be

$$\frac{R_s}{2} (4.3)^2 \left(\frac{20}{100}\right) .$$

With $R_s \sim 0.25$ ohm, this dissipation would be well within the rating of UM 7000 C diodes (14 W) and actually somewhat less than the dissipation due to the bias current, which is about 1 W per diode (i.e., 1.12 A at about 1 V dc).

An equivalent circuit for the reverse-bias case (code 00000....) is shown in Figure IV-2. From $C_1 = C_{max} = 6.15$ pF, one must have

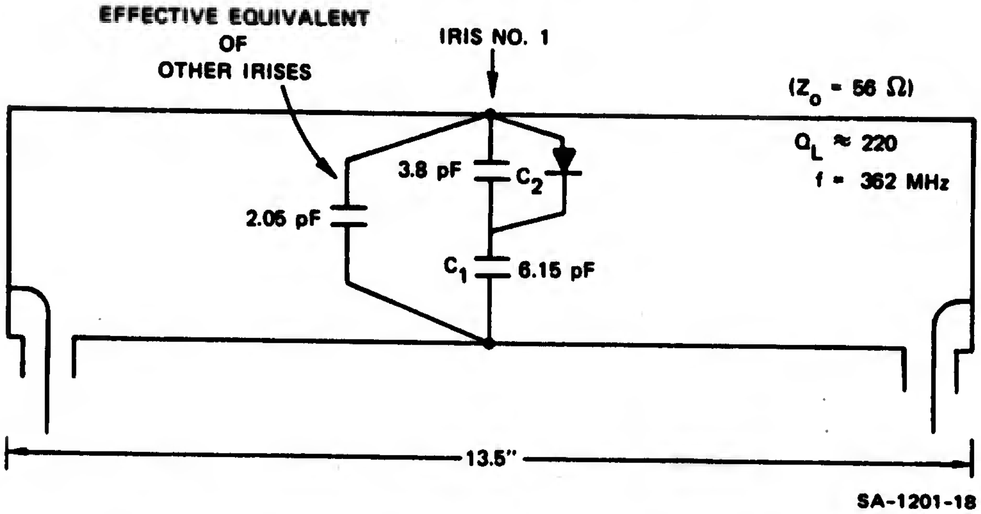

FIGURE IV-2 EQUIVALENT CIRCUIT OF FLAUTO I FILTER WITH ALL DIODES REVERSE-BIASED

$C_2 = 3.8$ pF to obtain $C_{min} = 2.35$ pF. The 2.05-pF capacitance must be the effective combined C_{min} of Irises 2 through 5, as required to give the resonance at 362 MHz. Using Eq. (IV-3), with $Q_L = 220$, f = 362 MHz, $P_0 = 100$ W, and C = 4.4 pF (the net central capacitance) one obtains

$$\hat{V} = 2100$$

as the total peak voltage at the center of the resonator. The fraction $C_2/C_1 + C_2$), or 800 V, appears across C_1, which is an air gap.* The remaining 1300 V appears across the back-biased diodes.

---

*For the forward-bias case, the peak RF voltage across the C_1 air gap is 1500 V--a larger value, and an indication that the metal there should be clean and free of sharp corners, etc.

According to the manufacturer, it is permissible for the instantaneous voltage on Unitrode PIN diodes to swing to about double the peak-inverse-voltage (PIV), or "breakdown" voltage, in the reverse direction, and also to some fraction of the PIV in the forward direction.* This possibility is a result of the RF period being small compared with the "turn-on" time of the diode. One may thus conclude that the Flauto I filter will handle a peak power of 100 W provided the diodes in Irises 1 and 2 have a PIV of 1000 V or more and are biased close to the PIV. This would require using UM 7010 C diodes in these irises. Theoretically, the RF voltage across the back-biased diodes in Iris 3 should be about half that for Iris 1, and for Iris 5, about one-fourth. Thus, diodes with lower PIV and less bias would be used for the "less-significant" irises. UM 7000 series diodes are available with PIV ratings of 1000, 800, 600, 400, and 200 V, and correspondingly lower prices. All have the same junction (same R_s, R_p, and C_d) and a junction breakdown voltage exceeding 1000 V; hence the PIV ratings are due only to different surface-leakage resistances. A surface-leakage resistance of the order of 10^7 ohms has no effect on the RF parameters since the RF resistance, R_p, shunting it is of the order of 10^5 ohms at UHF.

It should be noted that if it were possible to raise the loaded Q to 1000, to meet the original bandwidth specifications, all RF voltages in the filter would be about 2.2 times higher, and the diode selection and biasing problem would be quite serious unless peak input power levels were reduced. (While RF voltage swings peaking at two to five times the PIV or the bias voltage might not damage the diodes, they would very likely detune the filter and lower its Q.) Equation (IV-3)

---

*Application Note MW-70-1, Unitrode Corp., Watertown, Mass. 02172 (1970).

indicates that a substantial increase in the level of iris capacitance could lead to reduced diode voltages, but the corresponding decrease in Z_0 might not be feasible--e.g., from 56 ohms to 11 ohms.

B. Intermodulation Distortion

If two signals (whose frequencies are f_1 and f_2) simultaneously enter the filter, intermodulation distortion (IMD) will occur due to the presence of nonlinear elements in the filter. Assuming that care has been exercised in the construction to exclude metal/oxide interfaces that would constitute non-ohmic conducting paths, the IMD in Flauto I would be due to its PIN diode switches. If f_1 and f_2 are close to a passband, the third-order intermodulation products (IMPs) whose frequencies are $2f_1 - f_2$ and $2f_2 - f_1$, assuming $f_2 > f_1$, would also be near the passband and hence objectionable.

PIN diodes, with long carrier lifetimes, and heavily biased to the states of either maximum conduction or maximum insulation, where chosen as the solid-state devices generating the least IMD. However, objectionable IMD can be detected when, at high signal levels, RF current swings become comparable to $(2\pi f\tau)$ times the forward-bias current or when RF voltage swings become comparable to the reverse-bias voltage. The latter case is the one that applies in Flauto I and is due to a residual varactor effect, or a variation of diode capacitance with instantaneous junction voltage. It is evident that this effect would be at its worst in the reverse-biased diodes of Iris 1, and when f_1 and f_2 are both in-band, or very close to f_0, the filter resonance. The IMPs will then also be in-band and the most readily observable.

Equation (IV-3) indicates that the IMPs should be studied at the high end of the band (tuning code 00000...) where the contribution to C from the other irises is a minimum and Figure IV-2 remains the equivalent circuit. Using P_0 = 10 W (+40 dBm, the input-signal power specified for IMD evaluation) the peak RF voltage (calculated as before) would be 410 V across each diode, or 820 V peak-to-peak for each signal. Since this excursion is large relative to the bias voltage, one intuitively expects the varactor effects to be appreciable and the IMPs to be substantially greater than the desired -60 dBm (100 dB below signal level). This appears to have been confirmed experimentally, although the results suggest Flauto I could perform adequately where IMP specifications might be relaxed from 100 dB below signal to 65 dB below signal. Further theoretical speculations were not made, due to the difficulty of evaluating the effects of possible resonances in the system, at frequencies near $2f_1$ or $2f_2$, which strongly affect third-order IMPs. One such influence is the half-wave resonance of a bias choke.

Experimental observations were made (before addition of the fine-tuning irises) with the setup of Figure IV-3. The principal experimental problem is the masking of the filter IMPs by IMPs arising in the two lighthouse-triode transmitters (AIL type 124) due to residual coupling between them resulting from imperfect balance at the combining hybrid. Balancing the reflection coefficient of the filter under test with the 6-dB pad and sliding short was of some help, but the masking was still serious. The notch filters were then added. These have at least 45 dB (potentially infinite) insertion loss on resonance (when the loads are balanced) and about 2 dB off resonance (when they are highly unbalanced).* The high-Q resonators consist of large, welded aluminum, coaxial cylinders that have a quarter-wave resonance (with a few percent of capacitive tuning) and probe coupling that is overcoupled to give a 5:1 mismatch on resonance.

---

*The function of the notch filters could not be readily duplicated with bandpass filters nor with ferrite isolators.

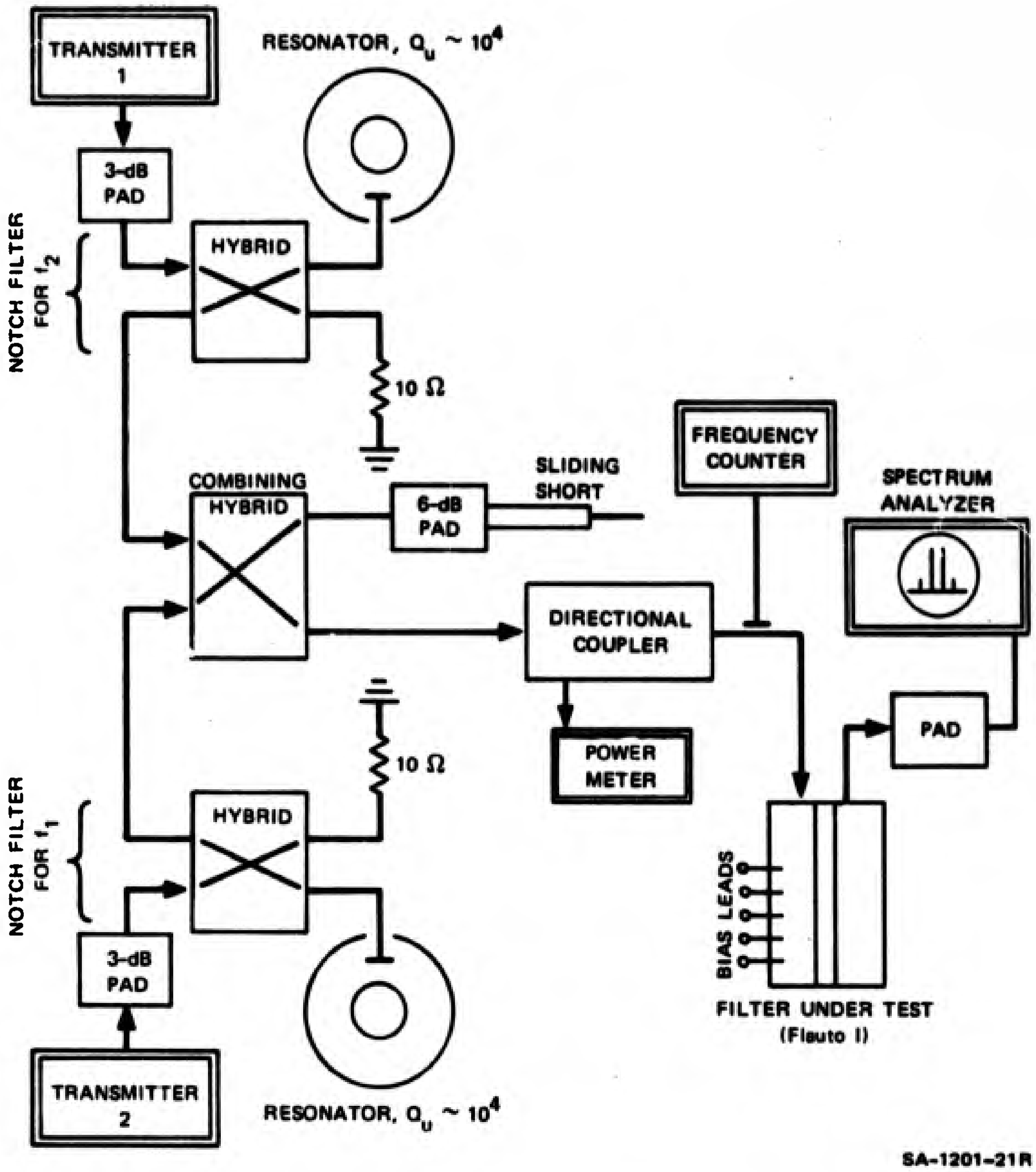

FIGURE IV-3 TEST SETUP FOR MEASURING INTERMODULATION DISTORTION IN UHF BANDPASS FILTER

The following frequencies were used:

f_0:	362.87 MHz
3-dB bandwidth:	1.63 MHz
(signal) f_1:	362.46 MHz
(signal) f_2:	363.06 MHz
(IMP) $2f_1 - f_2$:	361.86 MHz
(IMP) $2f_2 - f_1$:	363.66 MHz .

During a measurement, the notch filters are fine-tuned to minimize one or both IMPs. The remaining IMP amplitude is then assumed to be generated in the filter under test, especially if this amplitude is seen to vary with diode bias voltage.

Unfortunately, due to the notch-filter insertion loss and the 3-dB pads needed for buffering between them and the transmitters, only +30 and +34 dBm (average +32 dBm) of input power were available for filter inputs. (To increase these to +40 dBm, it should be possible to insert UHF power amplifiers ahead of the notch filters, and the isolation thus obtained for the transmitters would incidentally improve their stability.)

Using the above methods, the IMPs were observed to decrease as diode reverse-bias voltage was increased with the results as shown in Figure IV-4. It is seen that for the input-power levels stated, the lowest IMP level reached was -43 dBm at 500 V reverse bias. An increase in bias voltage to 1000 was planned, but the limited dynamic range of

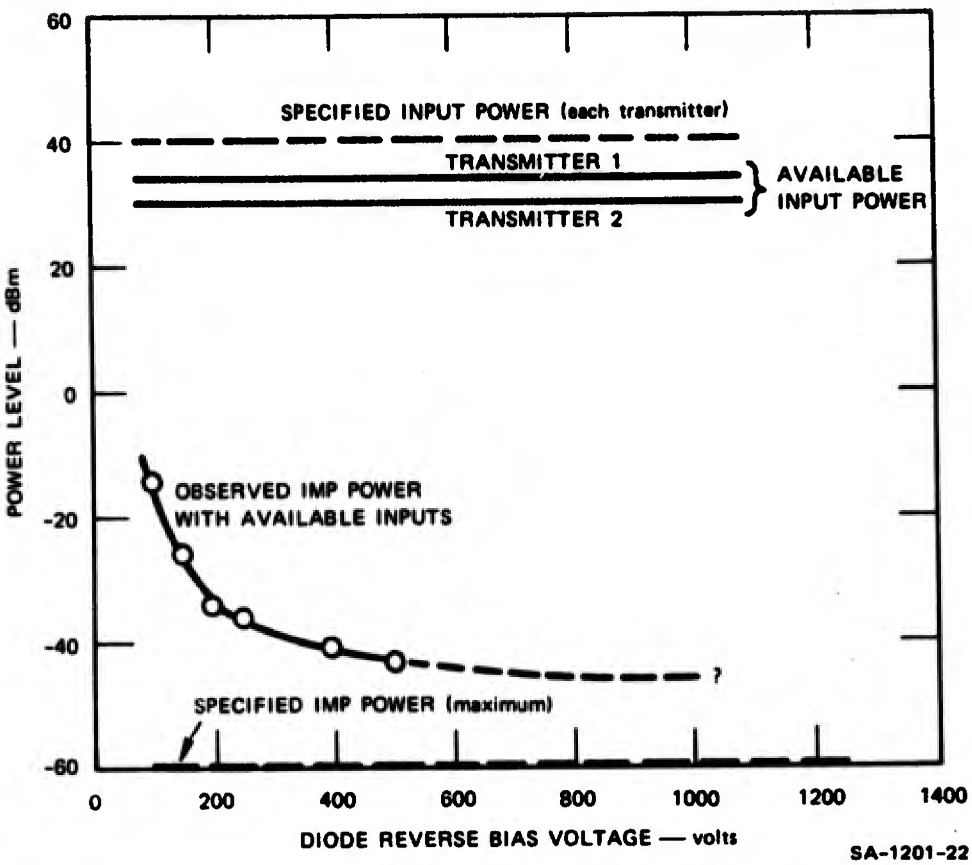

FIGURE IV-4 IMD DATA FOR FLAUTO I FILTER AT CHANNEL CODE 00000

the spectrum analyzer (HP Model 8551B/851B) would not then allow measurement of the lower IMP levels.*

Nevertheless, the data now on hand may be extrapolated to give an estimate of the IMD at +40 dBm input and 1000 V reverse diode bias. Since it appears that the IMP level is changing very slowly with bias voltage (beyond 400 V), it is likely that the IMPs would not be below

---

*The dynamic range of the spectrum analyzer could be increased by building notch filters for the transmitter frequencies and inserting them at the analyzer input. On the other hand, increasing transmitter power to +40 dBm might so increase the IMPs that the present dynamic range might be adequate.

-45 or -50 dBm at 1000 V. On the other hand, raising the input-power level by 8 dB (on the average) should cause a disproportionately larger rise in IMP level, in view of the RF voltage swings relative to the bias.* One may thus conclude that in-band IMP generation in Flauto I at rated RF input powers will be closer to the -20 or -25 dBm level (60 to 65 dB below input) than to the specified, desired, -60 dBm level (100 dB below input).

---

*The three-for-one law that generally applies for third-order IMPs would indicate a (roughly) 25-dB rise in IMP level.

V AUTOMATIC MULTICHANNEL-FILTER MEASUREMENT SYSTEM

This section is presented here because the novel measurement system described was used with the filter (Flauto I) discussed in the preceding two sections but not with the filter (Flauto II) discussed in the following section. Due to the large number of tuning channels, and the need to know minimum and maximum tuning increments and filter parameters over the entire tuning range as any one iris adjustment was made, the automatic system was essential to the completion of the project. Basically, the filter tuning is placed under computer control, with several operator-selected options.* At each tuning setting, phase-locking of a variable-frequency oscillator (VFO) establishes the channel center frequency and the frequencies for which the phase-shift increment is $\pm 45^{\circ}$. The network analyzer of which the VFO is a part measures insertion loss as well as the phase indications needed for the functions involving phase shift. The remainder of the system is concerned with data processing, including computation of parameters, compilation, tabulation, and display. Details are discussed on the following pages.

The system developed to automatically measure channel frequencies and associated insertion losses for the electronically tunable, high-power filter incorporates the Hewlett-Packard 8541A Automatic Network

---

*In a final system, computer control of tuning would be reduced to just a read only memory (REM) interposed between the "desired-frequency" input and the diode-biasing circuit control code. The REM program would be derived from Figure III-13. The desired-frequency command could actually be obtained from a transmitter-frequency counter rather than from an operator, although other means for tracking filter and transmitter are possible.

Analyzer* and the necessary hardware to interface the multichannel filter to the network analyzer's digital computer. Because of the limited memory available in this computer and because of the relatively slow speed at which its teleprinter operates, channel tuning code, frequency, and insertion-loss data were recorded on the network analyzer high-speed paper punch and subsequently processed by a CDC 6400 digital computer owned by the Institute. This section describes both the hardware and software aspects of the automatic measurement system.

A. Hardware for the Automated Measurement System

A block diagram of the measurement system used to automatically obtain filter-frequency and insertion-loss data is shown in Figure V-1. In addition to the computer, which acts as the measurement-system controller, the HP automatic network analyzer provides the RF signal source, and the microwave vector voltmeter that measures the amplitude ratio of, and the phase difference between, the filter RF input and output signals. The frequency of a sampled portion of the input signal to the filter is measured by means of a Systron-Donner, Model 7015 frequency counter.

The computer, through appropriate input/output (I/O) interface cards located within the computer itself, sets the frequency of the RF signal source, electronically tunes the filter, and commands both the vector voltmeter and frequency counter to measure, and then reads the results. The computer interface cards necessary to control both the RF signal source and vector voltmeter are part of the standard equipment supplied with the network analyzer and will not be discussed here. A general-purpose microcircuit interface card† was used to interface

---

*A description of the automatic network analyzer appears in Appendix B.

†This card is very similar to the Hewlett-Packard Interface Card, Model 12566A.

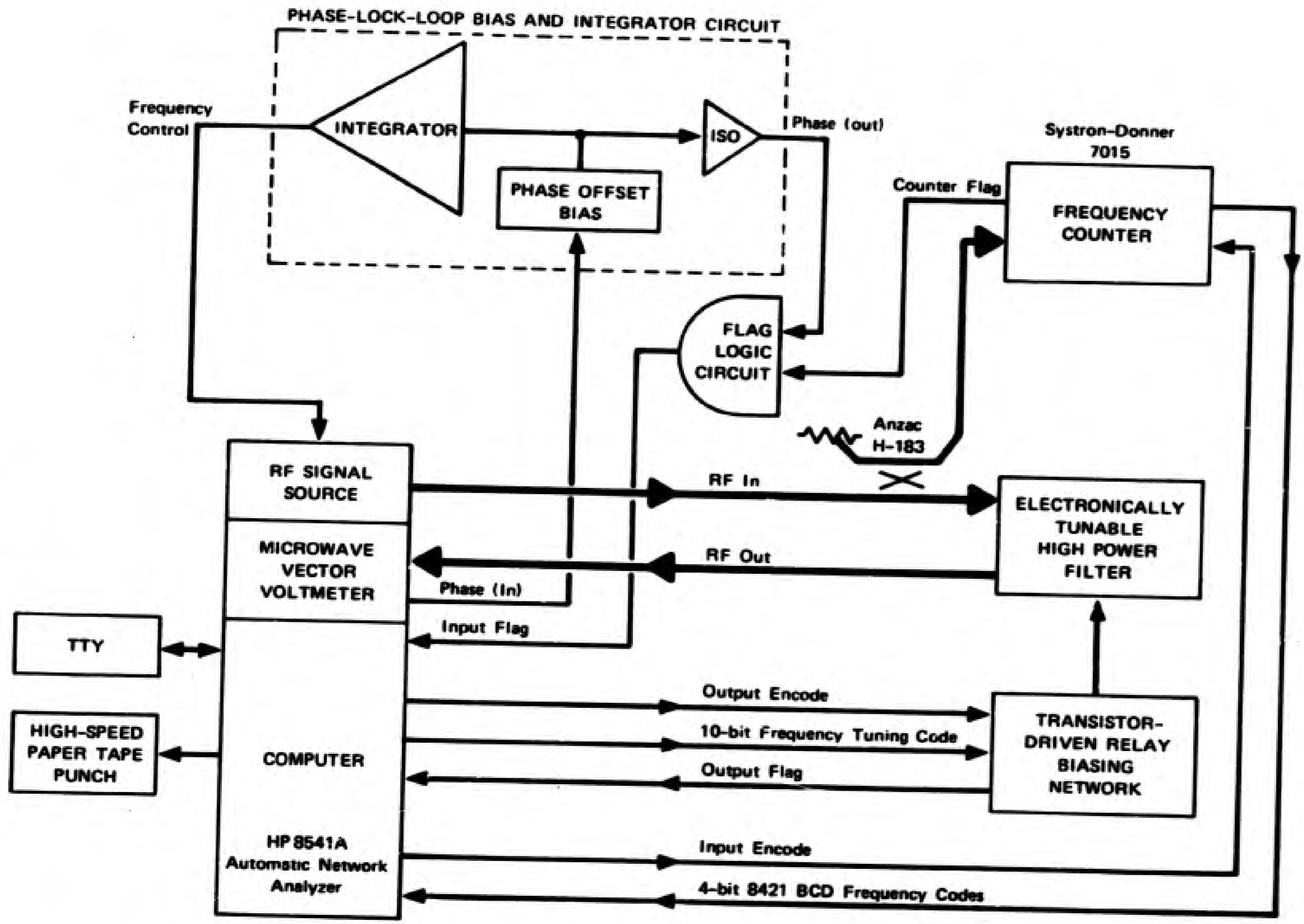

SA-1201-38

FIGURE V-1 AUTOMATED MEASUREMENT SYSTEM

the frequency counter and the filter to the computer. This card permits bidirectional interfacing to external I/O devices of TTL* compatible ground-true logic-level signals, and includes two independent 16-bit data registers (one for output and the other for input). In addition, the microcircuit interface card provides a positive-true encode signal which is used to command an external I/O device to begin its read or write operation, and accepts a ground-true flag signal generated by the external device to indicate the end of a read or write operation. Other standard computer interface cards connect the teletype machine (TTY) and the paper punch to the computer. The teletype machine provides user communication with the computer, and the punch is used to record the data obtained by the measurement system.

Additional interfacing is required between the microcircuit interface card and the high-power filter (see Figure V-1). This interfacing consists of heavy-duty relays† (P&B, Type PR5DY, SPDT, 25 A) required to switch the high-back-bias voltage across the filter diodes, and relay transistor-driver circuitry. Appropriate indicator devices are also included. Since ten or fewer irises were to be used to tune the filter, the relay biasing network was made up of ten identical relays and relay transistor-driver circuits as shown in Figure V-2. The transistors shown in the figure act as switches; a logic signal of +5 V from the computer causes the transistor to conduct, thus energizing its associated relay; during the other logic state (0 V), the transistor is cut off and its relay is deenergized. With the relay in its deenergized state, a

---

*Transistor-transistor logic.

†It is likely that solid-state circuits could eventually be devised to replace the mechanical relays used here for convenience.

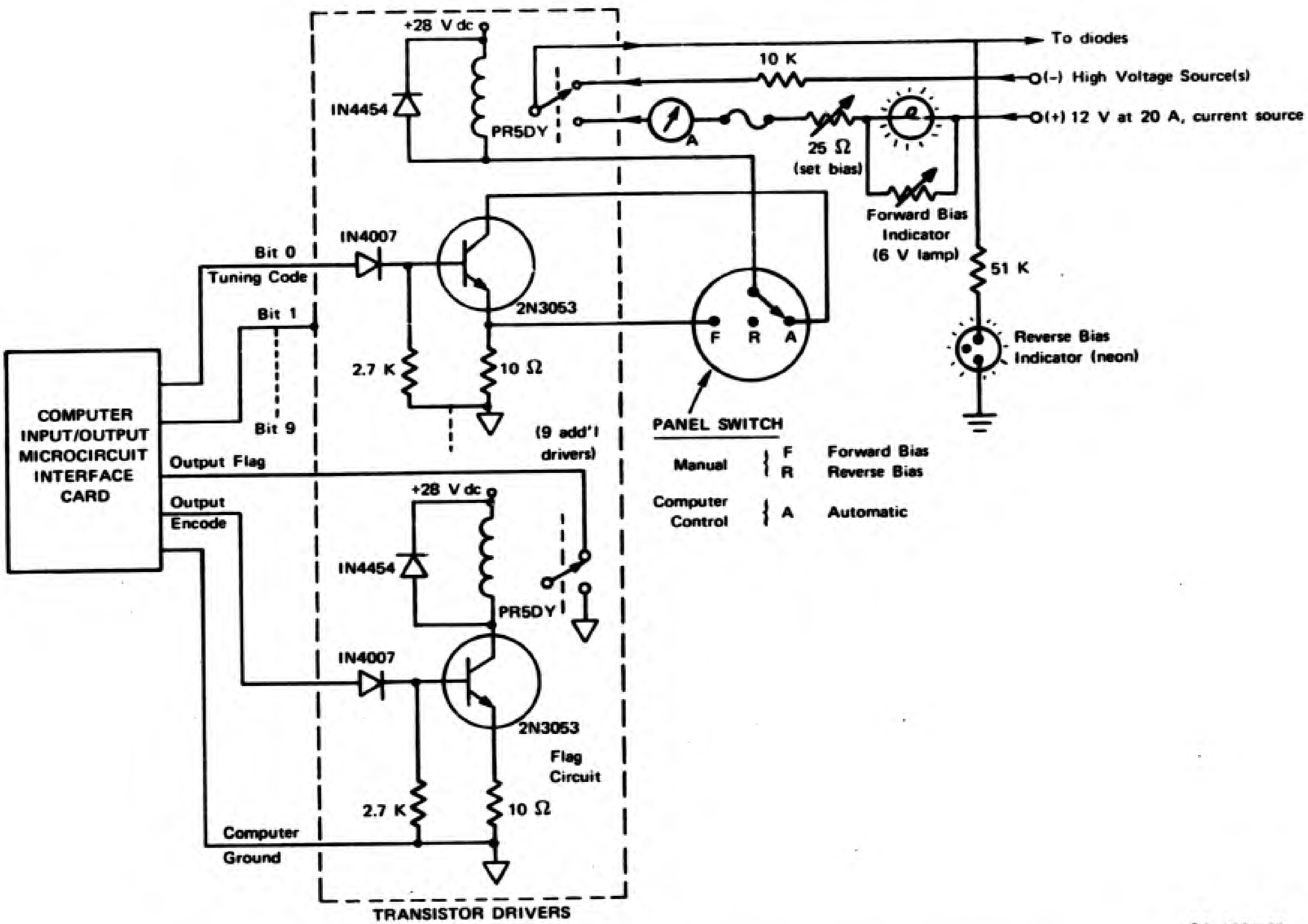

FIGURE V-2 TRANSISTOR-DRIVEN-RELAY BIASING CIRCUIT FOR EACH IRIS back-bias voltage is applied to the filter diode; when the relay is energized, a forward-bias current is applied. Both manual and automatic control of the diode bias is available through a front-panel switch as shown in Figure V-2. The eleventh transistor and relay combination make up the output-flag circuit. This circuit is necessary because the microcircuit interface card requires a flag after an output operation. The output encode signal, not necessary in this case to start the relay biasing network read operation (the network is continuously reading), is used to energize the flag circuit. Since the computer program will not continue after an output operation until receipt of the output flag, the program is delayed during the time (approximately 20 ms) that it takes the relay contacts to close. However, an additional delay is provided in the software to allow for the settling time of the relay switches.

The resonant frequency of the filter for any tuning code is established by means of a phase-lock loop controlling the RF signal source, as shown in Figure V-1. The phase-lock loop consists essentially of the microwave vector voltmeter (acting as a phase detector in this case), which produces a dc voltage proportional to measured phase, and an integrating amplifier shown in Figure V-3. The output of the integrating amplifier is a dc frequency-control (or error) voltage that remains constant as long as the input signal to the amplifier is zero. When the network-analyzer transmission reference plane is adjusted so that the vector voltmeter measures the phase difference between the signals at the input and output ports of the filter, the phase offset control on the vector voltmeter may be adjusted so that this input signal to the integrating amplifier will always be zero at filter resonance. This procedure is valid because the total phase shift through the filter is very nearly the same for all resonant (channel) frequencies. When the off-resonance condition exists, a dc voltage

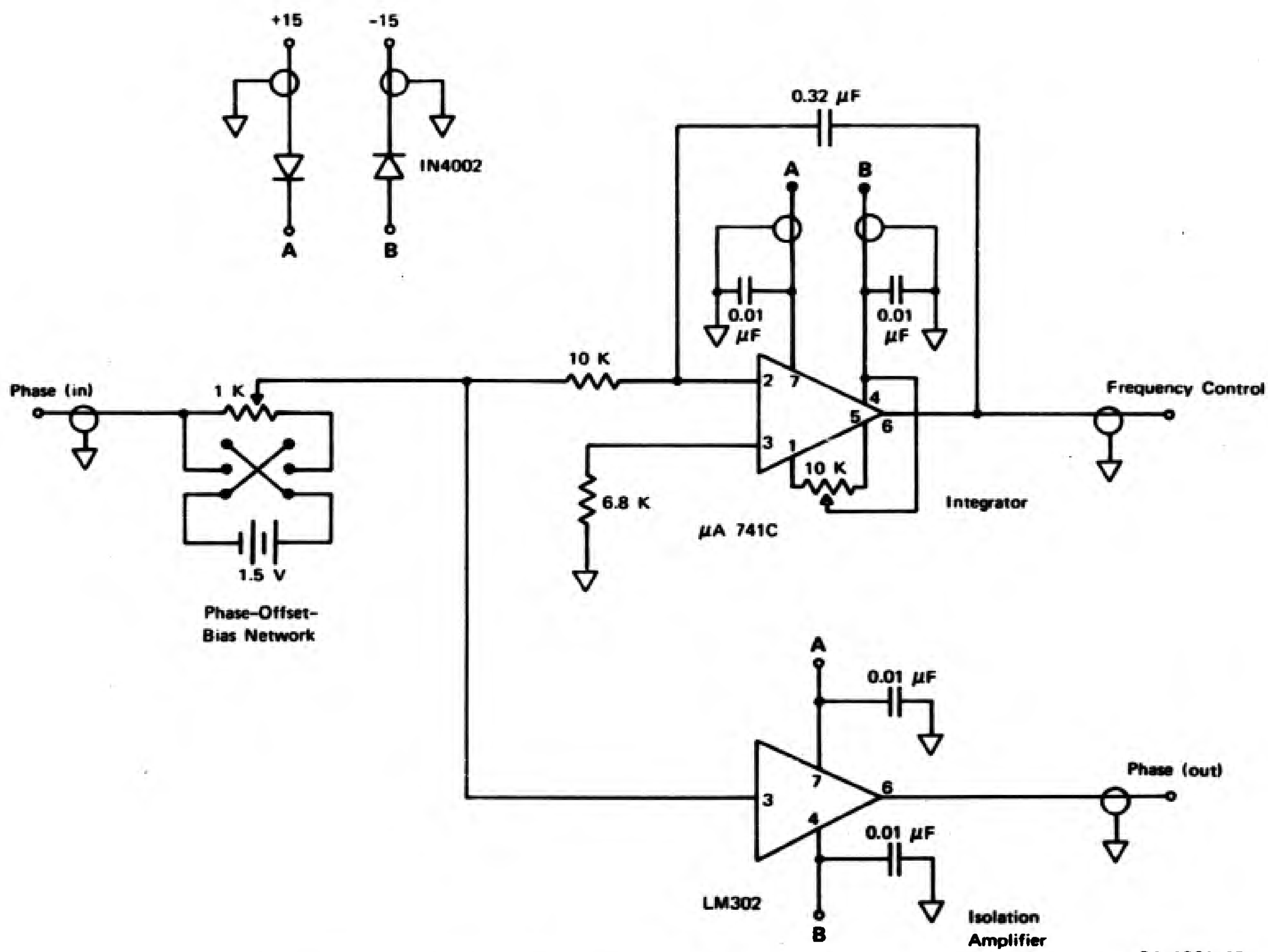

FIGURE V-3 PHASE-LOCK-LOOP BIAS AND INTEGRATOR CIRCUIT from the vector voltmeter [labeled "Phase (In)" in Figure V-1], proportional to the measured phase through the filter plus the phase offset, is generated and fed to the phase-lock-loop bias and integrator circuit. This voltage produces a changing frequency-control voltage to the RF signal source until the resonant frequency of the filter is obtained; at resonance the vector voltmeter voltage goes to zero and, as indicated above, the frequency-control voltage remains constant.

An additional phase-offset-bias network, shown in Figure V-3, was added in order that the 3-dB bandwidth at each resonant frequency of the filter could be measured. At the lower 3-dB bandedge frequency, the phase shift through the filter is $+45^{\circ}$ (theoretically) and at the upper bandedge frequency, -45°. Thus, by adjusting the phase-offset-bias network so that a voltage proportional to 45° (450 mV in this case) is added to the input of the integrator, the RF signal source will phase lock to the 3-dB bandedge frequency. The phase-offset-bias network switch determines the polarity of the bias voltage: a negative voltage will allow measurement of the lower 3-dB bandedge frequency and a positive voltage will allow measurement of the upper 3-dB bandedge frequency.

The input signal to the integrating amplifier is also used by the input-flag logic circuitry to be discussed below. An isolation amplifier, shown in Figure V-3, is used in order that the flag circuitry will not load down the input to the integrator.

Upon receipt of the computer-generated input encode command, the Systron-Donner Frequency Counter reads the frequency of the input signal to the filter. The input signal is coupled directly into the frequency counter by means of an Anzac, Model H-183, hybrid junction as may be seen from Figure V-1. At the completion of its count, the frequency counter sends a flag to the input-flag logic circuit and outputs the measured frequency in a 16-bit parallel-BCD* format to the computer. Four digits are transmitted, each requiring a 4-bit 8421 BCD code. Except for an inverter in the input encode circuit (shown in Figure V-4) necessary to convert the positive-true encode logic signal from the computer to a ground-true logic signal, no additional interfacing between the microcircuit interface card and the frequency counter was required. (This is possible because the frequency counter was completely TTL-compatible.)

The input-flag logic circuit, shown in Figure V-4, provides a ground-true logic signal to the computer when the RF signal source is phase-locked and when the frequency counter has completed its measurement (see Figure V-1). Two comparators (the LM306 operational amplifiers) are used to detect the phase-locked condition. This condition exists when the input voltage (or "phase(out)" voltage as indicated in Figure V-1) to the phase-lock-loop integrator is zero. The top comparator circuit is adjusted by means of the 100-ohm potentiometer to give a positive-true output-logic signal when its input signal falls below 4.5 mV; the bottom comparator circuit is adjusted to give a positive-true output-logic signal when its input signal is greater than -4.5 mV. The outputs of the comparator circuits are fed to a NAND gate. The two logic signals will be true when the "phase(out)" comparator input signal is within ±4.5 mV (representing $\pm 1^{\circ}$ of phase), indicating that phase-lock has been achieved. A third logic signal, the counter flag signal, is also fed to the NAND gate. The voltage divider in the counter flag circuit is necessary to reduce the +15 V signal, generated by the frequency counter at the completion of its count, to a +5 V logic signal. When all three input-logic signals to the NAND gate are true, the output

---

*Binary coded decimal.

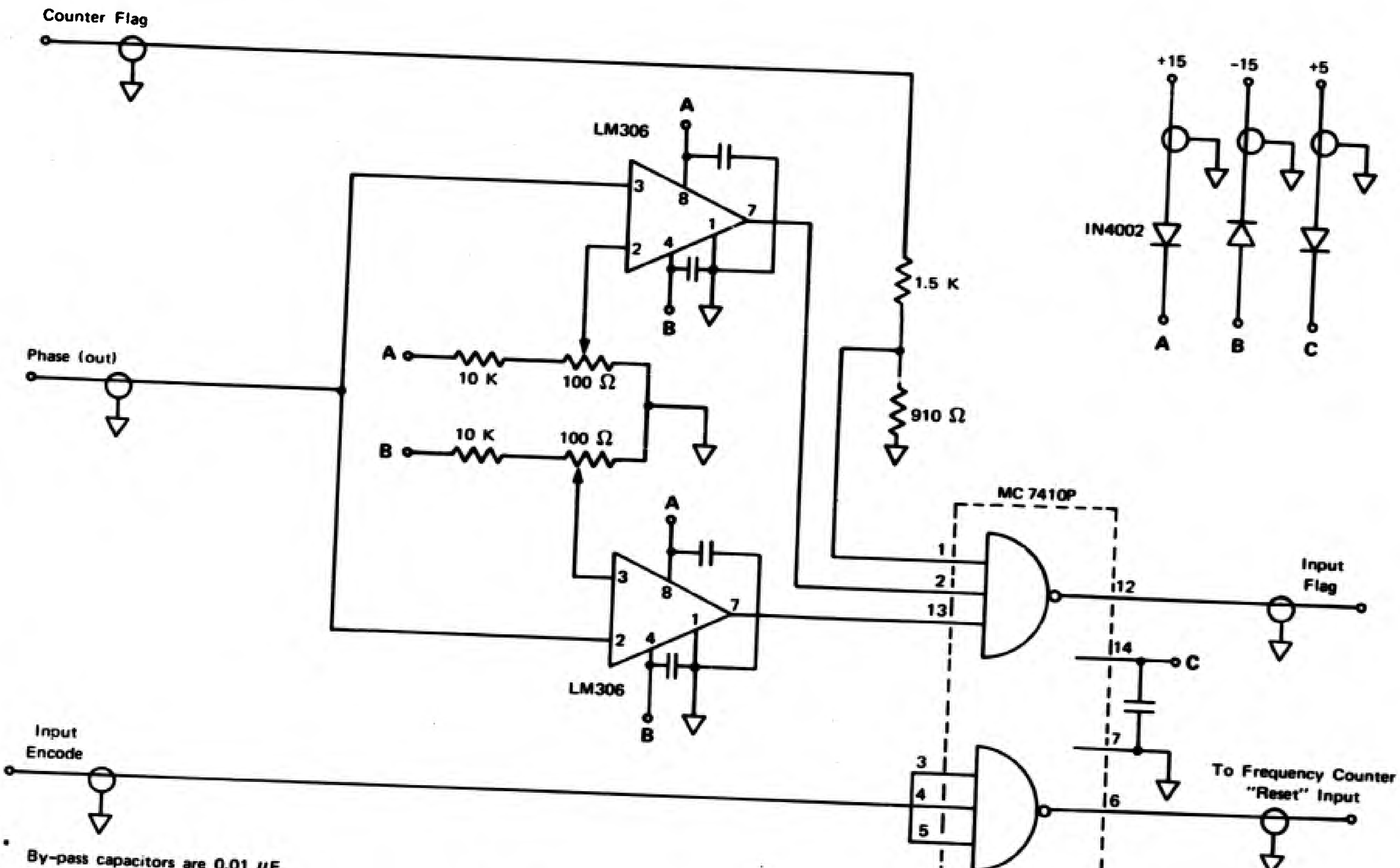

* By-pass capacitors are 0.01 μF.

FIGURE V-4 INPUT-FLAG LOGIC CIRCUIT

SA-1201-41

from the NAND gate, sent directly to the computer microcircuit interface card, will be ground-true, indicating that the RF signal source is phase-locked and that the frequency counter has completed its count.*

As indicated above, an inverter in the frequency-counter encode circuit was needed to convert the positive-true encode signal from the computer to a ground-true encode signal required by the frequency counter. For this purpose a NAND gate was used as shown in Figure V-4. This NAND gate is one of three identical but separate NAND gates built into a single MC7410P integrated circuit.

B. Software for the Automated Measurement System

Two computer programs were written for the multichannel-filter measurement system. The first program was written for the HP 2115A computer associated with the automatic network analyzer. This program provided the HP 2115 computer with instructions to automatically tune the multichannel filter and to measure and record for each channel the filter's resonant (or 3-dB-bandedge) frequency and insertion loss. The second program was written for the CDC 6400 computer, which was used to process the measured data and to provide output conducive to analysis of the frequency response of the filter.

1. HP 2115A Computer Program

The flow diagram for the HP 2115A computer program is shown in Figure V-5. The initial input data required by the program are

---

*Actually, the computer commands the frequency counter to measure twice, each time waiting for receipt of the input flag, and reads only the last measurement. This is done in case phase-lock occurred during the time the frequency counter was taking its first measurement.

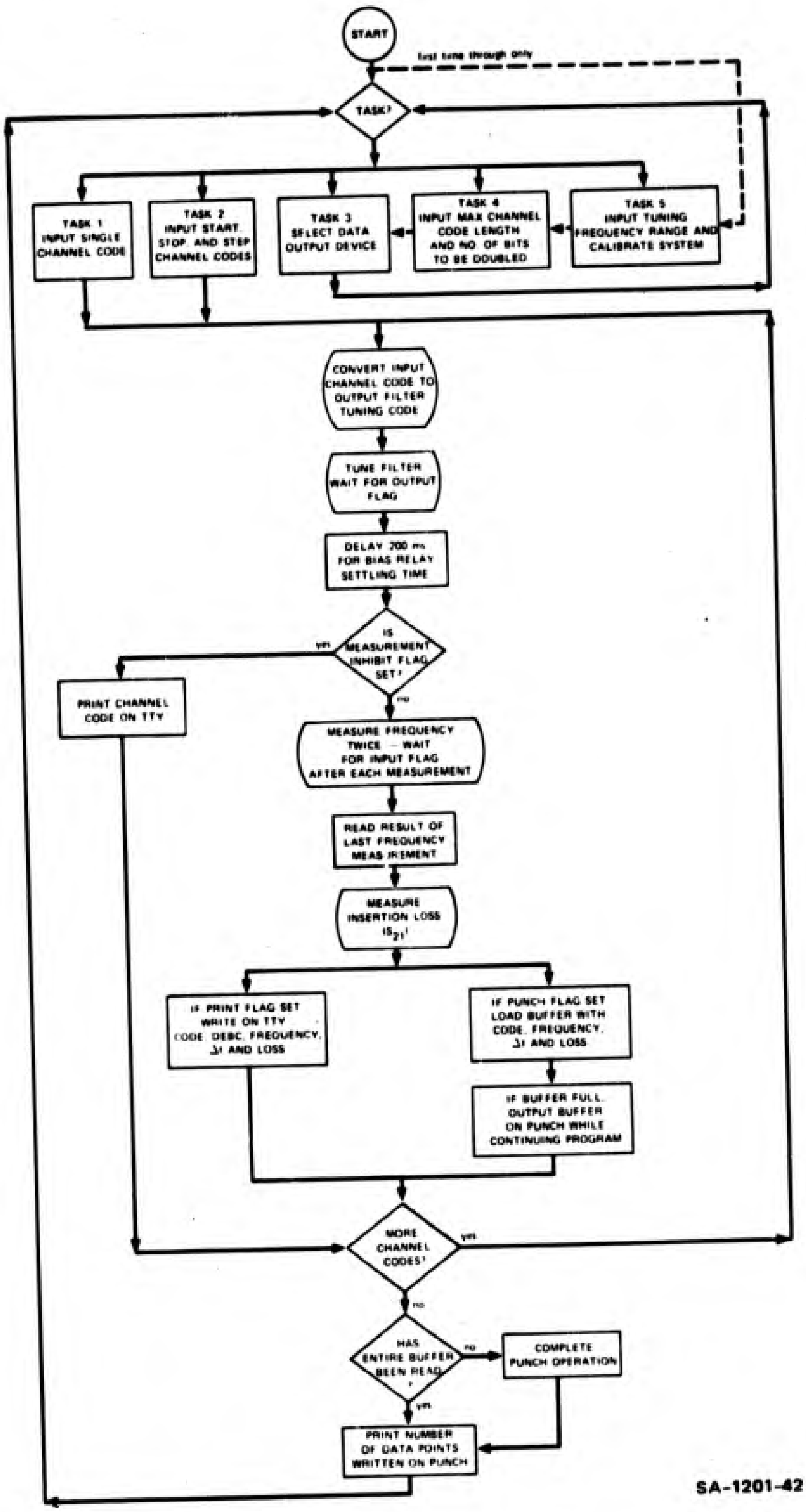

SA-1201-42

FIGURE V-5 HP 2115A COMPUTER PROGRAM FLOW DIAGRAM entered via the teletype under Tasks 1 through 5. For the first time through, inputs under Tasks 5, 4, and 3, in that order, are requested automatically; otherwise the user indicates the task under which input data are to be entered.

Task 1 requests entry of a single-channel code. After the entry is made, the filter is tuned, and frequency and insertion-loss measurements are obtained and recorded for this channel code only. Under Task 2, the filter is tuned and frequency and insertion-loss measurements are obtained and recorded for a number of channels. The start-, stop-, and step-channel codes are entered under this task and the program sequentially steps through channel codes beginning with the start-channel code and ending with the stop-channel code in increments of the step-channel code.

The device on which the measured data are to be recorded is selected under Task 3. Data may be recorded on the teleprinter, the high-speed paper-tape punch, or both.

Under Task 4, the length (i.e., the number of "1" bits) of the largest channel code for which frequency and insertion-loss measurements are to be made (under Task 2, this code is the stop-channel-code) is entered. Also, under this task the number of bits to be duplicated (beginning with the most significant bit) is entered. In effect, this number indicates the desire for a number of biasing circuits, beginning at the top of the control panel, to be switched in unison (both to forward bias or reverse bias) as the filter is tuned through its frequency range. For example, if there were eight irises in the filter so that 256 frequency channels existed, $2^8 - 1 = 255$* would be the largest

---

*Note that 0 is a valid channel code.

channel code (requiring eight binary digits) for which measurements would be obtained. Since there are ten biasing circuits to be controlled, the second entry under Task 4 must be 2 in this case. This means that, as the program sequentially steps through the channel codes 0 to 255, the first pair of biasing circuits (each of which is connected to the diode in an iris half), and the next pair, will each be controlled as one. When Flauto I was completed there were nine irises; thus the two halves of Iris 1 were wired separately to the top two bias-control circuits, while the halves of Irises 2 through 5 were tied together at the filter. Only 9-bit codes are therefore used for TTY "conversation," but internally the first bit is doubled to create compatibility with a 10-circuit control system.

System calibration takes place when Task 5 is called after the frequency range over which the filter is to be tuned is entered.* System calibration is accomplished by removing the filter and connecting together the RF cables from the network analyzer. The insertion loss due to the RF cables, as well as the loss introduced by the network analyzer itself, is then measured for five equally spaced frequencies over the frequency range entered under this task. During calibration, the phase-lock loop (Figure V-1) is disconnected and the five calibration frequencies are set under computer control. (Upon completion of calibration, the computer sets the RF-signal-source frequency to the middle of the Task 5 input-frequency range and the phase-lock loop is reconnected.) The calibration insertion-loss values are subsequently used to correct the measured insertion-loss values of the filter; when

---

*A value ≤ the lowest possible measured frequency and a value ≥ the highest possible measured frequency are entered here.

insertion loss (in dB) is measured for a channel frequency, the value of insertion loss for the calibration frequency closest to the channel frequency is subtracted from the measured value (in dB) to give the measured insertion loss of the filter alone.*

After the initial input data required by the program have been entered, the program proceeds to convert the first channel code to a binary filter tuning code (see Figure V-5). This code contains 10 significant bits, the value of each bit representing the bias state of the diodes in one of the 10 filter irises (or iris halves). A "0" bit will cause the diodes to be back-biased and a "1" bit will cause them to be forward-biased. The tuning code is the binary representation of the channel code with a number, as determined from the second entry under Task 4, of its most significant bits doubled. For the 256-channel example discussed above, the channel code 00001011 (decimal 11) would convert to 0000001011, but the channel code 01001011 (decimal 75) would convert to 0011001011 and the channel code 10001011 (decimal 139) would convert to 1100001011. Thus, for this example, an 8-bit channel code is converted to the required 10-bit tuning code. If the length of the binary channel code exceeds the maximum length entered under Task 4 (as will happen if the stop-channel code entered under Task 2 exceeds the maximum length) an error message will be printed on the teletype and the measurements for the remaining channel codes aborted.

After the tuning code has been constructed it is loaded into the output buffer of the microcircuit interface card, and the diodes

---

*The calibration insertion-loss values are actually printed out at the start of the run. Since these values have been found to be the same within ±0.1 dB across the band for the system used, it is seen that errors due to the stated method of interpolation should not exceed ±0.1 dB.

are then switched to the forward- or back-bias states indicated by the code. Again, for the above example, the tuning code for channel code 11 (binary 0000001011) will cause the diodes in three irises to be forward-biased and those in seven irises (or iris halves) to be reverse-biased. After the output buffer is loaded with the tuning code, an encode signal is sent to the relay biasing network (see Figure V-1). The program then waits for the output flag and upon its receipt delays 200 ms before continuing. This delay assures that the filter bias relays have settled prior to the measurement phase of the program.

At this point, the program checks to see if the "measurement inhibit" flag is set. The flag is set by a switch on the front panel of the computer. If this flag is set, the measurement phase of the program is bypassed. This feature allows use of the computer to automatically tune the filter while the network analyzer is in its manual mode of operation. When in this mode of operation, the RF signal source may be swept continuously in frequency (as opposed to being controlled by the computer and phase-lock loop in the automatic mode), and transmission-coefficient data (uncorrected for system and cable losses) versus frequency may be displayed on the network analyzer's rectangular and polar oscilloscopes. In this way, the swept-frequency response of the filter can be observed as the computer program steps through the specified channel codes.

If the "measurement inhibit" flag is not set, however, the program proceeds to its measurement phase. An encode signal is sent to the frequency counter to start the frequency measurement. The program waits until the input flag is received--an indication that the frequency counter has completed its measurement and that the system is phase-locked.* This sequence, beginning with the transmission of the frequency-counter encode signal, is repeated. This is done because of the possibility that system phase-lock can occur during the time the frequency counter is obtaining its first measurement. After the second input flag is received, the frequency is read from the microcircuit interface card. It was necessary, after measuring frequency, that the value be truncated to the nearest 10 kHz. Since the microcircuit interface-card 16-bit input buffer can accept only four decimal digits at a time,† two digits to the left and two digits to the right of the decimal point of the measured frequency value, in megahertz, are read by the input buffer. The most significant digit of the measured frequency value is not read by the input buffer. Instead, the value of this digit is determined by the computer program, multiplied by 100, and added to the value read by the input buffer. The value of the most significant digit can be determined by the program because the range of frequency values is known (entered under Task 5) and because it is known that the total tuning range of the filter is less than 100 MHz.

Measurement of insertion loss completes the measurement phase of the program. The microwave vector voltmeter obtains the loss measurement, which is then corrected for cable and system losses using the calibration data. The resulting filter insertion loss is converted to dB for output.

---

*If this flag is not received with 12 seconds, an error message is printed on the teletype and the measurements for that channel code are skipped.

†Four binary bits are required to represent a decimal digit.

The final phase of the program is the output phase. If the teletype was selected for output under Task 3, the following are printed: the binary channel code, the decimal equivalent of the binary channel code (DEBC), frequency, the difference between this frequency and the frequency obtained from the previous channel code measurement, and insertion loss. If the high-speed paper-tape punch is selected for output, then channel code, frequency, frequency difference, and insertion loss are stored in a buffer that is set aside within computer memory. This buffer is large enough to store the data obtained for 100 frequency channels. When the buffer has been filled, the punch is instructed to commence reading the data buffer directly in binary format. The punch continues to read until all of the buffer has been read. When the punch output operation is programmed in this way, the time it takes to obtain a large number of frequency-channel measurements is significantly reduced from the time it would take if the program were to wait for the punch to read currently measured data for a single-frequency channel before obtaining the measurement data for the subsequent frequency channel.

The channel-code conversion, measurement, and output phases of the program are repeated for all the channel codes for which measurements are required under Task 2. When the channel-code list is exhausted, the program checks to see if all the measurement data were read by the punch. If they were not, the punch operation is completed. The number of channel frequencies for which data were recorded on the punch is then printed by the teletype, and the program returns to one of its input tasks.

2. CDC 6400 Computer Program

The computer program written for the CDC 6400 processes the measured data from the multichannel, high-power filter that were previously recorded on paper tape. The objective of this program was to provide processed output data for the filter that would aid in the analysis of the tuning increment and frequency response of the filter as it was tuned through its frequency range of operation. Specifically, the program provided a means to easily observe channel codes that resulted in redundant resonant frequencies, or large frequency gaps that resulted when the filter was tuned sequentially through its channel codes. Furthermore, the variation of insertion loss about the specified value of 2.25 dB, as the filter channel codes changed, was also easily observed. With the output provided by this program, one quickly determined which filter irises required adjustment.

The data available on paper tape used by the CDC 6400 computer program were, for each tuning channel: channel code, frequency (MHz), and insertion loss (dB). These data were obtained with three separate measurement runs. For the first run, frequency and insertion-loss measurements were made when the effective phase shift* through the filter was zero; measurements were made during the second run when the effective phase shift was $+45^\circ$ and during the third run when it was -45°.† Each set of data was first read into the CDC 6400 computer memory. Next, the data, which originally were recorded in the 16-bit-word and floating-point format of the HP 2115A computer, are converted to the CDC 6400 computer 60-bit-word and floating-point format. The result is that for each channel frequency the following are stored into computer memory: a channel code and, associated with each channel code,

---

*The effective phase shift is the measured phase shift offset by the constant phase shift that occurs at filter resonance (refer to the vector voltmeter phase offset discussion in Section V-A.)

†The latter two runs were obtained by introducing a bias voltage, equivalent to $\pm 45^\circ$ phase shift, into the measurement-system phase-lock loop (see Figure V-3).

the resonant frequency (f_0), the $+45^{\circ}$ phase-shift frequency (f_1), the -45° phase-shift frequency (f_2),* and the insertion loss of the filter at each of the three frequencies.

After the conversion process, the raw data obtained from the paper tape are printed on a high-speed line printer. The purpose of printing the raw data is to assure that the data were read and converted correctly. The output is, for each channel frequency, the channel code (in both its binary and decimal representations), and for each measurement-phase-shift run (0, +45, and -45 degrees) the output is frequency, the difference between this frequency and the frequency measured for the previous channel code (both in megahertz), and the filter insertion loss in dB.

Data processing begins by rearranging all the resonant or channel frequencies in ascending order and assigning channel numbers to each, beginning with the number 1. The following data are printed on the high-speed line printer for the channel numbers in consecutive order:

(1) Resonant or channel frequency in megahertz.

(2) Binary channel code.

(3) Decimal channel code.†

(4) Filter insertion loss at resonance (dB).

(5) The 45°-phase-shift bandwidth in megahertz; this bandwidth is theoretically the 3-dB bandwidth at the resonant frequency.

---

*The frequencies f_1 and f_2 should theoretically be the 3-dB bandedge frequencies.

†Note that the channel code will not necessarily be listed in descending order, since in some cases adjacent channels overlap in frequency.

(6) The loaded Q of the filter derived from resonant frequency and the 45^{o}-phase-shift bandwidth:

$$Q_L = \frac{f_0}{f_2 - f_1} .$$

(7) The external Q of the filter derived from Q_L and the insertion loss at resonance:

$$Q_E = 2Q_L \cdot \text{antilog} \left[\frac{\text{insertion loss (dB)}}{20}\right] .$$

(8) The unloaded Q of the filter derived from the loaded and external Q's:

$$Q_u = \frac{Q_L Q_E}{Q_E - 2Q_L} .$$

(9) The predicted VSWR of the filter derived from the unloaded and external Q's:

$$\text{VSWR} = \frac{Q_u + Q_E}{Q_u} .$$

(10) The lower or positive 45^{o}-degree-phase-shift band frequency (f_1) in megahertz.

(11) The insertion loss of the filter at f_1 (in dB).

(12) The upper or negative 45^{o}-phase-shift band frequency (f_2) in megahertz.

(13) The insertion loss of the filter at f_2 (in dB).

(14) The frequency difference (in MHz) between two consecutive channel number frequencies.

With the use of the high-speed line printer, insertion loss versus channel (resonant) frequency (to the nearest 100 kilohertz) is also plotted. Frequency is continuously printed vertically over the ent 'e filter tuning band, every 100 kHz. On the same horizontal line, adjacent to its measured channel frequency, the channel number and channel code (both the binary and decimal representation) are printed; an X printed along a horizontal insertion-loss scale from 1.0 to 3.6 dB indicates the value of insertion loss at the channel frequency. The X is bounded horizontally by I points indicating a nominal measurement error of ±0.5 dB. Vertical "+" points indicate the filter-insertion-loss design objective of 2.25 dB. An example of this point plot may be seen in Figure III-12.

Finally, with the use of an oscilloscope in conjunction with a camera, plots of several parameters versus channel frequency are made. Unloaded, external, and loaded Q versus channel frequency (MHz) are plotted as shown in Figure III-14; insertion loss (in dB) at resonance versus channel frequency is plotted as shown in Figure III-15 (bottom); the broken horizontal line indicates the filter-insertion-loss design objective of 2.25 dB; predicted VSWR versus channel frequency is plotted as shown in Figure III-15 (top); the broken horizontal line indicates the filter VSWR design objective of 1.5; and the 45°-phase-shift bandwidth (MHz) versus channel frequency is plotted as shown in Figure III-15 (center).

VI MERCURY-FILM SWITCHES

A. General

Since it does not appear possible to meet the highest filter-performance specifications on bandwidth (via unloaded Q) and IMD through the use of PIN diodes, other switching devices have been sought. In particular, a higher open-switch resistance (R_p), and the elimination of biasing adjuncts in regions of RF field or current, would be especially advantageous. The Logcell mercury-film switch was therefore selected for study and found to be of promise, especially if it can be repackaged more specifically for the present application. A two-channel, high-power bandpass filter, Flauto II, was completed to demonstrate the use of these switches.

Mercury-film switches--of which the Logcell I (Figure VI-1) is but the original embodiment*--differ from the earlier hydrogen-filled mercury-wetted reed switches by being bounce- and noise-free, position-insensitive, and very much smaller, but the self-healing-contact feature and magnetic driving without electrical contact are retained. Logcells are also self-latching (but not necessarily, if not desired) and extremely shock- and vibration-resistant due to the high surface tension of the mercury film.† Mechanical motion does occur, but it is that of an element weighing 3 mg floating and gliding on a film of mercury within the hermetically sealed package. There are no hinges, bearings, springs, or

---

*"LOGCELL Mercury Film Relays and Switches," Bulletin 77, Fifth Dimension, Inc., Princeton, N.J. (1971); also W.D. Kinney, private communication.

†The switch is so small, no difficulty is foreseen in applying the localized heating that would permit operation at ambient temperatures below the freezing point of mercury.

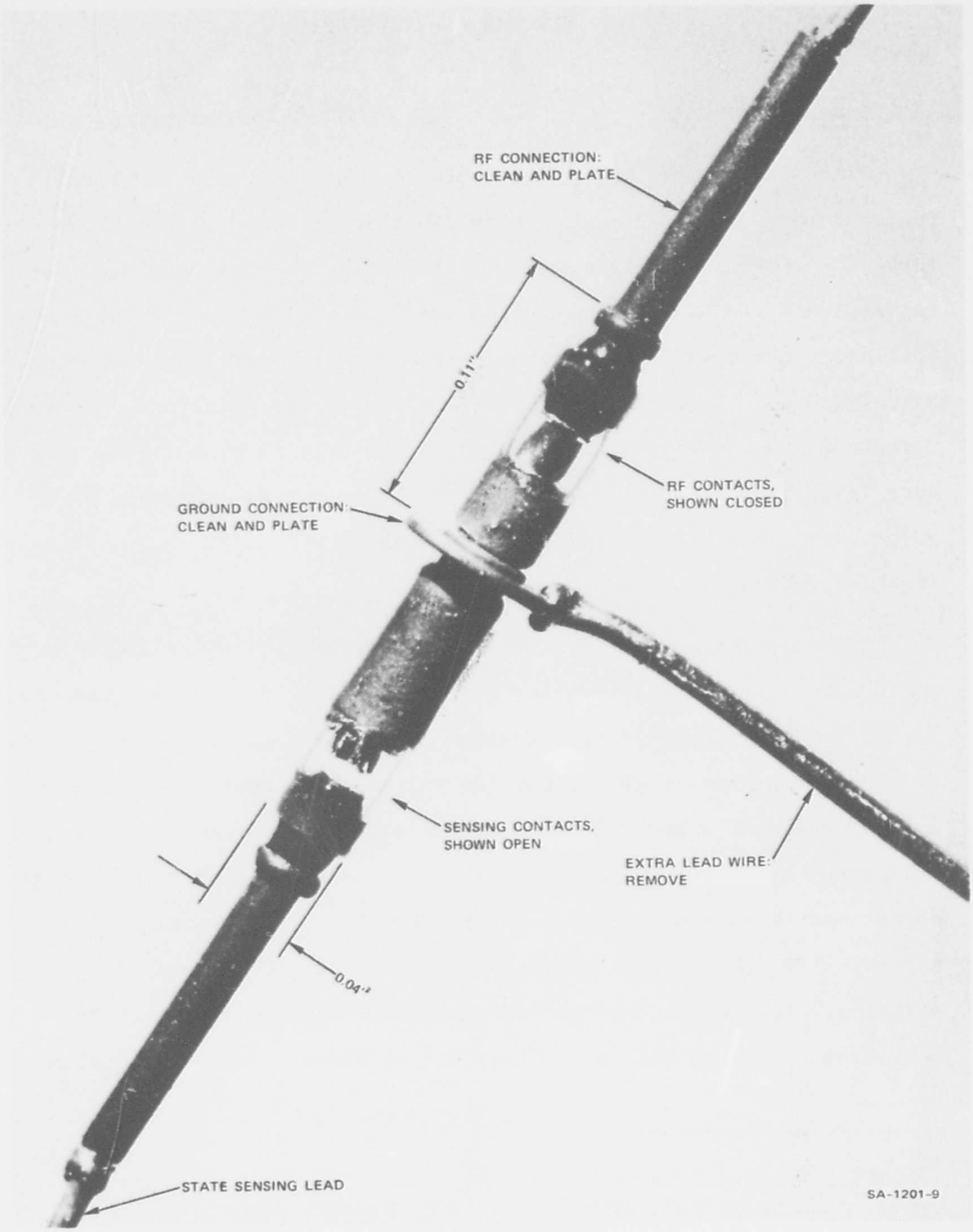

FIGURE VI-1 PHOTOGRAPH, APPROXIMATELY 15.5x, OF LOGCELL MERCURY-FILM SWITCH CAPSULE (Part No. 3000-1C-WL, Fifth Dimension, Inc., Princeton, N.J.)

other mechanical wear points, and the impact of the moving element is cushioned by the mercury. Indeed, the moving element is not actually a moving contact, but a mercury "driver," since the making and breaking of contacts is always between mercury and mercury. It therefore appears logical not to classify Logcells as mechanical, but as something unique, such as "liquid electronic." Actual performance of these switches bears this out; operating speeds faster than 5 ms, cycling rates to 150 Hz, and lieftimes to 10^8 cycles are typical, along with reliability, constancy of parameters, and repeatability of transients, as with electronic devices.*

The Logcell I capsule is shown in Figure VI-1. The metal parts are magnetic nickel-iron and the glass is soda-lime. Gas filling is of inert and reducing gases (argon and hydrogen) at 1.4 torr pressure. The moving part is a tape helix treated so that its external surfaces are mercury wetting while its internal surfaces are not. (This provides for the desired movement of the mercury.) In the present RF application, only the upper portion is inside the RF resonator. To make good contact, the connections are cleaned of oxide and gold plated. Nevertheless, a relatively long, highly-resistive path under the glass remains in the RF current loop, while the mercury path is short and contributes negligibly to the switch resistance at UHF. RF voltage and current ratings appear to be at least as high as those of the PIN diodes, but could be increased in a redesigned package. The lower end of the switch participates only in very low-power dc circuits for monitoring the state of the switch.

---

*This performance applies to Logcells that have been in operation in the actual assembly for a few dozen cycles, so that abnormal units will have been detected and discarded.

Major attractions of the Logcell switch are the very low capacitance across open contacts (0.02 pF) and the very high value of R_p, which at 400 MHz is about 24×10^6 ohms,* as deduced from filter Q_u measurements. Evaluation of IMD was attempted at RADC with open and closed Logcells in shunt and series, respectively, with a 50-ohm line. IMPs were found to be so much weaker than with PIN diodes that the limitations of the measuring system prevented identification of the origin of the IMPs as internal or external to the Logcells.

The closed-switch resistance, R_s, is found to be an increasing function of frequency, starting at about 0.03 ohms at very low frequencies. Values of R_s could be derived from component insertion-loss data (obtained by the manufacturer), from one-port measurements on the network analyzer, and from Q_u data on a filter resonator (for frequencies near 400 MHz only), and agreement was good. Below 400 MHz, R_s varies as the 1/2-power of the frequency, implicating skin effect in the highly-magnetic connections not coated with mercury. Actual data points are as follows:

f (MHz)	R_s (ohm)
10	0.10
100	0.35
200	0.52
300	0.68
400	0.80

*It can be shown that this value must arise from dielectric losses in the glass, and not from other sources of open-switch loss.

At higher frequencies, however, R_s climbs rapidly. Above 800 MHz it varies as the square of the frequency, with R_s = 2.1 and 10.0 ohms, respectively, at 1000 and 2000 MHz. No satisfactory explanation for this latter effect has been found. Fortunately, filters with Logcell I switches are not now contemplated for frequencies above 400 MHz.

Taking R_s as $\approx$ 0.75 ohm in the range 295 to 360 MHz, one might consider a parallel combination of about 15 Logcells as forming a switch having R_s = 0.05 ohm, R_p = 1.6 megohms, and C_d = 0.3 pF. If this composite switch took the place of each PIN diode in Iris 1 of Flauto I, one would not only have a very comparable filter, but one with Q_u raised to the desired value of 5000. The number of Logcells needed for the other irises could be progressively halved, in going from Iris 1 to Iris 2, to Iris 3, ..., hence the prospect of construction is not as formidable as at first supposed. Nevertheless, it remains much more attractive to develop a new Logcell package than to use parallel combinations of the old Logcell I.

The manufacturer (Fifth Dimension, Inc., Princeton, N.J.) is also marketing a non-latching, high-speed switch, called Logcell II, in which the floating magnetic mercury driver is a perforated disc rather than a helix. Logcell II is cheaper and extremely rugged, but its more rugged package adds so considerably to R_s, and to the capacitance, that it cannot be used for the present project. However, the performance is about the same in other regards, and in considering a UHF/microwave repackaging (as with molybdenum and ceramic), a disc armature might be considered as well as a helix.

The method of incorporating the fragile Logcell I capsule into the RF structure is shown in Figure VI-2. The connecting adjuncts, needed to avoid mechanical stress on the glass seals, increase the effective R_s by about 8%. The components for magnetically driving the switch,

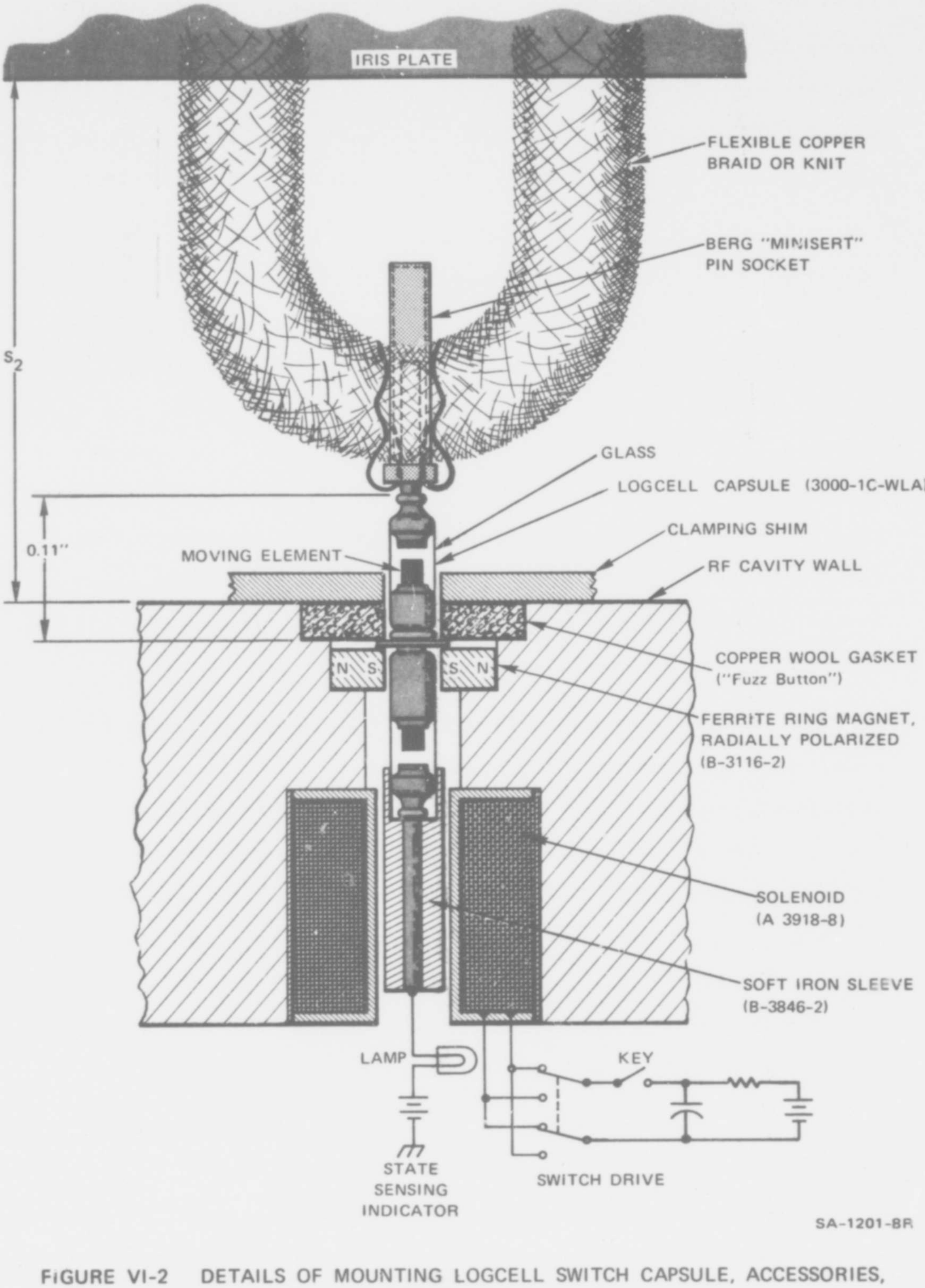

FIGURE VI-2 DETAILS OF MOUNTING LOGCELL SWITCH CAPSULE, ACCESSORIES, AND DRIVE COMPONENTS IN RF CAVITY which are completely isolated from the RF circuit, are also shown. The ferrite ring magnet polarizes the armature so that the solenoid field can both pull it down and push it up, depending on the polarity of the solenoid current. The solenoid is readily energized by the pulse from a discharging capacitor; a power of about 400 mW maintained for about 3 ms is adequate for the operation. The indicator lamp is a great convenience, since it will be lit when the RF contacts are open, and dark when they are closed.

About 10% of the new switches installed will not respond at first to being driven by the solenoid, but they will do so after several cycles of driving by the alternating poles of a strong, hand-held permanent magnet. Further, about 40 percent of the new switches installed cannot be made to push up by means of the solenoid, although they will pull down by this means, and can easily be moved both ways by the hand-held magnet. These switches simply have to be discarded and replaced, with a corresponding finite increase in effective material, labor, and time expense. Once the abnormal switches are culled out, operation is extremely reliable. In a working multi-iris filter, a single defective switch could easily be made to generate an alarm by including in the tuning program a test for error between the tuning code and the complement of a code derived from the state-sensing contacts. A corresponding alarm could not be so readily arranged in the case of PIN diode switches.

The manufacturer has some recent research results indicating that the abnormal capsules are actually the more perfect in construction. It appears that when the mercury wetting is entirely symmetrical, the force of the mercury surface tension is much more difficult to overcome.*

---

*Traces of oxygen can also increase the mercury surface tension excessively.

An uneven wetting, however, might give a place for "tearing loose" to begin. Apparently, the hand-held magnet always works because its field is unlikely to be coaxial with the switch and can thus initiate a tilting of the armature that aids in "tearing loose." With this new knowledge, it is possible that the yield of "good" switches can be raised by deliberately designing asymmetries into the solenoid, the ferrite ring magnet, or the wetted surfaces.

B. Flauto II Bandpass Filter

A high-power, high-Q, UHF bandpass filter, Flauto II, as shown in Figure VI-3, was prepared to demonstrate the use of Logcell I switches in this novel way. Since only one two-part iris was installed, there are only two channels--at 299.21 and 323.21 MHz--excluding the possibility of asymmetrical iris switching, which is disallowed in the case of truly low-loss switches or switch combinations.

An interior view is shown in Figure VI-4, where it is seen that the cross section is very close to that of Flauto I. The coupling loops are smaller in area, since Q_u is higher. The inner conductor does not run the full length of the coaxial resonator, but is only 7.88 inches long and brazed to the end wall near the coupling loops. The mode of resonance is thus "quarter-wave," as in Figure II-2, and there is a fringing capacitance at the "open" end of the inner conductor that could not be evaluated here due to the varying influence of the nearby iris in its two states. This mode of resonance was chosen because Eqs. (II-4) and (II-5) indicate that increasing the effective Z_0 will make Q_{ua} and Q_{ub} more nearly equal when R_s and R_p are greater than in the case of PIN diodes.

After some experimentation, it was decided to locate the switchable iris 4.63 inches from the shorted end of the resonator (59 electrical

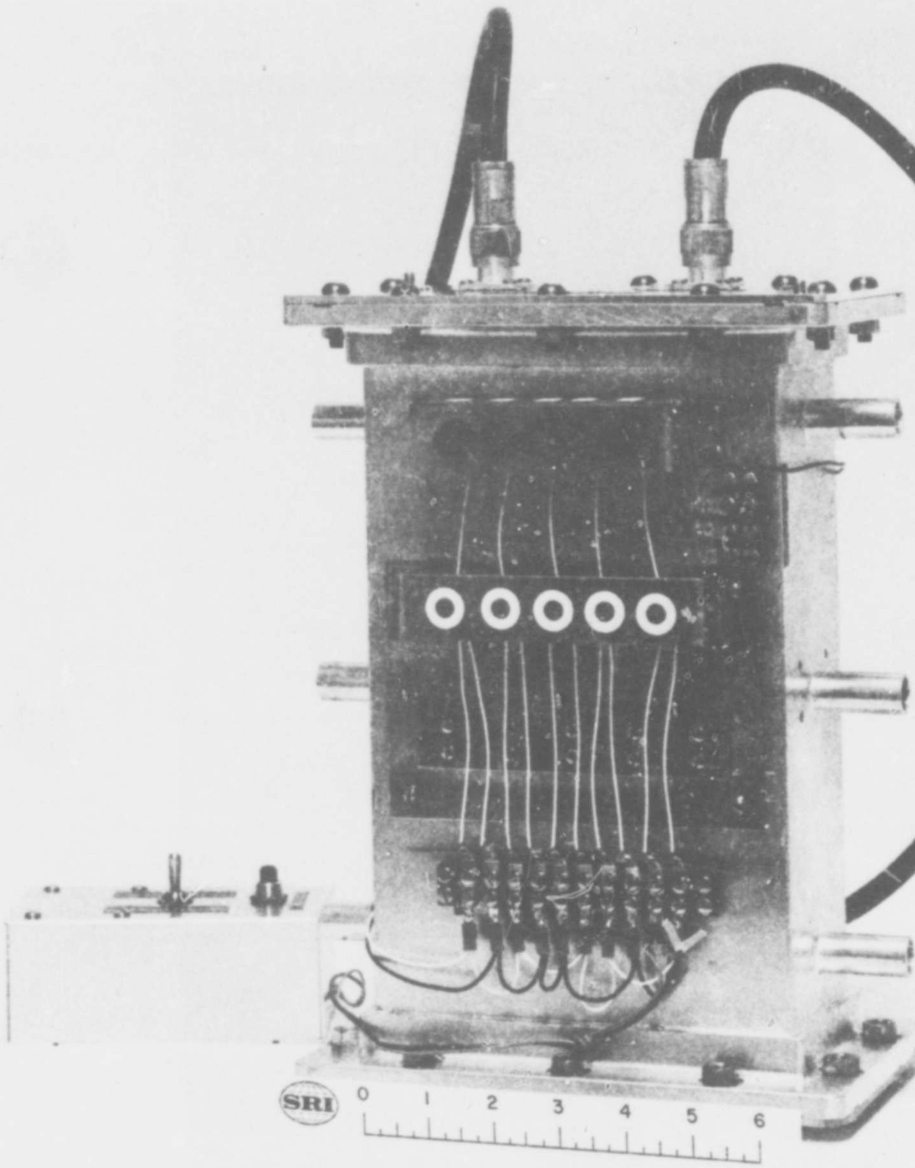

SA-1201-43

FIGURE VI-3 FLAUTO II, A TWO-CHANNEL (one-iris) ELECTRONICALLY TUNABLE, HIGH-POWER, HIGH-Q, UHF BANDPASS FILTER USING 10 LOGCELL I MERCURY-FILM SWITCHES

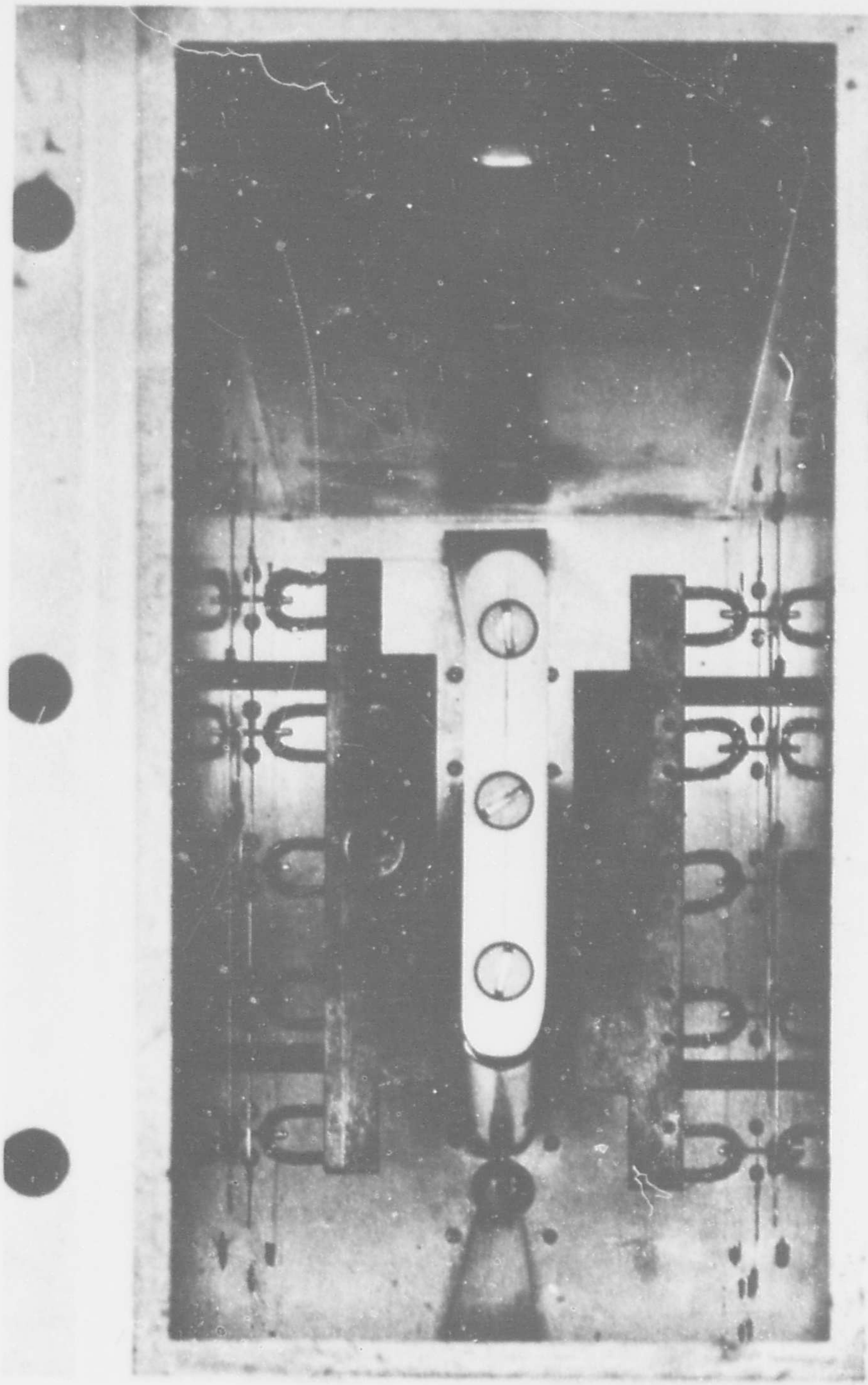

SA-1201-44

FIGURE VI-4 INTERIOR VIEW OF FLAUTO II FILTER degrees, neglecting the fringing capacitance). Details of the iris halves, with 10 Logcells installed, are seen in both Figures VI-4 and VI-5. Preliminary experiments with "dummy" switches revealed that only three switches per side (in the end and center positions) would be sufficient to render inductive effects and current-crowding losses negligible. However, more switches had to be paralleled to increase Q_{ua} due to the high R_s of a single switch. As will be seen, even more than 10 switches would have been preferable in Flauto II, if provisions had been made for installing them. (If additional irises were also installed, they would require, however, relatively fewer switches each.)

In Figure VI-3, the Logcells and their driving solenoids are installed behind the five white rings seen in the photograph.* State-sensing lamps (above) and solenoid terminals (below) are attached to the exterior resonator wall but do not connect to anything internal. These components are duplicated on the opposite side of the cavity.

Final measurements on Flauto II yielded the following parameters:

Channel:	Lower	Upper
RF contacts:	Closed	Open
Sensing lamps:	Off	On
Frequency, MHz	299.21	323.21
$\pm 45^{\circ}$ bandwidth, kHz	743	637
Insertion loss, dB	3.35	1.35
Q_L	402	507
Q_E	1190	1190

*The white rings are for aiming a pole of a hand-held permanent magnet toward a switch when the pulsed drive (from the small box) is to be overridden.

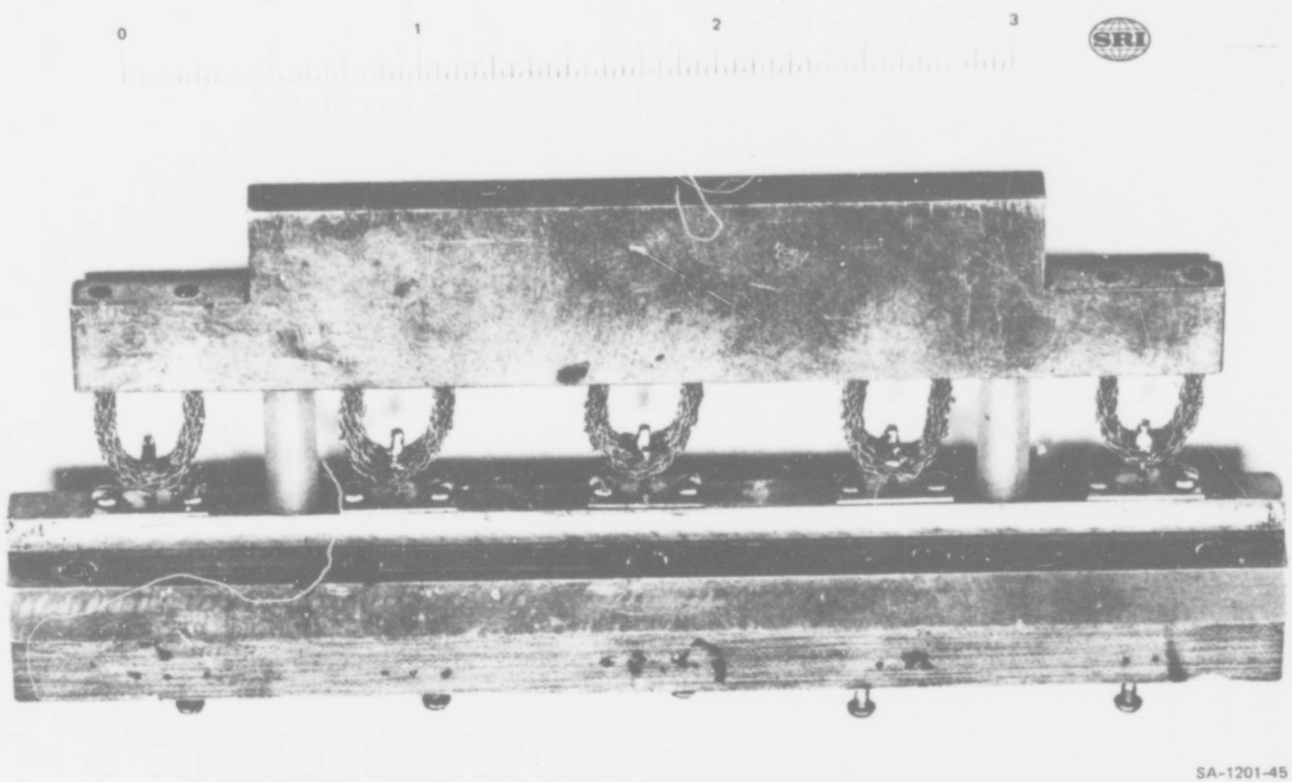

FIGURE VI-5 CLOSE-UP OF IRIS HALF FOR FLAUTO II FILTER, SHOWING TWO DIELECTRIC SPACERS AND FIVE LOGCELL I SWITCHES INSTALLED. (Magnetic drive components are concealed within the lower block.)

Q_u	1250	3440
Computed VSWR	1.95	1.35
Measured VSWR, input	1.95	1.22
Measured VSWR, output	2.0	1.44

It is seen that Q_{ua} and Q_{ub} are quite disparate, although their geometric mean, 2080, is much greater than was obtained with Flauto I. To realize $Q_{ua} \approx 2080$, it should suffice to increase the number of Logcells here from 10 to about 16, still ignoring resonator wall losses through they should not now be neglected.* Reconciling the above values with the loss parameters $R_s \approx 0.7$ ohms + 8%, and $R_p \approx 24 \times 10^6$ ohms, is difficult due to the uncertainty in the fringing capacitance here, which leads to a very great uncertainty in tan θ_a and tan θ_b, since θ_a and θ_b are close to $\pi/2$.

The coupling loops of Flauto II were adjusted so that the mean insertion loss and VSWR (for the two channels) would be close to the design objective and the values for Flauto I (2.25 dB and 1.5:1, respectively). Since the two filters are thus fairly comparable, the desirable twofold decrease in bandwidth (to the order of 700 kHz) for Flauto II can be appreciated.

C. Repackaging of the Logcell Switch

It appears possible to overcome the disadvantages of the presently available mercury-film switches (Logcell I and Logcell II) in application

---

*Referring to the equivalent circuit of Figure II-5, the resistance r was found to be 0.02 and 0.04 ohm, respectively, for the 373- and 411-MHz resonances of a half-wave resonator of the same cross section, and with the iris located centrally. These values would not apply to the Flauto II resonator too closely.

to VHF and UHF (and even microwave) filters of the Flauto type, by repackaging. Referring to Figure VI-1, the present high value of R_s can be accounted for by the extremely high RF resistivity of the kovar (nickel-iron, $\mu \sim 400$) cylinders to which the glass is sealed. By changing to molybdenum/ceramic seals it should be possible to reduce R_s several fold.* As for being magnetic, only two parts actually require it--the moving element, which is enveloped in mercury, and the lower contact, which is isolated from the RF circuit.

The proposed switch is sketched in Figure VI-6. The general arrangement and the diameters of the alumina ceramic tubing were chosen to be the same as in microwave solid-state device packages such as the Fairchild transistor shown in Figure VI-7. Yet, the Logcell I internal parts and magnetic circuit fit in well, provided the ceramic tubing is cut somewhat longer. The molybdenum is a superior RF and thermal conductor, has the required thermal coefficients for sealing to ceramic, and can be surface-treated to be wettable or non-wettable by mercury where required. Switching speed (3 ms), life, reliability, and shock and vibration resistance should be as before, or improved. Mechanical ruggedness would be greatly enhanced, and permit heavier, hence lower-loss, external connections. Power ratings should be superior. It is estimated that a filter $Q_u \approx 5000$ could be obtained with these new switches (with no IMD) with no more than five switches per iris half in Iris 1, and probably two or three per iris half in the less significant coarse-tuning irises.

---

*The ceramic would probably allow an increase in R_p, although this is not needed. Should Q_{ub} and Q_{ua} be too disparate because of an excessively high R_p, the C_2 gaps can be shunted with thin-film resistors.

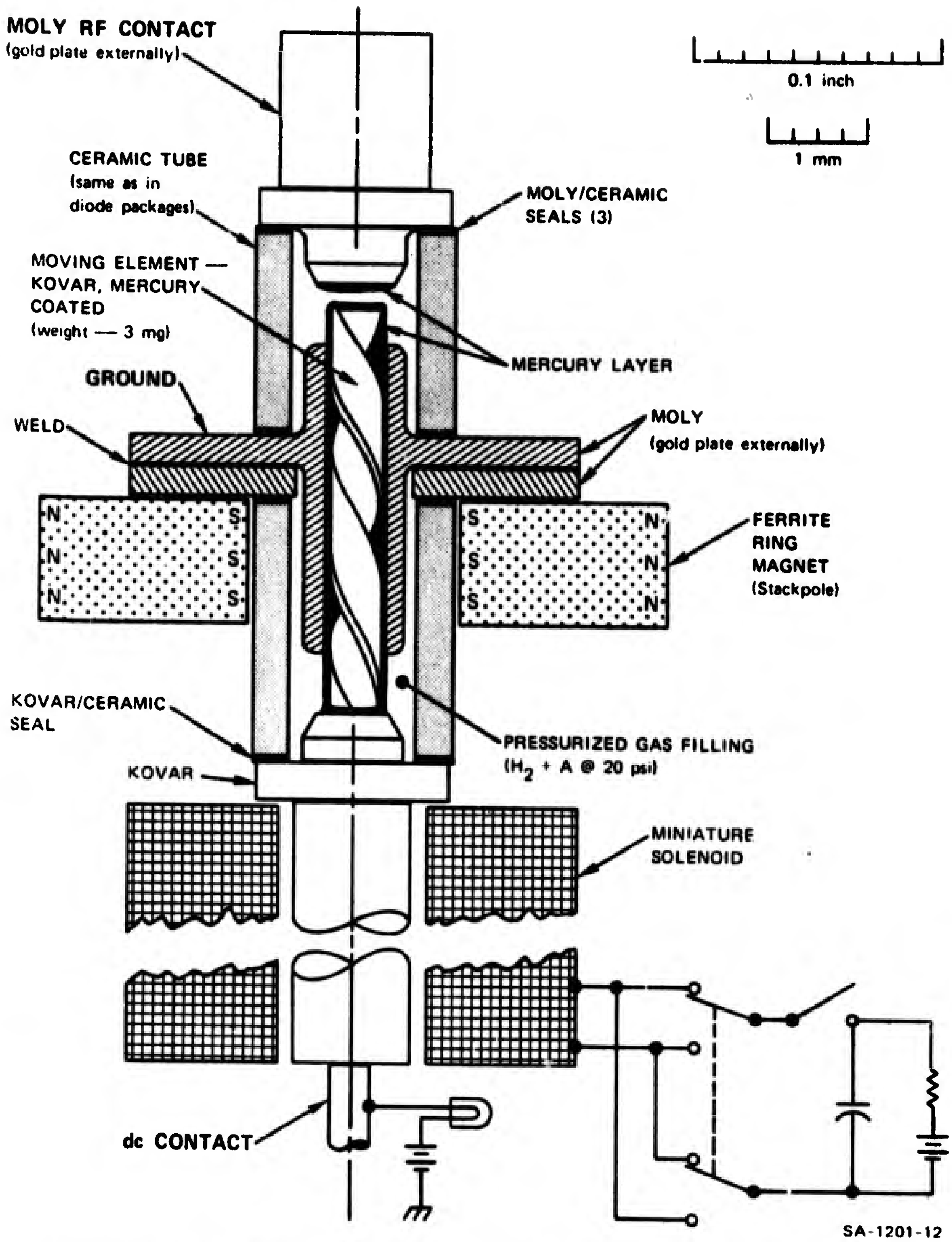

FIGURE VI-6 PROPOSED MOLYBDENUM/CERAMIC PACKAGE MODIFICATION OF LOGCELL SWITCH FOR HIGH-Q, HIGH-FREQUENCY, RESONANT CAVITY APPLICATIONS. (Drive components included.)

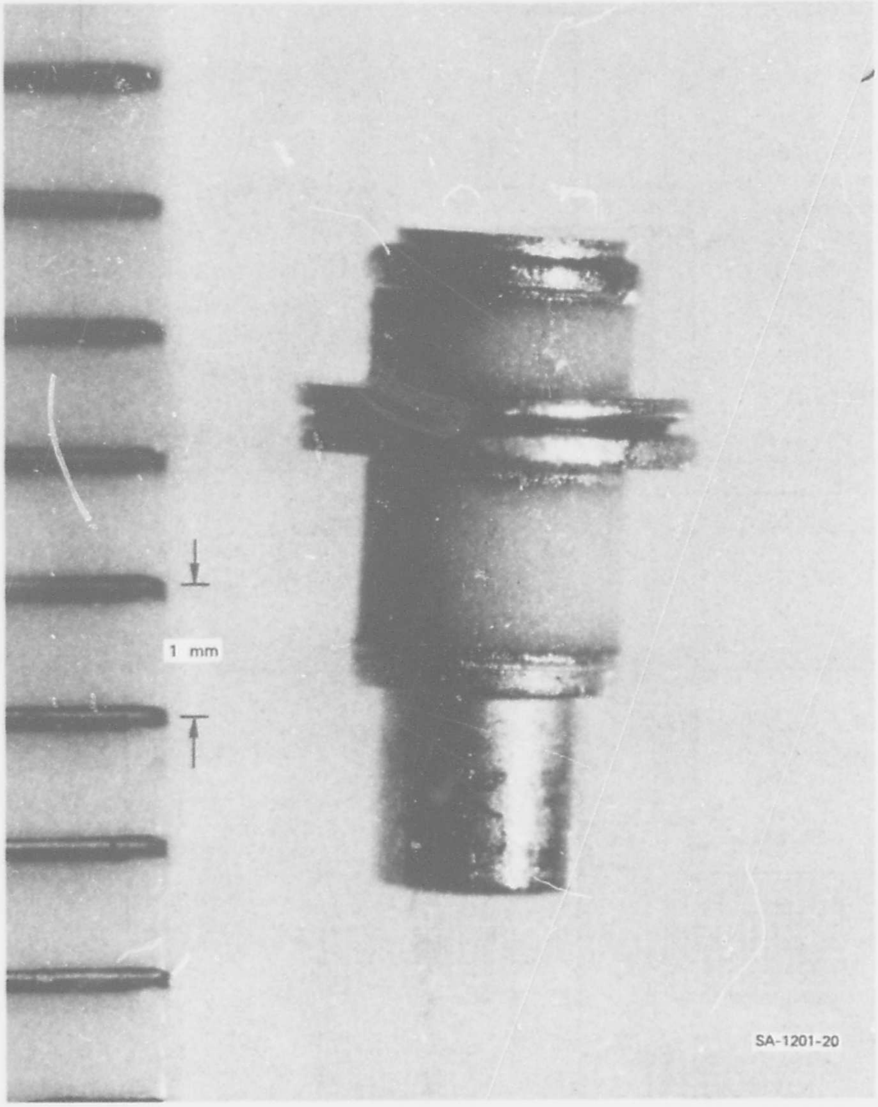

FIGURE VI-7 PROPOSED PACKAGE IDEA FOR HIGH-Q MERCURY-FILM SWITCH OF FIGURE VI-6

VII SUGGESTIONS FOR FUTURE WORK

Although the present contract has been successful in establishing feasibility of the design concept, generating design relations, and developing a working filter, several avenues remain open for further research and development. Future work should be aimed at making filters of the type under discussion more useful and/or reliable in the frequency bands of interest, not to mention other frequency bands (e.g., microwaves) where applications may well exist. Some suggestions for possible future work are as follows:

(1) For integration with the system.

(a) Design and construction of three additional filters ("Soprano," "Tenor," and "Bass") similar to Flauto I so that the range 225 to 400 MHz may be completely covered.

(b) Integration of all four filters with band-selection switches and control hardware/software for selection of any channel within the entire 225-to-400 MHz range.

(c) Development of hardware and software so that the filter subsystem may <u>automatically</u> track the <u>transmitter</u> of the communication system.

(d) Design and construction of a filter similar to Flauto I for the VHF band 116 to 150 MHz.

(e) Study of the feasibility of a four-pole (two coupled resonators) VHF/UHF filter based on the present principle, intended to give greater skirt selectivity.

(2) For enhancement of the general performance of Flauto I.

(a) Mechanical redesign for lower weight, smaller volume, increased ruggedness, temperature stability, etc.

(b) Refinement of the filter electrical design, including the input/output coupling loops, to make the bandwidth (and hence skirt selectivity) more nearly constant over the tuning range, and, if possible, somewhat narrower, through enhancement of Q_u and optimization of its variation over the tuning range.

(c) Refinement of the iris distribution pattern, and of the final trimming procedure, to enhance the uniformity of channel spacing and to minimize channel redundancies.

(d) Replacement of the relays in the diode bias-control circuits with solid-state devices.

(3) For improved understanding of high-power and IMD performance of filters with PIN diode-switched irises.

(a) Supplementation of analytical investigations of filter performance at full peak RF power input with experimental investigations.

(b) Continuation of IMD measurements over a range of RF input power levels, up to the rated maximum, and over the full range of bias voltage up to the PIV of the diodes.

(c) Analytical and experimental investigation of the mechanisms of third-order IMD generation in filters of the type under discussion, and correlation with specific filter design parameters (e.g., Z_0, $C_{i(min)}$, bias-choke resonances, etc.), and with specific diode parameters (e.g., doping levels, doping profiles, I-layer thickness, etc.).

(4) For obtaining substantial improvement in selectivity (unloaded Q) and IMD performance.

(a) Development of a rugged, low-loss repackaging of the mercury-film switch. [Barring a dramatic leap forward in the semiconductor art, for which there is no motivation from current users of PIN diodes as switches in low-Q circuits, mercury-film switches appear the only route to high-speed, reliable switching compatible with Q_u = 5000 and IMPs at 100 dB below signal. The Logcell manufacturers have shown interest in collaborating in this development, which is strongly urged by the authors. The technical resources available at SRI in the Physical Electronics Group (Information Sciences and Engineering Division), the Metallurgy and Ceramics Groups (Materials Laboratory, Physical Sciences Division), and other areas should ensure satisfactory and rapid development and pilot production of the new package, along with possible improvements in the basic mercury-film components and magnetic drive.]

(b) Investigation of FET (triode) switching for Flauto-type filters. (Preliminary estimates indicate that the effective R_s would be quite high, while the possibility of improvements in R_p and IMD performance is very speculative. Biasing adjuncts would add unwanted complexity.)

Since the above list of suggestions is extensive, it would be appropriate to assign priorities based on the application needs. If it is desired to prove system compatibility of the new form of filter, even with reduced selectivity, items (1a), (1b), and (1c) should receive priority. However, if it is not deemed worthwhile to go out into the field with the present relaxed specifications on selectivity and IMD performance, item (4a) would receive top priority, except for the following alternative: Increased selectivity, for the same unloaded Q and insertion loss, could be achieved by using two or more coupled resonators [suggestion (1e)], although IMD performance would not be improved.

Items (3a), (3b), and (3c) should be included in any program committed to the PIN-diode option, rather than to the repackaged-Logcell option.

VIII SUMMARY AND CONCLUSIONS

A novel concept for an electronically tuned, high-Q, high-power VHF/UHF bandpass filter suitable for Air Force communications systems was developed, and operating breadboard models were completed. The results of this work show that the concept has substantial merit and should see application in VHF and UHF (and, probably, microwave) systems in the near future.

The filter is obtained by distributively loading a high-Q, TEM-line resonator with N independent irises, each exhibiting a two-valued capacitance that is switched by means of low-loss RF switches within the iris. The placement of irises takes advantage of the sinusoidal distribution of electric field in the resonator so that the tuning increment resulting from the switching of an iris is weighted as the square of the sine of the electrical angle expressing the distance of that iris from the resonator end wall. The N distances are chosen so that the sequence of weightings follows the series 1, 1/2, 1/4, 1/8, ..., $1/2^{N-1}$, while the respective tuning increments follow the series 1/2, 1/4, 1/8, 1/16, ..., $1/2^N$, as fractions of the tuning range. The electronic tuning program thus follows a binary logic and the exercising of all switching-control codes of N binary digits yields 2^N tuning channels that are (very nearly) uniformly distributed over the tuning range.

During the development of the design concept and the experimental confirmation of its validity, mathematical modeling of the filter was achieved with regard to iris placement, the effects of switch losses, and the RF voltages and currents in individual switches at high power levels. Design relationships were developed for the case of non-ideal switches, and the resulting limitations on filter selectivity were predicted. Two kinds of RF switching device--high-voltage PIN diodes and Logcell I mercury-film switches--were evaluated.

Using UM 7000-C-series PIN diodes, an operating bandpass filter was completed having 512 tuning channels in the range 294 to 350 MHz. Worst-case third-order intermodulation generation in this filter was evaluated. Hardware and software were developed to rapidly tune this filter through a list of tuning channels and automatically measure, record, tabulate, and display the corresponding filter parameters.

Using Logcell I mercury-film switches, a demonstrational bandpass filter was completed having two tuning channels (at 299 and 323 MHz) with superior selectivity. An improved packaging for mercury-film switches was proposed as the means for achieving much greater unloaded Q and selectivity, and much less intermodulation distortion, in a filter of the type under consideration. Recommendations for future research and development work on these filters and the systems employing them were compiled for the PIN-diode option as well as the repackaged-mercury-film-switch option.

A summary of design objectives and performance parameters for the completed filters is given in Table VIII-1.

Table VIII-1

SUMMARY OF DESIGN OBJECTIVES AND PERFORMANCE PARAMETERS

Parameter	Original Specification	Working Design Goal[a]	Filter Model Flauto I	Filter Model Flauto II
Frequency range, MHz	225-400	1/4 this range	294-359	299,323
Tuning increment, kHz	100	300, max	300, max	(c)
3-dB bandwidth, kHz	400, max	(b)	1200-1800	743,637
30-dB bandwidth, MHz	14, max	(b)	32-48	(d)
Passband insertion loss, dB	2.25, max	2.25, max	1.3-2.7	3.35,1.35
Passband VSWR	1.5, max	1.5, max	1.3-1.7	2.0,1.3
Power rating, peak, W	100	100	(e)	(e)
Power rating, average, W	20	20	(f)	(f)
Input impedance, ohms	50	50	50	50
Tuning time	1 s	1 s	< 5 μs[f]	< 5 ms[f]
Volume, ft^3	0.5, max	0.5/4, max	(g)	(g)
Weight, lb	15, max	15/4, max	(g)	(g)
Third-order intermodulation products with two inputs at +40 dBm	-60 dBm, max	(b)	-25 dBm (estim.)	(e)
Unloaded Q	5000	(b)	890-1560	1250,3440

(a) Established after review of limitations imposed by use of PIN diodes.

(b) Best obtainable, considering switch limitations.

(c) Not applicable.

(d) Not measured.

(e) Meets specifications, according to calculations.

(f) Exceeds specifications.

(g) Acceptable, following mechanical redesign.

Appendix A

FILTER CIRCUIT REQUIREMENTS AND RELATIONS

Appendix A

FILTER CIRCUIT REQUIREMENTS AND RELATIONS

As shown below, a filter consisting of one resonator will fulfill requirements with respect to filter skirt characteristics, passband insertion loss, and passband VSWR, provided the unloaded Q of the filter does not fall below a certain minimum value of $Q_{u(min)}$.

1. Filter Skirt Characteristics*

The attenuation of a bilateral lossless bandpass filter is readily computed from the formula for the low-pass prototype filter in the ω' plane:

$$L_A(\omega') = 10 \log_{10}\left[1 + \epsilon\left(\frac{\omega'}{\omega_1'}\right)^2\right] \tag{A-1}$$

where

$$\epsilon = \left[\left(\text{antilog}_{10} \frac{L_{Ar}}{10}\right) - 1\right] \tag{A-2}$$

$$\omega_1' = \text{cutoff frequency} \tag{A-3}$$

and L_{Ar} is the attenuation of the passband edge in decibels. Here, L_{Ar} = 3 dB at $\omega' = \omega_1'$ and $\epsilon = 1$. In the case of the original design objectives, ω_1' corresponds to the 400-kHz bandwidth in the bandpass filter. At $\omega' = 35\ \omega_1'$, corresponding to the 14-MHz bandwidth in the bandpass filter,

---

*General reference: G.L. Matthaei, L. Young, and E.M.T. Jones, Microwave Filters, Impedance-Matching Networks, and Coupling Structures (McGraw-Hill Book Company, New York, N.Y., 1964).

 Preceding page blank

the attenuation is

$$L_A(\omega_1) = 10 \log_{10} [1 + (1)(35)^2] \text{ dB} = 31 \text{ dB} \quad . \qquad \text{(A-4)}$$

Since 30-dB attenuation is specified, a single resonator is adequate. Although the filter will not be lossless, as was assumed in the above computation, the skirt characteristics are not affected by such loss in the high-attenuation (30-dB) region. Therefore, the conclusion that one resonator is adequate is still correct, even when dissipation loss is considered.

2. Passband VSWR

A bilateral single-resonator filter with loss may be represented at resonance as a series (or shunt) resistance, as shown in Figure A-1. The maximum allowable value of this equivalent resistance is determined by the system impedance and the allowable VSWR. For a 50-ohm system and a maximum allowable VSWR of 1.5:1, the equivalent resistance Z_{series} is 25 ohms. This resistance is one of several controlling factors with respect to loaded Q, and it also determines the insertion loss in the passband.

3. Passband Insertion Loss

The passband insertion loss is computed from the passband insertion voltage ratio

$$T = \frac{2}{2 + (Z_{series})/Z_0} \qquad \text{(A-5)}$$

which gives

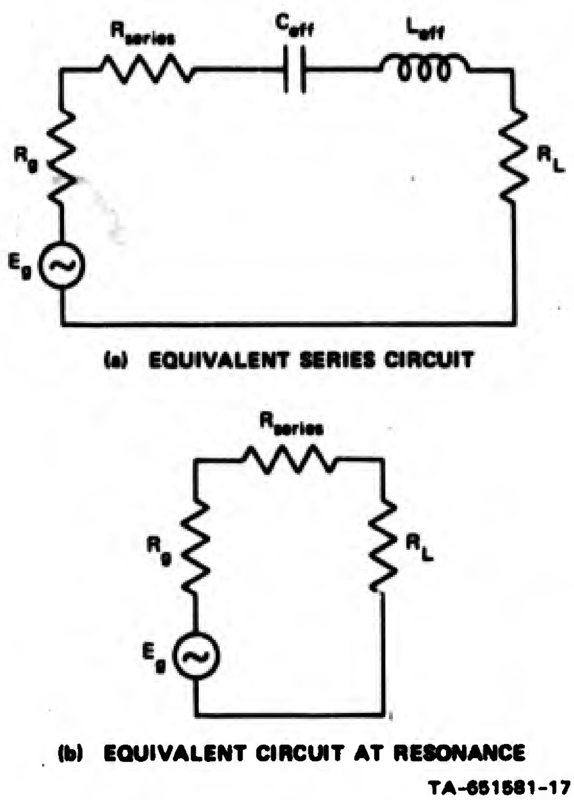

FIGURE A-1 EQUIVALENT CIRCUITS OF A SINGLE-RESONATOR BANDPASS FILTER WITH LOSS

$$T = \frac{2}{2 + 25/50} = 0.8 \quad .$$

The insertion loss is

$$L_{A0} = 20 \log_{10} \left(\frac{1}{T}\right) = 1.94 \text{ dB}$$

which is less than the specified maximum of 2.25 dB.

4. Filter Unloaded Q

The minimum allowable value of unloaded Q is determined from the filter circuit at resonance and the maximum loaded Q.

The maximum value of loaded Q occurs at the highest frequency in the range,

$$Q_{L(max)} = \frac{f_{max}}{\text{3-dB bandwidth}} = \frac{400 \text{ MHz}}{0.4 \text{ MHz}} = 1000 \quad . \qquad \text{(A-6)}$$

The minimum value of unloaded Q is

$$Q_{u(min)} = Q_{L(max)} \left(\frac{R_G + R_L + R_{series}}{R_{series}}\right) = 1000 \, \frac{50 + 50 + 25}{25} \qquad \text{(A-7)}$$

$$Q_{u(min)} = 5000 \quad .$$

5. Resonator Structure

In order for switch losses, rather than resonator losses, to set an upper limit on Q_u of the filter, the resonator alone should have a Q_u substantially larger than 5000. If coaxial, the optimum ratio of O.D. to I.D. for a given O.D. is 3.5. For copper, in this case,

$$Q_u = 3400 \text{ (O.D. in inches)} \left[\text{(f in MHz)}^{1/2} \right] \tag{A-8}$$

and

$$Z_0 = 75 \text{ ohms} \quad .$$

If limited by the undesirable possibility of exciting a higher-order mode in the coaxial line, the O.D. could be as large as 14.6 inches. An O.D. of six inches, however, would be chosen because of volume limitations. In this case, for copper,

$$Q_u = 12{,}900$$

neglecting end-wall losses and those due to current crowding near irises.

6. General Relations

$$Q_L = \frac{\text{Center frequency}}{\text{3-dB bandwidth}} = \frac{f_0}{(\Delta f)_3} \quad . \tag{A-9}$$

For equal input and output coupling loops,

$$Q_{E1} = Q_{E2} = Q_E \tag{A-10}$$

$$L_{A0} = 10 \log_{10} (Q_E^2/4(Q^2)_L) \tag{A-11}$$

$$\frac{1}{Q_L} = \frac{2}{Q_E} + \frac{1}{Q_u} \tag{A-12}$$

and

$$\text{VSWR} = \frac{Q_u + Q_E}{Q_u} \quad . \tag{A-13}$$

Appendix B

HEWLETT-PACKARD 8541A AUTOMATIC NETWORK ANALYZER

Preceding page blank

Appendix B

HEWLETT-PACKARD 8541A AUTOMATIC NETWORK ANALYZER

The Hewlett-Packard Automatic Network Analyzer, shown in Figure B-1, is a combination of a microwave vector voltmeter, RF signal generators, output displays, and a digital computer. At the extreme left in the figure is the teletypewriter and teleprinter for communicating with the computer. The network analyzer comes in three sections. The section on the left contains a high-speed punched-tape reader. The middle section contains a polar display (at the top), a phase-gain meter (which displays degrees or decibels), the control units for the oscillator heads (which cover a frequency band from 0.11 to 12.4 GHz), a test set to connect components under test from 1.5 to 12.4 GHz, and a high-speed tape punch (at the bottom). The section on the right contains the X-Y plotter, a test set to connect components under test from 0.11 to 2.5 GHz, and the RF sweep oscillators (at the bottom).

In addition to providing more accurate data, this instrument greatly facilitates generation of design data for new microwave passive and active components and systems. This automatic network analyzer has the capability to generate RF energy in the frequency range from 0.11 to 12.4 GHz, tune the frequency under computer control, measure the magnitude and phase of waves incident on the two input ports, correct the measured data for system errors, do computations for data reduction, and present the results. The results can be presented as tabulations on the teleprinter, plotted on rectangular or polar oscilloscopes, plotted on the X-Y recorder, punched on paper tape, or as various combinations of these outputs.

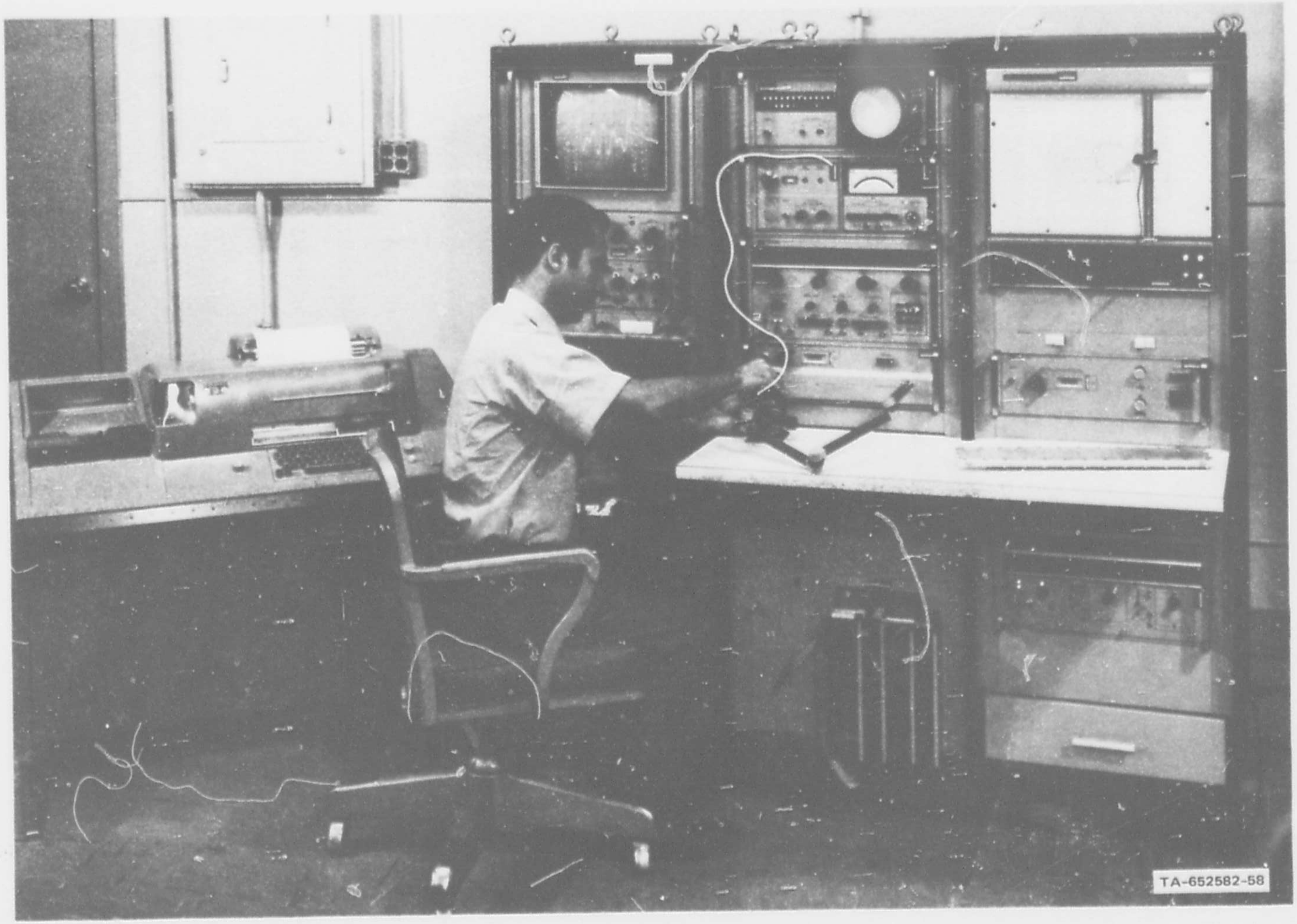

FIGURE B-1 COMPUTER-CONTROLLED AUTOMATIC NETWORK ANALYZER (Hewlett-Packard Model 8541A) USED TO MEASURE VHF, UHF, AND MICROWAVE COMPONENTS AT STANFORD RESEARCH INSTITUTE

The fundamental parameters measured by the network analyzer are the scattering parameters (S-parameters) of one-, two-, or multi-port devices. These are the complex reflection and transmission coefficients. Once the S-parameters are measured, the digital computer can convert them to other parameters such as VSWR, return loss, gain in dB, insertion loss in dB, input impedance or admittance, phase shift, and group time delay. For transistor measurements, the data can be converted to h, y, or z parameters, as well as voltage gain with a conjugate match at the input, the output, or both.